2018

Polypyrrole (PPy) Coated Patterned Vertical Carbon Nanotube (pvCNT) Dry ECG Electrode Integrated with a Novel Wireless Resistive Analog Passive (WRAP) ECG Sensor

Mohammad Jomah I. Abu Saude

Polypyrrole (PPy) Coated Patterned Vertical Carbon Nanotube (pvCNT) Dry ECG Electrode Integrated with a Novel Wireless Resistive Analog Passive (WRAP) ECG Sensor

By

Mohammad Abu Saude

A Dissertation

Submitted in Partial Fulfillment of the

Requirements for the Degree of

Doctor of Philosophy

Major: Electrical and Computer Engineering

The University of Memphis

December 2018

ACKNOWLEDGMENTS

First and above all, praises and thanks to God, for His helpings and blessings to complete this dissertation successfully.

I would like to thank my research supervisor, Dr. B. Morshed, professor for Electrical Engineering and Computer Engineering, University of Memphis, for giving me the opportunity to complete my Ph.D. degree, providing great guidance throughout the work, and helping me to complete my degree.

I want to thank the members of my committee: Dr. Eddie Jacobs, Dr. Firouzeh Sabri, Dr. Madhusudhanan Balasubramanian, and Dr. Amy L de Jongh Curry for their invaluable advice and feedback on this research.

I am also thankful to other students working at the ESARP lab, for helping me and giving me suggestions throughout my work. I also acknowledge the funding provided by the FedEx Institute of Technology.

I could have never achieved my dissertation without my family. They have always supported me emotionally and financially throughout my degree.

Mohammad J. Abu-Saude

ABSTRACT

Abu-Saude, Mohammad. The University of Memphis. October 2018. Polypyrrole (PPy) Coated Patterned Vertical Carbon Nanotube (pvCNT) Dry ECG Electrode Integrated with a Novel Wireless Resistive Analog Passive (WRAP) ECG Sensor. Major Professor: Dr. Bashir I. Morshed.

Biopotential signals such as electroencephalography (EEG), electrocardiography (ECG or EKG), electrooculogram (EOG), and electromyography (EMG) play vital roles in health and clinical diagnoses, monitoring, and therapy. In addition, these signals are required for many nonclinical applications such as Neurofeedback and Brain-Computer Interface (BCI). The quality of the measurement relies on the electrical and mechanical properties of the electrode. Conventional wet or gel impedimetric electrodes provide an excellent signal due to the conductive fluids or gel, which reduces the skin-contact impedance and maintains contact during movement. However, they operate for a short duration; the quality of the signal degrades due to the fluid or gel drying out. Dry electrodes promise the ability for long duration sensing and avoiding the drawbacks of the wet/gel electrodes. However, dry electrodes suffer from high interfacing impedance. In this work, dry electrodes based on Carbon Nanotube (CNT) are presented. The CNTs were fabricated in a Vertical Pattern (pvCNT) on a circular stainless steel foil substrate with a diameter of 10 mm and thickness of 2 mils. The pattern on the substrate was developed with a custom shadow mask using sputter coating with Al2O3 and iron. Electrically conductive multi-walled CNTs were grown in patterned pillar formation with a square base of 100 µm each side, with an inter-pillar spacing of 50, 100, 200 and 500 µm, and heights between 1 to 1.5 mm. The impedances of the electrodes were 1.92, 3.11, and 8.15 Ω for 50, 100, and 200 µm spacing, respectively. A comparative in vitro study with commercial wet and gel electrodes showed pvCNT electrode has lower interfacial impedance for a long-term period, comparable signal capture quality, and ability

to be used for stimulation. Coating the electrodes by a conductive polymer (Polypyrrole or PPy) is used to improve the mechanical properties of the CNTs. The coating procedure involved applying 10 µL of PPy after preparing the pvCNT with 70% ethyl alcohol solution and flash drying at 300°C. The impedance of the coated version of pvCNT has slightly increased compared to the non-coated pvCNT version and stayed lower than the electrical impedance of the commercial electrodes. Mechanical tests showed the PPy coated pvCNT has stronger adhesion to the Stainless Steel (SS) substrate. The results demonstrate the feasibility of coating pvCNT dry electrodes with PPy for robustness. Furthermore, we explore the use of this dry electrode for wearable ECG sensors. Fully passive sensors, which are zero power and battery-less, can make wearable devices more practical by eliminating the contact wires subsequently decreasing the weight, costly and high-maintenance batteries. We have previously developed a novel technique of Wireless Resistive Analog Passive (WRAP) sensor based on resistive transducers. The scanner transmits an RF signal at an ISM frequency band (e.g. 8.37 MHz) which is amplitude modulated based on the resistive changes by a transducer. The modulated signal is then captured and analyzed on the scanner or downstream on the user's smartphone. In this work, we have proposed a novel conjugate coil pair technique for WRAP sensors and demonstrated the capability for differential signal capture, such as electrocardiogram (ECG or EKG). The WRAP ECG sensor uses an N-channel dual-gate MOSFET (depletion mode) to convert the biopotential signal to the correlated resistive variation of R_{SD} (Source to Drain Resistance). The system was able to cancel the common mode signal and only transmitted differential mode signals. The results show that connecting a pair of sensors in this way could allow accurate measurement of a differential biopotential. This work demonstrates voltage sensitivity down to 40 µV towards realizing a battery-less, body-worn WRAP ECG sensor for monitoring ECG signals while the signal is collected using pvCNT electrodes.

PREFACE

This dissertation includes three Journal articles as chapters. I am the first author of these articles. Article 1 entitled “Patterned Vertical Carbon Nanotube (pvCNT) Dry Electrodes for Impedimetric Sensing and Stimulation”, listed as Chapter 2, is published by the IEEE Sensors Journal and is available online with the citation: Mohammad J. Abu-Saude, Bashir I. Morshed, “Patterned Vertical Carbon Nanotube (pvCNT) Dry Electrodes for Impedimetric Sensing and Stimulation”, IEEE Sensors Journal, Vol. 15(10), pp. 5851-5858, Oct. 2015.

Article 2 entitled “Characterization of a Novel Polypyrrole (PPy) Conductive Polymer Coated Patterned Vertical CNT (pvCNT) Dry ECG Electrode” listed as Chapter 3, is accepted by the Chemosensors and is available online with the citation: Mohammad Abu-Saude, Bashir Morshed, “Characterization of a Novel Polypyrrole (PPy) Conductive Polymer Coated Patterned Vertical CNT (pvCNT) Dry ECG Electrode”, Chemosensors, vol. 6, pp. 27, 2018.

Article 3 entitled “Accessing Differential Measures with a Conjugate Coil-pair for Wireless Resistive Analog Passive (WRAP) ECG Sensors with PPy Coated pvCNT” listed as Chapter 4 and ready for submission to IEEE Sensors Journal.

TABLE OF CONTENTS

LIST OF FIGURES

Chapter 1: Introduction

1. Overview

Biopotential signals are generated from electrochemical activity in certain cells of the nervous, muscular, or glandular tissue. When these cells are stimulated, they create an action potential due to the ions exchanged through the cell membrane. This action potential can be measured using electrodes at the body surface through several methods such as electroencephalography (EEG), electrocardiography (ECG or EKG), electrooculogram (EOG), and electromyography (EMG) [1, 2]. The amplitude of the ECG signal range from hundreds of microvolts to a few millivolts in the frequency range from 0.1 Hz to several hundred Hz [1] as shown in Fig. 1. 1.

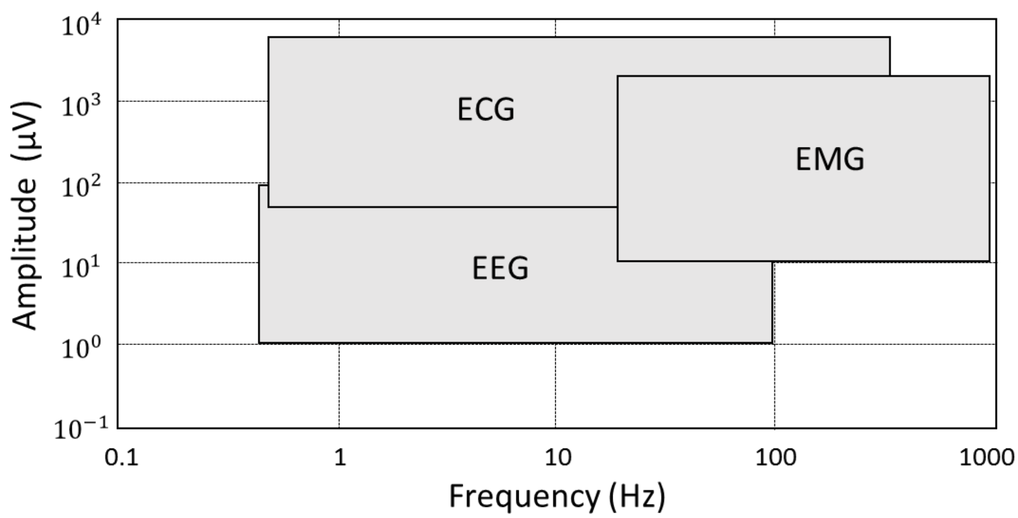

Fig. 1. 1 The characteristics of the biopotential signals: ECG, EEG, and EMG [1].

Biopotential signals are sensed by transducing ionic currents into electric currents with the use of electrodes and electronic instrumentation for signal amplification, filtering, and processing. This transducing mechanism requires an electrically conducting electrode to be in contact with the electrically conducting ionic solutions of the body. For wet or gel electrodes, a chemical reaction (oxidation-reduction) can occur at the solution-electrode interface such that the charge can be transferred through the electrolytes in the solution and the metal conductor of the electrode. Thus, the electrical characteristics of the wet electrode can be described as a parallel capacitance and resistance of the interface between the electrode and the electrolyte in series with the half-cell potential and the resistance of the electrolyte [3]. However, for the dry electrodes, the resistance of the electrolyte is not applicable.

Biopotential signal acquisition systems suffer from biological interference from skin, electrodes, or motion and noise sources from the surrounding environment (e.g., power lines, electromagnetic or radio frequencies). These noises can be classified into two categories: environmental and contact noise [4-6] and consequently electrodes require very carefully tailored designs in order to effectively reject or suppress most of these interference noise sources [2].

The contact noise is generated from the unstable interface between the skin and the electrode. In the case of the wet electrodes, the skin-gel interface is the most significant source of noise. Half-cell noise as discussed before appears at the interface between the gel and the electrode due to the diffusion of the gel in the top layer of the skin [6]. Any mismatch of the half-cell potential on different electrodes and the reference electrode will produce a differential DC offset voltage.

Wet electrodes use a conductive solution at the interface between the electrode and the skin. The traditional impedimetric interfacing electrodes are made up of silver metal (Ag) coated with silver chloride (AgCl) layer. A gel-based electrolyte is used to decrease the contact impedance and the artifact of motion and to increase the dielectric constant between the skin surface and the electrode [7]. The stratum corneum (SC) – the top layer of the skin - has a high impedance, while the biopotential signals are transmitted using the ionic water below the SC layer. The gel will make an easier path between the surface of the metal part of the electrode and the skin below the SC layer. These sensors only operate optimally for a short duration because of gradual degradation of conductivity, as the electrode interface impedance deteriorates over time due to evaporation, and leads to signal quality degradation [3, 8-10]. In addition, wet or gel electrodes usually require skin preparation to remove dirt, skin debris, and oil from the skin surface and this preparation is usually performed precisely by an expert (e.g. clinician). Furthermore, the gel is a key source of the contact noise [11] and could cause a skin allergy. Wet or gel electrodes lead to detrimental reliability over a long period; hence, the current practice is to periodically replace the electrodes, burdening the user and the operator-in-the-loop (e.g., clinician). This is a technological barrier for pervasive patient-centric care and continuous, all day health/wellness monitoring (e.g., neuro-physiological signal monitoring for prolonged periods) in natural environments [12-14]. These wet Ag/AgCl electrodes are still widely used for clinical and research purposes. Most wet electrodes have an adhesive attached to the skin, which makes it hard and painful to remove after recording and uncomfortable to wear for a long period of time, and a metal snap to be attached to the electrode.

As an alternative, Carbon Nanotubes (CNTs) are highly conductive material and have the potential to be used in many applications [15]. In the work described in this dissertation, we first studied the feasibility of using CNTs for ECG type bioelectric signal sensing (referred as impedimetric sensing) because of the desirable properties of CNTs.

Measuring biopotential signals requires electronics, power source, and wires thus the cost and the size of the device will be increased. Wireless and fully passive sensors can be suitable in situations where a wired connection is inconvenient or impractical such as body-worn, implantable, and remote sensors. Wireless Resistive Analog Passive (WRAP) sensors are chip-less and zero-power that operate by modulating the amplitude of the transmitted RF signal. The sensor is composing of a loop antenna, a tuning capacitor, and resistive transducer. We have previously developed this type of sensor, which is suitable for biosignal (using resistive transducers) and biopotential sensing. The resistor-based transducer can be replaced by a metal-oxide-semiconductor field-effect transistor (MOSFET) to convert the biopotential signal to its corresponding resistive variation of the drain-source resistor (R_{DS}). The RF signal is transmitted from the scanner and amplitude modulated based on R_{DS} changes according to the biopotential signal that is measured through the gate of the MOSFET. In depletion-mode MOSFETs N-channel, a thin layer of silicon N-type is placed below the gate. This layer is insulated from the gate by a silicon dioxide insulating layer. Therefore, a current of free electrons can flow between the source and drain when V_{GS} is zero due to the conductive channel between the source and the drain. The depletion mode MOSFETs are suitable for use as a voltage-control resistance. We have investigated the use of the depletion-mode MOSFETs in WRAP biopotential sensor due to its special construction as shown in Figure 1.2.

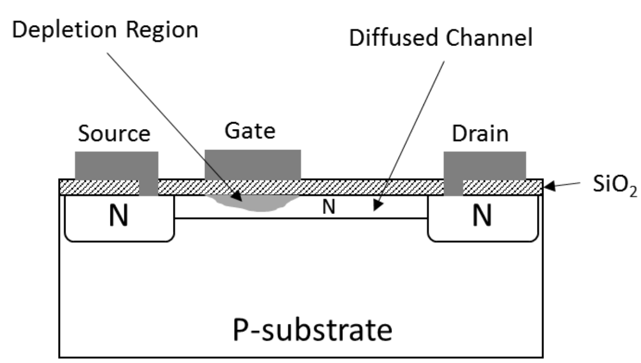

Fig. 1. 2 Cross-section view of a depletion-mode MOSFET N-channel

2. Related works

Dry electrodes are designed to sense the biopotential signal in the absence of the gel/electrolyte, which makes it more suitable for longer duration impedimetric sensing compared to wet electrodes. Sensing with dry electrodes occurs without the degrading of impedances, however, suffer from inferior impedances and noise [6-8,14]. A conductive polymer, such as polypyrrole (PPY) thin film on a copper substrate [16] or planar polydimethylsiloxane (PDMS) [14], are promising dry electrode technologies; however, surface connectivity at the skin-electrode interface is poor. Improved surface connectivity and penetration through hair were achieved with PDMS based flexible pin dry electrode, which has relatively high impedances [17]. Pin structure was also demonstrated using micro-electromechanical systems (MEMS) chips with limited pin height (250 µm) [18]. Spring-loaded mechanical metal pin electrode is another promising dry electrode with low impedance and ability to penetrate through thick layers of hair [19,20]; however large and uncomfortable for all-day usage. Conductive sponge [21] and foam [3] provide comfortable interfaces, but have high electrode impedance (e.g. more than 10 kΩ below 100 Hz). An inkjet-based dry electrode using silver ink has low electrode impedances [22], but toxicity and surface connectivity issues remain. Finally, non-contact capacitive sensors have drawn significant recent interest [23], but it mandates complex active circuitry for each sensor to deal with changing distance between sensor and scalp due to motion, high interfering noise, and issue related to sensing of potential versus charge. In general, various dry electrodes suffer from one or more unresolved issues such as low contact surface, high contact potential, polarization and high interfacial noises [4,24]. In addition, non-contact electrodes are more sensitive, compared to contact electrodes, to any motion of the electrode with respect to the body as the capacitance can be dramatically changed by a factor of 10 by only moving the electrode by100 µm vertically [25]. Hence, a significant research effort has been devoted towards a high-performance dry electrode [26].

In vitro studies have demonstrated that CNT-based biosensors can provide reliable interfacing to neuronal signals [27]. Furthermore, at a low concentration external to the body, CNT-based biosensors do not show toxicity [28-30]. Previous attempts to use CNTs for neurological and physiological electrodes as dry electrode interfaces have only limited success [5,31-33]. Other techniques that utilized CNTs as dry electrodes primarily involve integration of CNTs within other polymers or substrates (such as PDMS) [34,35] that do not have good electrical conductivity, and suffer from the issues like the top surface of the composite electrode is planar, thus would not make proper contact with a rough skin surface.

Wireless analog passive sensors (WAPS) have been demonstrated for remote signal capturing based on varactor and Surface Acoustic Wave (SAW) resonator [36-39]. The capacitive changes were used in these WAPS for modulation by shifting the resonance frequency based on the recorded signal [38, 39]. In previous work, we showed a new type of Wireless Resistive Analog Passive (WRAP) sensor that can be used for capturing physiological and biopotential signals. We have previously shown that this WRAP sensor is able to capture a biopotential signal as low as 10 mV over a distance of 21.5 mm between the antennas [40].

3. Research Objective, Approach, and Scope

The work in this research attempts to develop a new dry electrode that can be used for daily and long-term monitoring and transmit the biopotential signals using wireless passive technology with zero power. The key research objectives of this study are:

1. To develop dry biopotential electrodes using Multi-walled carbon nanotubes (MWCNT) due to its high conductivity property.
2. To evaluate the CNT-based electrode compared to the traditional wet/gel electrodes *in vitro* and *in vivo*.
3. To improve the adherence stability of the CNT pillars to the substrate by using an electrically conductive polymer (Polypyrrole, PPy) coating.

4. To build a battery-less wireless resistive analog passive (WRAP) sensor that can transmit biopotential signals (i.e. ECG) using an resistor-inductor-capacitor (RLC) tank resonator with zero-power.
5. To integrate the CNT-based electrodes with WRAP sensor to meet the demand of finding an alternative method for the daily and ease-of-use monitoring system.

The patterned vertical CNT (pvCNT) is an ensemble of an array of MWCNT that forms pillars vertical to the circular stainless steel (SS) substrate (diameter of 10 mm, 2 mils thick). Each pillar was grown on 100 µm squared base, and the height was between 1 - 1.5 mm with four different spacings between the pillars (50, 100, 200, and 500 µm) in an array formation. The pvCNTs were synthesized using Chemical Vapor Deposition system (CVD). The PPy was used due to its easy preparation process, high electrical conductivity, and environmental safety. In order for this work to be useful for daily and long duration measurement, we have demonstrated the feasibility of a novel Wireless Resistive Analog Passive (WRAP) sensor for biopotential measurement. The WRAP sensor is an RLC resonator with a damping factor (Q). Thus, the variation of the resistive load changes the damping factor that modulates the carrier RF signal accordingly, which can be captured from the scanner using an envelope detector.N-channel dual-gate depletion-mode MOSFETs were used to capture the ECG signal. The dual gate MOSFET acts as a resistor load that changes accordingly to the biopotential signal that is connected to the gate.

6. Achievements

<u>Patent Application:</u>

1. B. I. Morshed and M. Abu-Saude, "Apparatus and Method to Capture Body Signals with Conjugate Coils and Paired Coils", USPTO Provisional Patent Application, No. 62/664,329, Filed on Apr. 30, 2018.

Journal Articles as the first author:

1. Mohammad Abu-Saude, Bashir Morshed, "Accessing Differential Measures with a Conjugate Coil-pair for Wireless Resistive Analog Passive (WRAP) ECG Sensors with PPy Coated pvCNT", *IEEE Sensors Journal*. (Manuscript in preparation), 2018.
2. Mohammad Abu-Saude, Bashir Morshed, "Characterization of a Novel Polypyrrole (PPy) Conductive Polymer Coated Patterned Vertical CNT (pvCNT) Dry ECG Electrode", *Chemosensors*, vol. 6, pp. 27, 2018.
3. M. J. Abu-Saude, and B. I. Morshed, "Patterned Vertical Carbon Nanotube (pvCNT) Dry Electrodes for Impedimetric Sensing and Stimulation", *IEEE Sensors J.*, vol. 15, no. 10, pp. 5851-5858, 2015.

Refereed Conference Publications:

1. Mohammad Abu-Saude, and Bashir I. Morshed, " Accessing Differential Measures with a Conjugate Coil-pair for Wireless Resistive Analog Passive (WRAP) ECG Sensors", IEEE Electro-Information Theory (EIT) Conf., Oakland, MI, (in press), May 3-5, 2018.
2. M. Abu-Saude, and B. I. Morshed, "Polypyrrole (PPy) Conductive Polymer Coating of Dry Patterned Vertical CNT (pvCNT) Electrode to Improve Mechanical Stability", IEEE Topical Conf. Biomedical Wireless Technologies, Networks, and Sensing Systems (BioWireleSS), Jan. 24-27, 2016. (DOI: 10.1109/BIOWIRELESS.2016.7445569).

3. M. Abu-Saude, S. Consul-Pacareu, and B. I. Morshed, "Feasibility of Patterned Vertical CNT for Dry Electrode Sensing of Physiological Parameters", IEEE Biowireless Conf, pp. 1-4, 2015. (DOI: 10.1109/BIOWIRELESS.2015.7152124).

<u>Other Publications during this period:</u>

1. S. Consul-Pacareu, R. Mahajan, and M. J. AbuSaude, and B. I. Morshed, "NeuroMonitor: A Low-power, Wireless, Wearable EEG Device with DRL-less AFE", The IET Circuits, Devices, & Systems 11, no. 5, pp.471-477, Mar. 2017.
2. R. Mahajan, S. Consul-Pacareu, M.J. AbuSaude, M.N. Sahadat, and B. I. Morshed, "Ambulatory EEG Neuromonitor Platform for Engagement Studies of Children with Development Delays", SPIE Proc. Smart Biomedical & Physiological Sensor Tech X, vol. 8719, pp. 87190L(1-10), May 2013.

<u>Awards:</u>

1. The conference paper titled "Accessing Differential Measures with a Conjugate Coil-pair for Wireless Resistive Analog Passive (WRAP) ECG Sensors" by Mohammad Abu-Saude and Bashir I. Morshed has received the First Place award at the 18th Annual IEEE Intl. Conf. on Electro Information Technology (EIT2018), May 3-5, 2018 at Rochester, Michigan, USA.
2. Awarded third best poster in the Department of EECE Poster Competition held at the University of Memphis on 24 April 2015. (Poster title: "Patterned Vertical Carbon Nanotube (pvCNT) Dry Electrodes for Impedimetric Sensing and Stimulation")

7. References

[1] Yazicioglu RF, VanHoof C, Puers R. “Bio-potential Readout Circuits for portable Acquisition Systems”, *Berlin: Springer Verlag*, 2009.

[2] Nitish V. Thakor, “The Measurement, Instrumentation and Sensors Handbook”, *CRC Press LLC*, Chapter 74, 1999.

[3] Y. M. Chi, T. Jung, G. Cauwenberghs, “Dry-contact and noncontact biopotential electrodes: methodological review”, IEEE Reviews in Biomedical Engineering, vol. 3, pp. 106-119, 2010.

[4] E. Huigen, A. Peper, and C. A. Grimbergen, “Investigation into the origin of the noise of surface electrodes,” Medical & Biological Engineering & Computing, vol. 40, pp. 332-338, 2002.

[5] J.G. Webster, Medical Instrumentation, J. Wiley & Sons, 1998.

[6] G. Ruffini, S. Dunne, E. Farres, J. Marco-Pallares, C. Ray, E. Mendoza, R. Silva, and C. Grau, “A dry electrophysiology electrode using CNT arrays”, Sensors and Actuators A, vol. 132, no. 1, pp. 34-41, 2006.

[7] Dinglong Hu , Tin Kei Cheng, Kai Xie and Raymond H. W. Lam, “Microengineered Conductive Elastomeric Electrodes for Long-Term Electrophysiological Measurements with Consistent Impedance under Stretch”, Sensors, 15.10:26906-26920, 2015.

[8] C. Lin, L. Liao, Y. Liu, I. Wang, B. Lin, J. Chang, “Novel dry polymer foam electrodes for long-term EEG measurement”, IEEE Trans. Biomed. Eng., vol. 58, no. 5, pp. 1200-1207, 2011.

[9] A. Searle and L. Kirkup, “A direct comparison of wet, dry and insulating bioelectric recording electrodes,” Physiol. Meas., vol. 21, pp. 271–283, 2000.

[10] C. Gurger, G. Krausz, B.Z. Allison, and G. Edlinger, “Comparison of dry and gel based electrodes for P300 brain-computer interfaces”, Front Neurosci., vol. 6, no. 60, pp. 1-7, 2012.

[11] G. Ruffini, S. Dunne, E. Farres, J. Marco-Pallares, C. Ray, E. Mendoza, R. Silva, and C. Grau, “A dry electrophysiology electrode using CNT arrays”, Sensors and Actuators A, vol. 132, no. 1, pp. 34-41, 2006.

[12] S. Patel, H. Park, P. Bonato, L. Chan, M. Rodgers, “A review of wearable sensors and systems with application in rehabitation”, J. NeuroEngineering and Rehabilitation, vol. 9, no. 21, 17 p., 2012.

[13] H. Alemdar, C. Ersoy, “Wireless sensor networks for healthcare: a survey”, Computer Networks, vol. 54, pp. 2688-2710, 2010.

[14] B. He, T. Coleman, G. M. Genin, X. Hu, N. Johnson, T. Liu, S. Makeig, P. Sajda, and K. Ye, “Grand challenges in mapping the human brain: NSF workshop report”, IEEE Trans Biomed Eng, vol. 60, no. 11, pp. 2983-2992, 2013.

[15] Nanoscience instruments (http://www.nanoscience.com/applications/education/overview/cnt-technology-overview/)

[16] S. Jamadade, S. Jadhav, V. Puri, “Electromagnetic properties of polypyrrole thin film on copper substrate”, Physics Res, vol. 1, no. 4, pp. 205-210, 2010.

[17] L. Wang, J. Liu, B. Yang, C. Yang, “PDMS based low cost flexible dry electrode for long-term EEG measurement”, IEEE Sensors J., vol. 12, no. 9, pp. 2898-2904, 2012.

[18] J. Chiou, et al. “Using novel MEMS EEG sensors in detecting drowsiness application”, IEEE Biomedical Circuits and Systems Conf., London, pp. 33-36, 2006.
[19] R. Matthews, P.J. Turner, N. J. McDonald, K. Ermolaev, T. Mc Manus, R. A. Shelby, M. Steindorf, “Real time workload classification from an ambulatory wireless EEG system using hybrid EEG electrodes”, IEEE Eng. Med. Biol. Soc. Conf., pp. 5871-5, 2008.
[20] C. Grozea, C. D. Voinescu, S. Fazli, “Bristle-sensors – Low-cost flexible passive dry EEG electrodes for neurofeedback and BCI applications”, J. Neural Eng., vol. 8, pp. 025008 (14 pages), 2011.
[21] A. Gruetzmann, S. Hansen, J. Muller, “Novel dry electrodes for ECG monitoring”, Physiol. Meas., vol. 28, pp. 1375-1390, 2007.
[22] L. Xie, Y. Geng, M. Mäntysalo, L.-L. Xu, F. Jonsson and L.-R. Zheng, Heterogeneous Integration of Bio-Sensing System-on-Chip and Printed electronics, IEEE Journal of Emerging and Selected Topics and Systems, vol. 2, no. 4, pp. 672-682, 2012.
[23] T. J. Sullivan, S. R. Deiss, G. Cauwenberghs, T. Jung, “A low-noise, low-power EEG acquisition node for scalable brain-machine interfaces”, SPIE Bioengineering and Bioinspired Systems III, vol 6592, p. 659203 (8 pages), 2007.
[24] C. Gondran, E. Siebert, P. Fabry, E. Novakov, and P. Y. Gumery, “Non-polarisable dry electrode based on NASICON ceramic”, Medical & Biological Engineering & Computing, vol. 33, pp. 452-457, 1995.
[25] J. M. Lee, F. Pearce, A. D. Hibbs, R. Matthews, and C. Morrissette, "Evaluation of a capacitively-coupled, non-contact (through clothing) electrode or ECG monitoring and life signs detection for the objective force warfighter," Combat Casualty Care in Ground Based Tactical Situations: Trauma Technology and Emergency Medical Procedures, DTIC Document, 2004, pp. 25-1 - 25-10.
[26] S. Ha, C. Kim, Y. M. Chi, A. Akinin, C. Maier, A. Ueno, G. Cauwenberghs, “Integrated circuits and electrode interfaces for noninvasive physiological monitoring”, IEEE Trans. Biomed. Eng., vol. 61, no. 5, pp. 1522-1537, 2014.
[27] Y. Zhang, Y. Bai, B. Yan, “Functionalized carbon nanotubes for potential medicinal applications”, Drug Discovery Today, vol. 15, no. 11/12, pp. 428-435, 2010.
[28] L. Bareket-Keren, Y. Hanein, “Carbon nanotube-based multi electrode arrays for neuronal interfacing: progress and prospects”, Frontiers in Neural Circuits, vol. 6, article. 122, pp. 1-16, 2013.
[29] S.K. Smart, A.I. Cassady, G.Q. Lu, D.J. Martin, “The biocompatibility of carbon nanotubes”, Carbon, vol. 44, pp. 1034-1047, 2006.
[30] J. Chlopek, B. Czajkowska, B. Szaraniec, E. Frackowiak, K. Szostak, F. Beduin, “In vitro studies of carbon nanotubes biocompatibility”, Carbon, vol. 44, pp. 1106-1111, 2006.
[31] G. Ruffini, S. Dunne, E. Farres, P.C.P. Watts, E. Mendoza, S. R. P. Silva, C. Grau, J. Marcho-Pallares, L. Fuentemilla, B. Vandecasteele, “ENOBIO – First tests of a dry electrophysiology electrode using carbon nanotubes”, Proc IEEE EMBS Int. Conf, NY, pp. 1826-1829, 2006.
[32] G. Ruffini, S. Dunne, L. Fuentemilla, C. Grau, E. Farres, J. Marco-Pallares, P.C.P. Watts, S.R.P. Silva, “First human trials of a dry electrophysiology sensor using a carbon nanotube array interface”, Sensors and Actuators A, vol. 144, pp. 275-279, 2008.
[33] J. K. Radhakrishana, H. Bhusan, P.S. Pandian, K. U. B. Rao, V. C. Padaki, K. Aatre, J. Xie, J.K. Abraham, V. K. Varadan, “Growth of CNT array, for physiological monitoring applications”, Proc. SPIE, vol. 6931, pp. 69310P1-5, 2008.

[34] H. B. Baskey, “Development of carbon nanotube based sensor for wireless monitoring of electroencephalogram”, DRDO Science Spectrum, pp. 161-163, 2009.
[35] H. Jung, J. Moon, D. Baek, J. Lee, Y. Choi, J. Hong, S. Lee, “CNT/PDMS composite flexible dry electrodes for long-term ECG monitoring”, IEEE Trans Biomed. Eng., vol. 59, no. 5, pp. 1472-1479, 2012.
[36] Z. Popovic, E.A. Falkenstein, D. Costinett, and R. Zane, Low-power far-field wireless powering for wireless sensors, Proc. IEEE, vol. 101, no. 6, pp. 1397-1409, 2013.
[37] W. Luo, Q. Fu, J. Deng, G. Yan, D. Zhou, S. Gong, Y. Hu, An integrated passive impedance-loaded SAW sensor, Sensors and Actuators B: Chemical, vol. 187, pp. 215-220, 2013.
[38] H.N. Schwerdt, W. Xu, S. Shekhar, A. Abbaspour-Tamijani, B.C. Towe, F.A. Miranda, and J. Chae, A fully-pasive wireless microsystem for recording of neuropotentials using RF backscattering methods, J. Microelectromech Syst., vol. 20, no. 5, pp. 1119-1130, 2011.
[39] J. Riistama, E. Aittokallio, J. Verho, and J. Lekkala, “Totally passive wireless biopotential measurement sensor by utilizing inductively coupled resonance circuits”, Sensors and Actuators A, vol. 157, pp. 313-321, 2010.
[40] S. Consul-Pacareu, D. Arellano, and B. I. Morshed, “Bodyworn Fully-Passive Wireless Analog Sensors for Biopotential Measurement Through Load Modulation”, IEEE Biowireless Conf., (in press), 2015.

Chapter 2: Patterned Vertical Carbon Nanotube (pvCNT) Dry Electrodes for Impedimetric Sensing and Stimulation

1. Introduction

All bioelectric neurological and physiological (neuro-physiological) signals require impedimetric interfacing with the skin for sensing of bioelectric signals or bio-impedances, such as electroencephalography (EEG), electrocardiography (ECG/EKG), electromyography (EMG), and Galvanic Skin Response (GSR) [1,2]. These neuro- physiological signals are of clinical significance for disease diagnosis, patient monitoring, and therapy administration. Current impedimetric interfacing sensors are wet or gel based Ag/AgCl electrodes. These sensors only operates well for a short duration because of gradual degradation of conductivity, as the electrode interface impedance deteriorates over time due to evaporation, leading to signal quality degradation [3-6]. In addition, these wet or gel electrodes usually require skin preparation to remove dirt, skin debris, and oil from skin surface. Thus, the electrophysiology measurements suffer from two types of noises: environment and contact noise [7,8]. The gel is a key source of the contact noise [9]. Wet or gel electrodes lead to detrimental reliability over long period; hence, the current practice is to periodically replace the electrodes, burdening the user and the operator-in-the-loop (e.g., clinician). This is a technological barrier for pervasive patient-centric care and 24/7 health/wellness monitoring at naturalistic environments that require neuro-physiological signal monitoring for prolonged periods [10-12]. Dry electrodes are more suitable for long duration impedimetric sensing without degrading of impedances, however suffer from inferior impedances and noise [3-5, 12]. Conductive polymer, such as polypyrrole (PPY) thin film on copper substrate [13] or planar polydimethylsiloxane (PDMS) [14], are promising dry electrode technologies; however, surface connectivity at the interface is poor. Improved surface connectivity and penetration through hair was achieved with PDMS based flexible pin dry electrode, which has high impedances [15]. Pin structure was also demonstrated using micro-electromechanical systems (MEMS) chips with limited pin height (250 μm) [16]. Spring-loaded mechanical metal pin electrode is another promising dry electrode with low impedance and ability to penetrate through thick layers of hair [17, 18]; however large and uncomfortable for 24/7 usage. Conductive sponge [19] and foam [3] provide comfortable interfaces, but have low electrode conductivities (e.g. more than 10 kΩ below 100 Hz). Inkjet-based dry electrode using silver ink has low electrode impedances [20], but toxicity and surface connectivity issues remain. Finally, non-contact capacitive sensors have drawn significant recent interest [21], but it mandates complex active circuitry for each sensor to deal with changing distance between sensor and scalp due to motion, high interfering noise, and issue related to sensing of potential versus charge. In general, various dry electrodes suffer from one or more unresolved issues such as low contact surface, high contact potential, polarization and high interfacial noises [8,22]. Hence, significant research effort to search for a high performance dry electrode is still ongoing [23].

In this paper, we report a novel dry interfacing electrode based on pattered vertical carbon nanotubes (pvCNT) that has very stable, low electrode impedance. The bristle-like electrode enables contact over rough skin surfaces and is breathable, thus promising high signal qualities for a prolong period of sensing. Preliminary findings were reported elsewhere [24], which is extended and elaborated here. This paper is organized as follows: Section II describes the pvCNT electrode fabrication, Section III outlines the experimental setup, Section IV details the experimental results in the same order, Section V provides some discussion items, and Section VI has concluding remarks.

2. pvCNT Fabrication

Carbon nanotube (CNT) is an extremely high aspect ratio material made of pure carbon atoms that possesses excellent electrical conductivity, thermal conductivity, mechanical strength, and chemical stability - properties that are particularly suitable to develop biosensors [25]. Multi-walled CNT (MWCNT) and some configurations of single-wall CNT (SWCNT), such as armchair configuration, show metal-like electric-conductivity properties [26]. In vitro studies have demonstrated that CNT based biosensors can provide reliable interfacing to neuronal signals [25]. Furthermore, at a low concentration external to the body, CNT based biosensors do not show toxicity [27-29]. Even though attempts were made to develop neurological and physiological electrodes with CNT, previous attempts for direct use of CNT as dry electrode interfaces had only limited success [9,30-32]. We note two prime limitations that might have hampered the potential of CNT electrodes: (1) CNTs were uniformly grown on the substrate without any gap, which led to a dense surface of CNT tips at the top of the electrode, unable to make good contact through skin roughness and pores, and (2) the height of the grown CNTs were small, in the range of tens of µm, which would not cause any significant penetration through the skin ridges. Other techniques that utilized CNT as dry electrodes primarily involve integration of CNT within other polymers or substrates (such as PPY, and PDMS) [33-35] that do not have good electrical conductivity, and suffer from the issues like the top surface of the composite electrode is planar, thus would not make proper contact through the rough skin surface.

The prototyped pvCNT electrode is different than previously developed CNT electrodes in the aspect that the CNTs are grown in custom patterns resulting in bristle-like structure. Furthermore, the growth of CNT is vertically aligned and can be long (e.g., 1.5 mm); that is sufficient to penetrate through pores and ridges of the skin. The electrode fabrication was performed through a commercial CNT fabrication facility (NanoLab, Boston, MA). Briefly, the procedure was as follows. Typical catalyst deposition processing for aligned nanotube growth was used, which includes the deposition of 10 nm of Al2O3, followed by 1-2 nm of iron, both by sputtering processes. For a patterned array, the photoresist is imaged and developed, and both alumina and iron are subsequently deposited through the holes in the mask. After sputtering, the resist is stripped, and the patterned substrates are subjected to thermal growth of carbon nanotubes. Aligned nanotube growth is typically accomplished in several steps: heat-up, anneal, growth, and cool-down. During the heat-up and annealing stage, the catalyst film breaks into islands, which will determine the diameter and site density of the carbon nanotubes that will be nucleated. The substrates are loaded into a 500˚C furnace for rapid annealing and then removed until the system is at the growth temperature, where the substrate is reinserted for CNT growth.

For this study, we have fabricated pvCNT electrodes using MWCNT primarily due to its superior electrical (conductivity) and mechanical (elasticity and tensile strength) properties [9]. The fabricated pvCNT electrode is an ensemble of an array of MWCNT in pillar formation of 100 µm-squared footprints. The square grid formation array of pillars was grown on a circular stainless steel (SS) foil substrate (∅ = 10 mm, 2 mils thick). The pvCNT pillars had heights of 1 to 1.5 mm and were grown vertically. Here, we report results from three spacing between the pillars: 50, 100 and 200 µm. These initial prototypes were fabricated in simple square geometric patterns for proof-of-concept, but the fabrication of other geometric patterns is trivial. Fabrication process and pvCNT samples with different spacing are depicted in Figure 2.1.

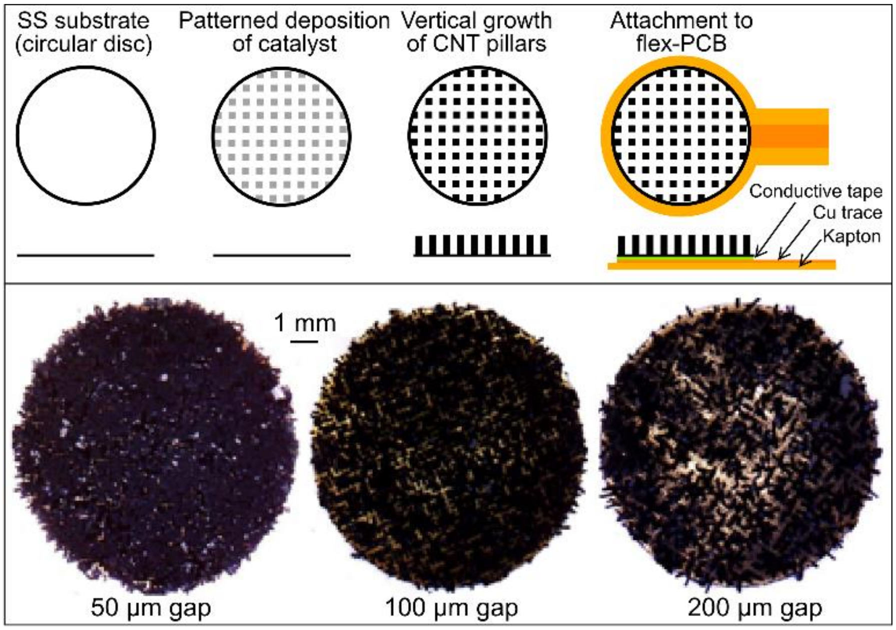

Fig. 2. 1. (Top) Schematic diagram of the pvCNT electrode fabrication process. (Bottom) Photographs of three pvCNT electrodes with various pillar separations (50, 100, and 200 µm).

Optical microscopy and Scanning Electron Microscopy (SEM) images revealed the top of the electrodes have bristle-like arrangements. SEM images were captured at the Integrated Microscopy Center (IMC) of the University of Memphis. In Figure 2.2, a SEM image shows the corner of a pvCNT pillar depicting aligned individual CNT fibers, while an optical microscope image shows the top of the pillar arrangement of a 100 µm spaced pvCNT electrode. Note that even though the pvCNT pillars were patterned in square array formations at the substrate, the top of the pvCNT pillars appear in a non-uniform formation due to natural bending of the pvCNT pillars (height vs width aspect ratio is greater than 10:1), as evident in the SEM and optical images of Figure 2.2.

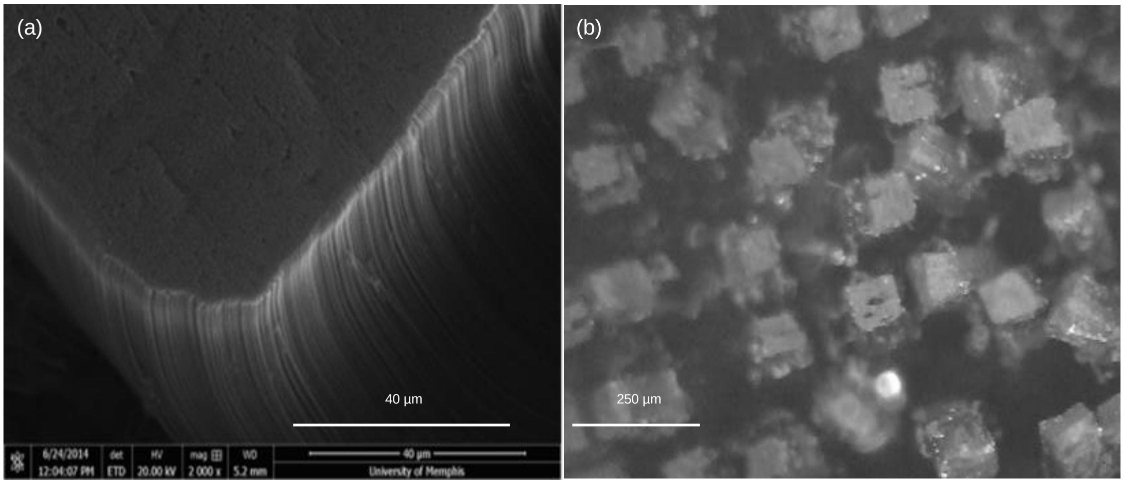

Fig. 2. 2. (a) A SEM image of a pvCNT pillar top corner depicting individual CNT strands aligned vertically. (b) An optical microscope image showing the bristle-like arrangement of the pillars (100 µm spacing).

3. Experimental Setup and Procedure

A. Impedance measurements

The impedance of the prototyped pvCNT electrodes of various spacing and that of some commercial electrodes (GS-26, Bio-Medical Instruments, USA, and Emotiv, San Francisco, CA) were analyzed by Agilent 4294A Precision Impedance Analyzer (Agilent Technologies Inc., Santa Clara, CA, USA) using two fixtures (16451B and 16089B) at room temperature (~23ºC). Prior to each measurement, all fixtures were compensated and calibrated as per manufacturer instruction to ensure accurate measurements. Two software tools, MATLAB (MathWorks, Natick, MA, USA) and Microsoft Excel (Microsoft Corp, Redmond, WA, USA) were utilized to periodically collect data via a GPIB to USB cable and to analyze the collected data from the impedance analyzer.

1) Sensor impedance measurement using a dielectric fixture

Agilent 4294A Impedance Analyzer (IA) with a Dielectric Fixture 16451B was used to measure the impedance of the pvCNT and GS-26 electrodes. The electrodes were positioned between the parallel plates of the fixture. During the pvCNT measurement, it was ensured that the two plates barely contacted the bottom surface, i.e. SS substrate of the pvCNT electrode (Figure 2. 3. a). Measurement of the impedance of pvCNT electrodes was collected using Fixture 16451B with barely touching CNT tips (at single click of the torque knob). The same procedure was applied for the GS-26 electrode measurement. The frequency range of the impedance analyzer was set to scan from 40 Hz to 100 kHz.

2) Interfacial impedance measurement with agar gel

For interfacial impedance measurements, a skin phantom model was built with agar gel. Briefly, the preparation of agar was as follows. First, 4.35 gm of sodium chloride (NaCl) and 15 gm of agar powder (A10752, Alfa Aesar) were added to 500 mL of water. The solution was then boiled at 75ºC for a few hours, then poured into an Al foil wrapped petri dish, and naturally cooled. A flexible PCB (flex-PCB) was designed and prototyped (Cirexx Intl., CA, USA), which allowed pvCNT sensor to be attached at one end and provides low impedance electrical connectivity at the other end. A pvCNT electrode was affixed on the exposed Cu pad ($\varnothing = 10$ mm) of the flex-PCB via a double-sided z-axis conductive tape (Electrically Conductive Adhesive Transfer Tape 9703, 3M Company, MN, USA). The electrode was placed (pvCNT facing down) on top of agar and connected to the impedance analyzer via Agilent Fixture 16089B, while the other terminal of the fixture was connected to the Al foil (Figure 2. 3. b).

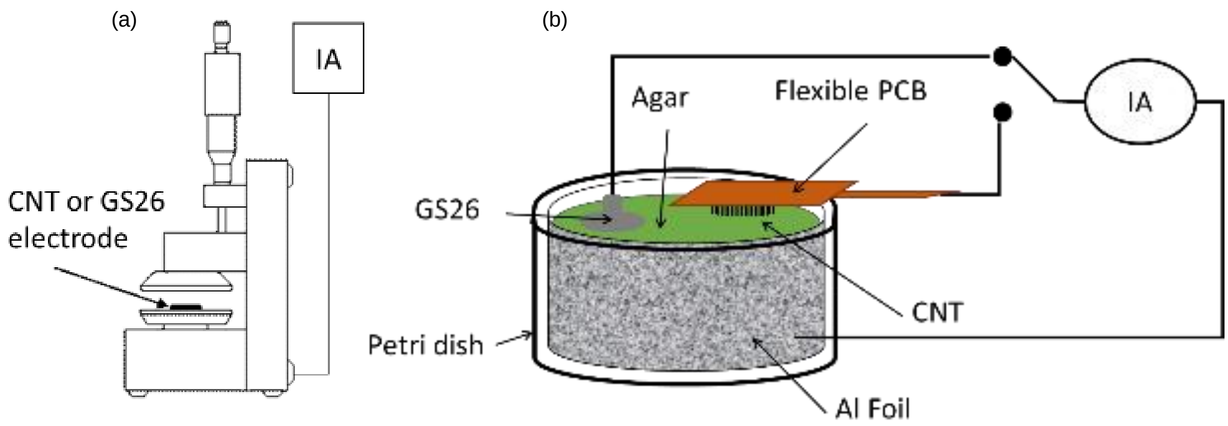

Fig. 2. 3. Impedance measurement setups: (a) Fixture 16451B setup for sensor impedance measurement. (b) Interfacial impedance measurement with agar gel setup. (IA: Impedance Analyzer).

B. Long duration study

One of the significant benefits of dry electrodes is their stable operation over a long duration. For this stability test, we tested impedances of commercial gel and wet electrodes (GS-26 and Emotiv, respectively) in contrast to pvCNT dry electrodes. As electrolyte is used in wet or gel electrodes to reduce skin-electrode interfacial impedance, based on chemical compositions, these interfaces become dry within hours due to evaporation of the electrolyte leading to significant increases or fluctuations of the impedances. In these long duration studies, the pvCNT, GS-26, and Emotiv electrode impedances were monitored over for 24 hours and for 7 days. Fixture 16451B was used in this study and the data acquisition software was programmed to automatically collect impedance data every 1 hour (for 24-hour study) or every 4 hours (for 7-day study).

C. Signal capture in bench test

When the electrodes capture neuro-physiological signals from human body, there are number of factors that affect the measurements. For instance, half-cell potential is usually observed for wet or gel electrode, which arises from the potential differences across the interface between anions and cations. This shows up as a DC offset in ECG, EMG and other bioelectric signal capture electrodes. For dry electrodes, motion artifact and micro-movement are sources of noise in these measurements, which stems from relative movements of the electrodes with respect to the skin surface (micro-movement) producing fluctuations in measurements. We have used agar gel as skin phantom model in a bench-top setup to study quality of the captured signals. The signal was applied to an Al foil at the bottom, while measurements were taken with the sensors (GS-26 and pvCNT electrodes) at the top of the agar.

D. Stimulation study using pvCNT

For stimulation experiments with the electrodes, the same procedure as mentioned in the signal capture section was used, except the signal was applied to the top surface of the agar gel using the pvCNT electrode (stimulated signal), while the signal was recorded from the Al foil (measured signal).

E. Compression and peel tests

Mechanical compression was applied with the test fixture 16451B, where a small pressure can be applied by twisting the torque screw. Scanning electron microscopy (SEM) pictures were taken before and after the experiments. To measure tensile strength of the pvCNT with the substrate, peel tests were conducted by holding the bottom of the sensor to a double sided tape, while a drafting tape was attached to the top surface of the carbon nanotubes and then peeled off at a ~ 45° angle. A mini-digital microscope camera (Vividia 2.0MP Handheld USB Digital Microscope, Oasis Scientific Inc., Taylors, SC, USA) was used to inspect the samples after each peel test.

4. Experimental Results

The experimental results are described in this section in the same order of experimental setup described in the last section.

A. Impedance measurement

1) Sensor Impedance measurement using a dielectric fixture

The results here are presented in terms of the amplitude (|Z|) and the phase angle (θ) of the impedance. Figure 2.4 shows the plot of the absolute impedance (|Z|) for electrodes with 50, 100, and 200 µm gaps between pvCNT pillars. At 40 Hz, the impedance of 50, 100, and 200 µm spacing electrodes were 1.92, 3.11, and 8.15 Ω, respectively. Higher variation of impedance with frequency was observed for larger spacing. For instance, the variation of impedance for 50 µm spacing of electrodes from 40 Hz to 100 kHz is 6 mΩ, whereas for 200 µm spacing, the variation is 243 mΩ. A lower spacing between pillars leads to a higher number of pillars per unit area; therefore, the corresponding impedance is lower. As expected, the pvCNT electrode with the least spacing (50 µm) showed the least impedance (as a higher number of pillars per unit area are conducting in parallel), compared to other samples (where lesser numbers of pillars are conducting per unit area).

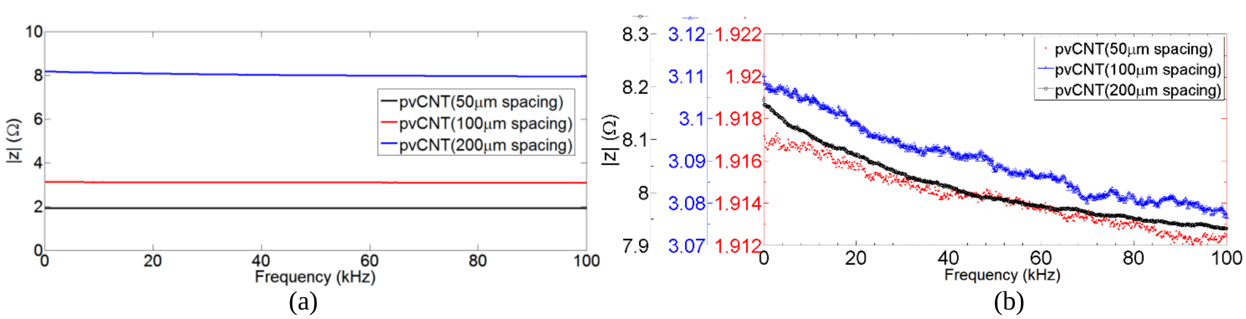

Fig. 2. 4. (a) The amplitude of the impedance of pvCNT electrode with three pillar spacings (50, 100, and 200 µm). (b) The amplitude variations of the impedances are magnified using three separate y-axis markers, which show slight decrease of impedance with higher frequencies.

To measure the impedance of a single pillar (100 µm × 100 µm base area), we have manually plucked all the pillars of an electrode using tweezers except one pillar at the center of the substrate. The resistance of the single pillar is measured to be 7.6 kΩ at 40 Hz. Using this information, resistances for various gaps can be calculated and correlated with the corresponding measured values. For instance, the number of the pillars for 200 µm spacing can be calculated to be 873 pillars using a geometric approximation approach. Hence, the calculated total resistance is 8.82 Ω, as pvCNT pillars are in parallel formation. The computed result closely matches with the experimental measurement of 8.15 Ω (Figure 2.4). The impedance of a single pvCNT pillar on an SS substrate and a table shows the measured and calculated values of pvCNT electrode resistances for various inter-pillar gaps are shown in Figure 2.5.

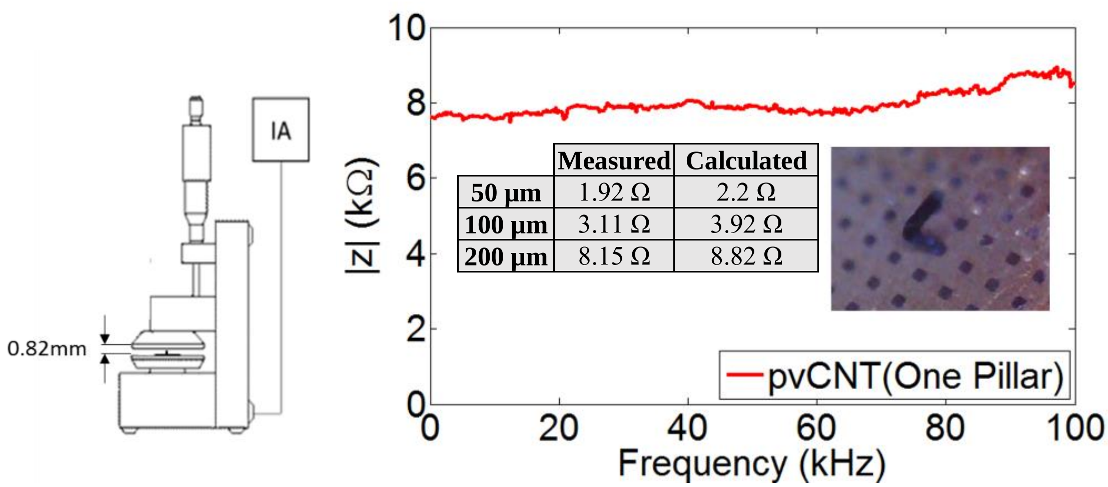

	Measured	Calculated
50 µm	1.92 Ω	2.2 Ω
100 µm	3.11 Ω	3.92 Ω
200 µm	8.15 Ω	8.82 Ω

Fig. 2. 5. The amplitude of the impedance of single pillar of the pvCNT electrode. The table inset shows measured (Meas) and calculated (Calc) resistances for various spacing of pvCNT electrodes.

2) Interfacial impedance measurement with agar gel

As described in the method section, two electrodes were tested in these experiments: a commercial gel type ECG electrode (GS-26), and a pvCNT dry electrode. The pvCNT electrode was mounted on a flex-PCB using z-axis conductive tape as mentioned in the previous section. Figure 2.6 (a-c) presents the photographs of the mounted pvCNT electrode. Figure 2.6 (d-e) shows plots of interfacial impedances (amplitude and phase) of both electrodes with agar gel model of skin (Figure 2.3b).

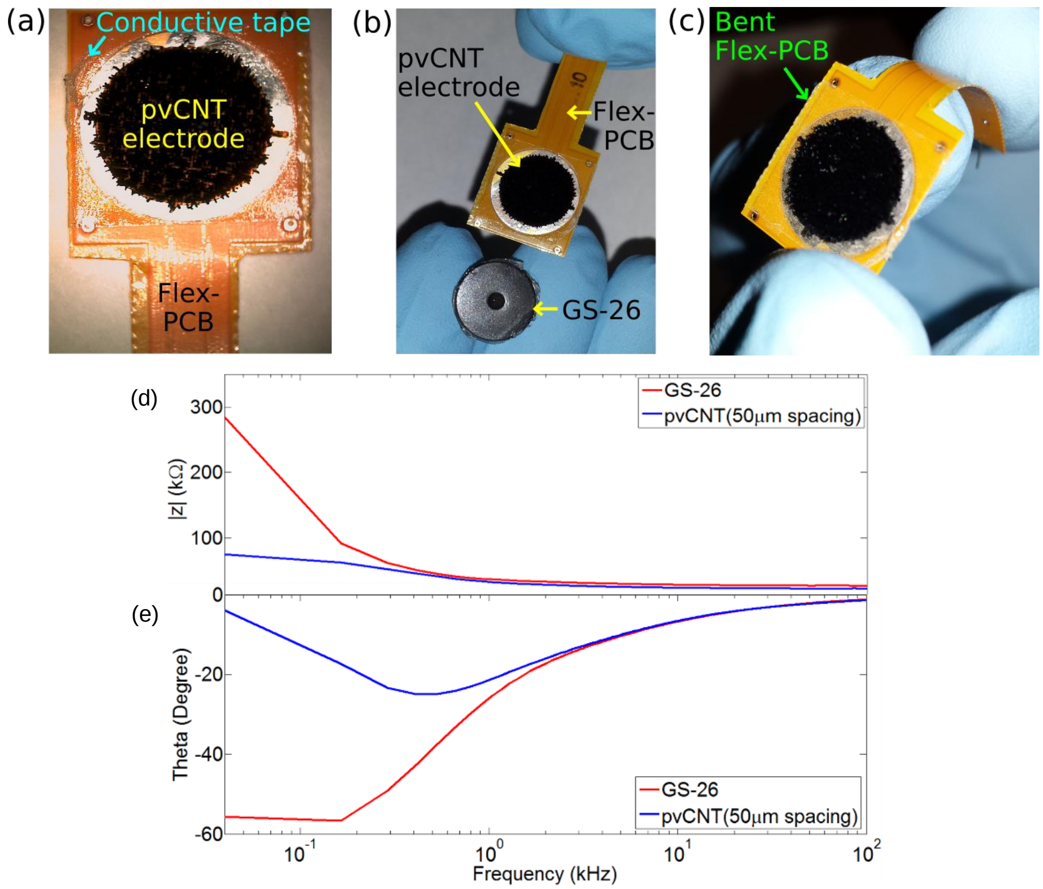

Fig. 2. 6 (a-c) Photographs of the pvCNT electrode on flex-PCB. (d-e) The interfacial impedance (magnitude and phase) with agar gel using two electrodes: gel electrode (GS-26) and prototyped pvCNT electrode.

This interfacial impedance includes a series combination of the impedance of the electrode, the impedance of the agar, the impedance of the Al foil, the electrode-agar contact impedance, and the Al foil-agar contact impedance. The impedance of the pvCNT in range up to 300 Hz is significantly lower than the impedance of the gel electrode, while the phase distortion is superior up to kHz range. Furthermore, the worst-case impedance and phase distortion are equivalent to commercial gel electrode. As the electrode impedance itself is very small (Figure 2.3), it is plausible that at higher frequencies, the agar impedance dominates over the electrode impedance as the electrode-agar interfacial reactance decreases, thus both electrode characteristics show similar performances.

B. Long duration study

In the first experiment of long duration study, the impedance measurements were captured for over 24 hours for pvCNT and GS-26 gel electrodes. The impedance data were recorded for the frequency ranges of 40 Hz to 100 kHz. Figure 2.7 shows the measurements of these electrodes for two frequencies (40 Hz and 10 kHz) for 24 hours. In the case of pvCNT electrodes, the amplitude and the phase of the impedance values change very slightly over the duration (within 1 Ω and 1° variations over 24 hours). In the case of GS-26 gel electrode, the impedance changes more significantly, especially after 8 hours, the average amplitude and phase of the impedance variation were over 10 Ω and 10°, respectively. The frequency response of GS-26 (compared between 40 Hz and 10 kHz) also changes widely, while pvCNT electrodes show very stable behavior on both frequencies. The frequency dependent impedance difference for 40 Hz and 10 kHz are is about 5 mΩ as shown in the insets of the Figure 2.7 (a).

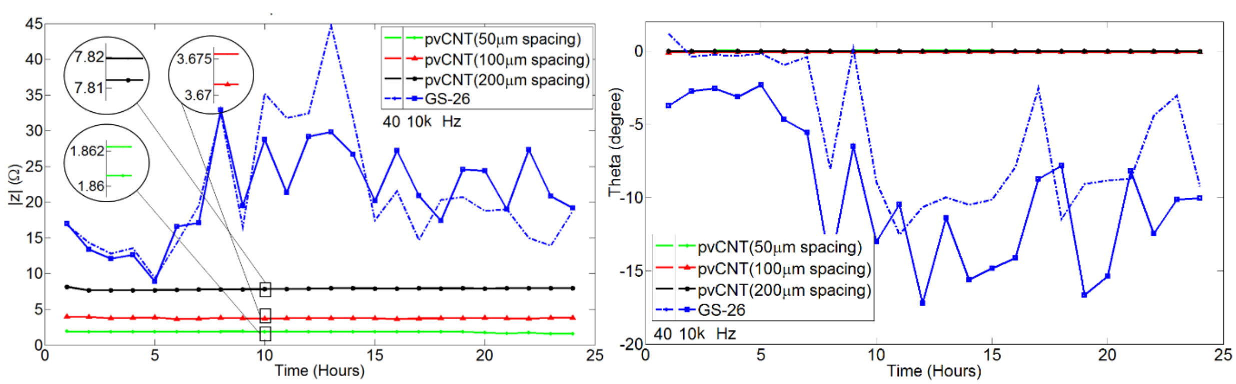

Fig. 2. 7. The amplitude and the phase results from impedance measurement of four electrodes over 24 hours.

The pvCNT electrode was also tested for weeklong experiments to show that the degradation of the impedance is minimal. The software was programmed to collect the data every 4 hours over

11.5 days. Figure 2.8 shows a representative impedance (magnitude and phase) changes over 7 days using an electrode with 50 μm spacing.

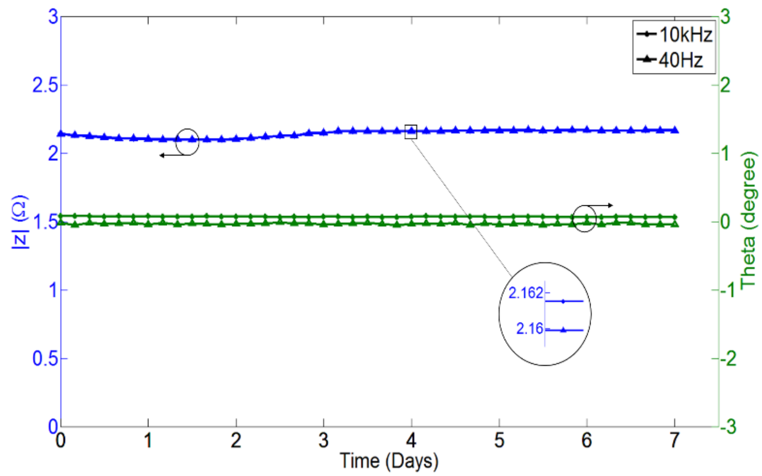

Fig. 2. 8. A long-term study result of the impedance of pvCNT dry electrodes (50 μm spacing) over 7 days.

Another experiment compared a commercial Emotiv wet electrode (Emotiv, San Francisco, CA) in contrast to pvCNT electrodes. Figure 2.9 shows the results of this experiment over a 24-hour duration. As the Emotiv electrode is a wet type, it becomes dry within a few hours. Thus, the amplitude and the phase of the impedance change significantly, and signal capture becomes unreliable. After 24 hours, the amplitude of the impedance of wet electrode has increased by about two orders of magnitude (Figure 2.9), while the pvCNT dry electrode impedance remained very stable for the same period.

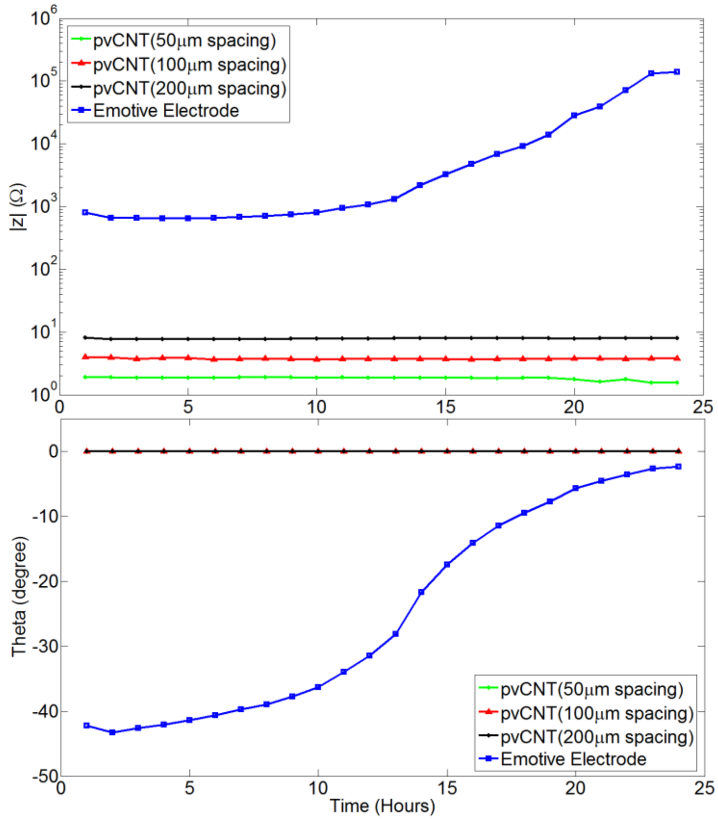

Fig. 2. 9. The impedance of a wet electrode in comparison to the prototyped pvCNT dry electrodes (50, 100 and 200 µm spacing) over 24 hours.

C. Signal Capture in bench test

It is important to determine the half-cell potential for the pvCNT electrode. Experimental results showed that the potential drops of the electrodes interfaced with Al foil are 809.4 mV and 15 mV for GS-26 electrode and pvCNT electrode, respectively. A snapshot of captured signal is shown in Figure 2.10 (a) where the applied signal was sinusoidal of 100 Hz. Figure 2.10 (b) shows the snapshot of a signal captured in bench test with agar using a simulated ECG signal from a function generator applied to the Al foil at the bottom surface of the agar (setup as shown in Figure 2.10). Data captured from the electrodes (GS-26 and pvCNT) shows comparable signal capture capabilities of both electrodes.

(a)

(b)

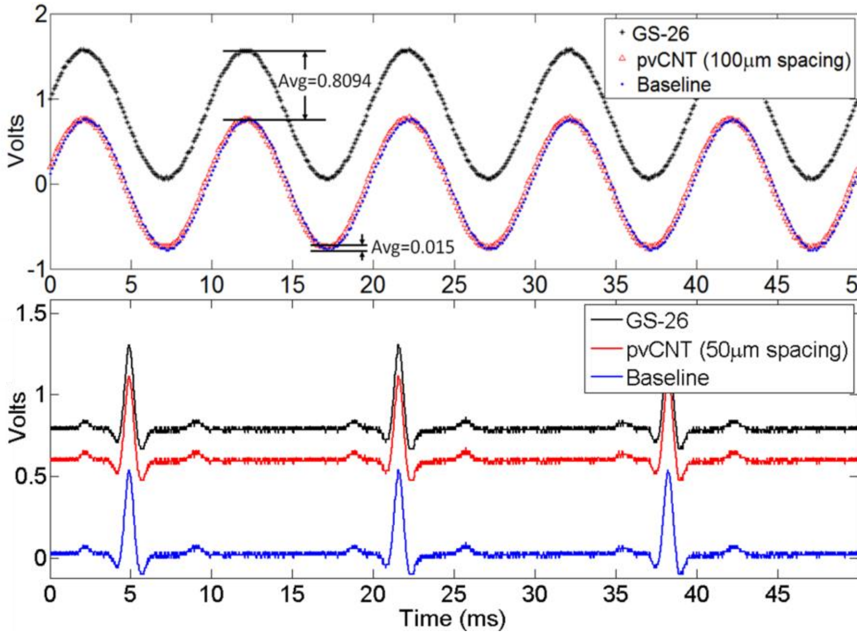

Fig. 2. 10. (a) Signal capture by pvCNT electrode and GS-26 electrode interfaced with an Al foil. (b) Signal capture by pvCNT electrode and GS-26 electrode interfaced with an agar gel phantom model.

D. Stimulation study using pvCNT

A pulse signal is applied to the top of the agar every one-second with 200 ms of duty cycle and pvCNT is used as stimulations electrode for this experiment. The signals were measured from the other side of the agar gel (Al foil). Figure 2.11(a) shows that the phase shift between the stimulated and the measured signal is 0.8 ms, whereas the potential drops on the electrode and agar interface are -592 mV. There was no extra weight or force applied during the experiment and there was an insignificant change of the pvCNT pillars from the stimulation experiments, as shown in Figure 2.11 (b).

(a)

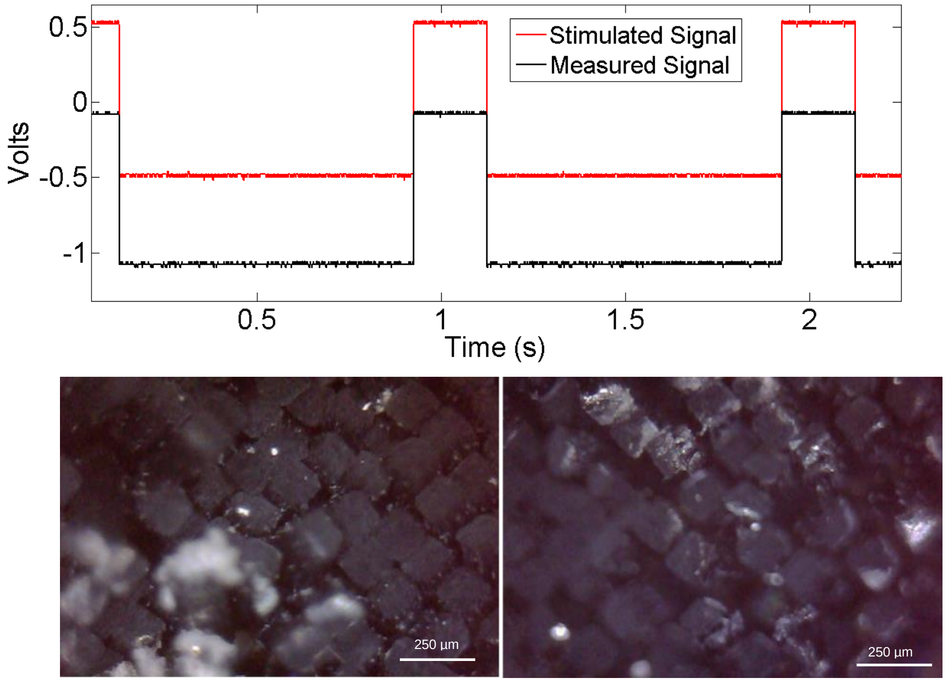

(b)

Fig. 2. 11. (a) Signal stimulated by the pvCNT electrode and measured from the AL foil. (b) The changes of the pvCNT pillars from the stimulation experiments, before (left) and after (right).

E. Compression and peel tests

We have conducted compression and peel tests to test mechanical stability. Some representative results are depicted in Figure 2.12. In Figure 2.12(a), SEM images of the pvCNT electrode are shown after the compression test experiments. It is observed that the pvCNT pillars bend with compression force. High compression force can even cause disintegration of pvCNT pillar formation as evident from Figure 2.12(a). The peel test demonstrated that pvCNT pillars could be dislodged with the drafting tape test as depicted in Figure 2.12(b), showing three successive peel test on a pvCNT electrode.

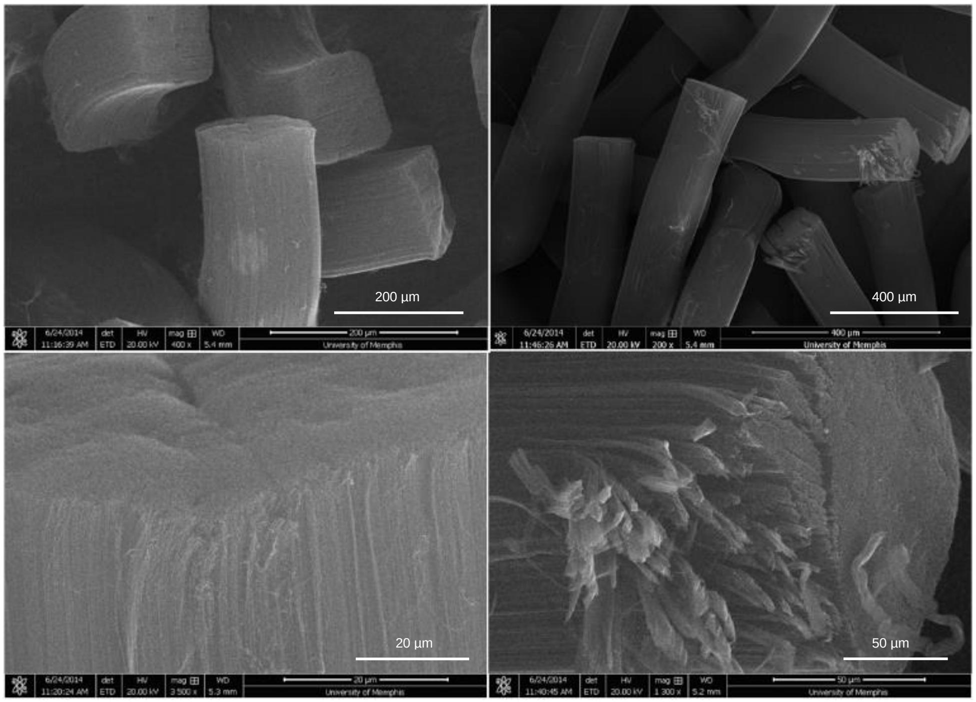

(a)

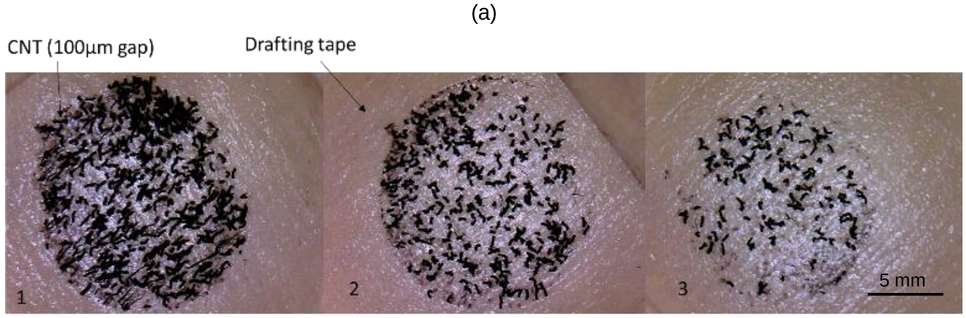

(b)

Fig. 2. 12. (a) SEM images of pvCNT electrodes after the compression experiments. Top: Bending of pvCNT pillar (Left: 100µm spacing, Right: 200µm spacing). Bottom: Breakdown of pvCNT pillar after the compression experiments (Left: Slight peeling effect, Right: Complete break-down). (b) A representative result of peel tests showing peeled pillars on the drafting tape in 3 successive attempts (labeled as 1-3) with a pvCNT electrode (100 µm spacing).

5. Discussions

The impedances of dry polymer foam [44] and printed [22] electrodes were reported to be almost similar to commercial wet electrodes, and that of PDMS-based dry sensor [16] was about one order smaller. In comparison, the pvCNT electrode impedances were measured to be two orders smaller than that of the wet electrodes. The foam electrode was reported to be stable for 5 hours [2], whereas this long duration study showed that pvCNT electrodes had stable impedances for one week. Furthermore, in contrast to the other dry electrodes, due to the structure of pvCNT pillars with spacing that allows airflow, the pvCNT electrode has better breathability. The bristle-like arrangement of the pvCNT electrode will also promote good contact over rough skin surfaces and pores. A small concentration of carbon nanotubes is shown to be not toxic on the epidermal tissue and due to low possibility of skin puncture, the pvCNT electrode can possibly be safer to use.

6. Conclusion

A novel dry pvCNT electrode is demonstrated in this paper for physiological and neurological bioelectric or impedimetric signal capture. The electrodes were fabricated by patterning vertically aligned CNT pillars on a circular disk (Ø = 10 mm) of SS foil. The characteristics of pvCNT were assessed against a commercial gel electrode (GS-26) and a wet electrode (Emotiv). The pvCNT has shown stable impedance over short and long durations. The impedances of pvCNT electrodes were found to be a function of the pillar spacing. The pvCNT electrodes also showed a lower electrical impedance and comparable signal capture in bench test with simulated signals. Results show that pvCNT dry electrode can be a very suitable for long duration neuro-physiological signal collection. The pvCNT electrode was also tested for stimulation. This study demonstrates the pvCNT electrode as a promising technology for dry electrode for impedimetric sensing and stimulation over long durations.

7. References

[1] S. Grimnes, and O.G. Martinsen, “Bioimpedance & bioelectricity basics”, Academic Press: Bodmin, Cornwall, UK, 2000.
[2] R. Plonsey, and R.C. Barr, “Bioelectricity: a quantitative approach”, 3rd ed., Springer: New York, NY, USA, 2007.

[3] C. Lin, L. Liao, Y. Liu, I. Wang, B. Lin, J. Chang, "Novel dry polymer foam electrodes for long-term EEG measurement", *IEEE Trans. Biomed. Eng.*, vol. 58, no. 5, pp. 1200-1207, 2011.

[4] A. Searle and L. Kirkup, "A direct comparison of wet, dry and insulating bioelectric recording electrodes," *Physiol. Meas.*, vol. 21, pp. 271–283, 2000.

[5] Y. M. Chi, T. Jung, G. Cauwenberghs, "Dry-contact and noncontact biopotential electrodes: methodological review", *IEEE Reviews in Biomedical Engineering*, vol. 3, pp. 106-119, 2010.

[6] C. Gurger, G. Krausz, B.Z. Allison, and G. Edlinger, "Comparison of dry and gel based electrodes for P300 brain-computer interfaces", *Front Neurosci.*, vol. 6, no. 60, pp. 1-7, 2012.

[7] E. Huigen, A. Peper, and C. A. Grimbergen, "Investigation into the origin of the noise of surface electrodes," *Medical & Biological Engineering & Computing*, vol. 40, pp. 332-338, 2002.

[8] J.G. Webster, Medical Instrumentation, J. Wiley & Sons, 1998.

[9] G. Ruffini, S. Dunne, E. Farres, J. Marco-Pallares, C. Ray, E. Mendoza, R. Silva, and C. Grau, "A dry electrophysiology electrode using CNT arrays", *Sensors and Actuators A*, vol. 132, no. 1, pp. 34-41, 2006.

[10] S. Patel, H. Park, P. Bonato, L. Chan, M. Rodgers, "A review of wearable sensors and systems with application in rehabitation", *J. NeuroEngineering and Rehabilitation*, vol. 9, no. 21, 17 p., 2012.

[11] H. Alemdar, C. Ersoy, "Wireless sensor networks for healthcare: a survey", *Computer Networks*, vol. 54, pp. 2688-2710, 2010.

[12] B. He, T. Coleman, G. M. Genin, X. Hu, N. Johnson, T. Liu, S. Makeig, P. Sajda, and K. Ye, "Grand challenges in mapping the human brain: NSF workshop report", *IEEE Trans Biomed Eng*, vol. 60, no. 11, pp. 2983-2992, 2013.

[13] S. Jamadade, S. Jadhav, V. Puri, "Electromagnetic properties of polypyrrole thin film on copper substrate", Physics Res, vol. 1, no. 4, pp. 205-210, 2010.

[14] J. Baek, J. An, J. Choi, K. Park, and S. Lee, "Flexible polymeric dry electrode for long-term monitoring of ECG", Sensors and Actuators A, vol. 143, pp. 423-429, 2008.

[15] L. Wang, J. Liu, B. Yang, C. Yang, "PDMS based low cost flexible dry electrode for long-term EEG measurement", *IEEE Sensors J.*, vol. 12, no. 9, pp. 2898-2904, 2012.

[16] J. Chiou, et al. "Using novel MEMS EEG sensors in detecting drowsiness application", IEEE Biomedical Circuits and Systems Conf., London, pp. 33-36, 2006.

[17] R. Matthews, P.J. Turner, N. J. McDonald, K. Ermolaev, T. Mc Manus, R. A. Shelby, M. Steindorf, "Real time workload classification from an ambulatory wireless EEG system using hybrid EEG electrodes", IEEE Eng. Med. Biol. Soc. Conf., pp. 5871-5, 2008.

[18] C. Grozea, C. D. Voinescu, S. Fazli, "Bristle-sensors – Low-cost flexible passive dry EEG electrodes for neurofeedback and BCI applications", *J. Neural Eng.*, vol. 8, pp. 025008 (14 pages), 2011.

[19] A. Gruetzmann, S. Hansen, J. Muller, "Novel dry electrodes for ECG monitoring", *Physiol. Meas.*, vol. 28, pp. 1375-1390, 2007.

[20] L. Xie, Y. Geng, M. Mäntysalo, L.-L. Xu, F. Jonsson and L.-R. Zheng, Heterogeneous Integration of Bio-Sensing System-on-Chip and Printed electronics, *IEEE Journal of Emerging and Selected Topics and Systems*, vol. 2, no. 4, pp. 672-682, 2012.

[21] T. J. Sullivan, S. R. Deiss, G. Cauwenberghs, T. Jung, “A low-noise, low-power EEG acquisition node for scalable brain-machine interfaces”, *SPIE Bioengineering and Bioinspired Systems III*, vol 6592, p. 659203 (8 pages), 2007.

[22] C. Gondran, E. Siebert, P. Fabry, E. Novakov, and P. Y. Gumery, “Non-polarisable dry electrode based on NASICON ceramic”, *Medical & Biological Engineering & Computing*, vol. 33, pp. 452-457, 1995.

[23] S. Ha, C. Kim, Y. M. Chi, A. Akinin, C. Maier, A. Ueno, G. Cauwenberghs, “Integrated circuits and electrode interfaces for noninvasive physiological monitoring”, *IEEE Trans. Biomed. Eng.*, vol. 61, no. 5, pp. 1522-1537, 2014.

[24] M. Abu-Saude, S. Consul-Pacareu, and B. I. Morshed, “Feasibility of Patterned Vertical CNT for Dry Electrode Sensing of Physiological Parameters”, IEEE Radio Wireless Conference (BioWireleSS), (in press), Jan. 2015.

[25] Y. Zhang, Y. Bai, B. Yan, “Functionalized carbon nanotubes for potential medicinal applications”, *Drug Discovery Today*, vol. 15, no. 11/12, pp. 428-435, 2010.

[26] C. T. White, T. N. Todorov, “Carbon nanotubes as long ballistic conductors”, Nature, vol. 393, pp. 240-243, 1998.

[27] L. Bareket-Keren, Y. Hanein, “Carbon nanotube-based multi electrode arrays for neuronal interfacing: progress and prospects”, Frontiers in Neural Circuits, vol. 6, article. 122, pp. 1-16, 2013.

[28] S.K. Smart, A.I. Cassady, G.Q. Lu, D.J. Martin, “The biocompatibility of carbon nanotubes”, *Carbon*, vol. 44, pp. 1034-1047, 2006.

[29] J. Chlopek, B. Czajkowska, B. Szaraniec, E. Frackowiak, K. Szostak, F. Beduin, “In vitro studies of carbon nanotubes biocompatibility”, *Carbon*, vol. 44, pp. 1106-1111, 2006.

[30] G. Ruffini, S. Dunne, E. Farres, P.C.P. Watts, E. Mendoza, S. R. P. Silva, C. Grau, J. Marcho-Pallares, L. Fuentemilla, B. Vandecasteele, “ENOBIO – First tests of a dry electrophysiology electrode using carbon nanotubes”, Proc IEEE EMBS Int. Conf, NY, pp. 1826-1829, 2006.

[31] G. Ruffini, S. Dunne, L. Fuentemilla, C. Grau, E. Farres, J. Marco-Pallares, P.C.P. Watts, S.R.P. Silva, “First human trials of a dry electrophysiology sensor using a carbon nanotube array interface”, *Sensors and Actuators A*, vol. 144, pp. 275-279, 2008.

[32] J. K. Radhakrishana, H. Bhusan, P.S. Pandian, K. U. B. Rao, V. C. Padaki, K. Aatre, J. Xie, J.K. Abraham, V. K. Varadan, “Growth of CNT array, for physiological monitoring applications”, *Proc. SPIE*, vol. 6931, pp. 69310P1-5, 2008.

[33] H. B. Baskey, “Development of carbon nanotube based sensor for wireless monitoring of electroencephalogram”, *DRDO Science Spectrum*, pp. 161-163, 2009.

[34] H. Jung, J. Moon, D. Baek, J. Lee, Y. Choi, J. Hong, S. Lee, “CNT/PDMS composite flexible dry electrodes for long-term ECG monitoring”, *IEEE Trans Biomed. Eng.*, vol. 59, no. 5, pp. 1472-1479, 2012.

[35] P. S. Kumar, P. Rai, S. Oh, H. Kwon, V. K. Varadan, “Flexible capacitive electrodes using carbon nanotube and acrylic polymer nanocomposites for healthcare textiles”, *Smart Nanosystems in Eng. Med.*, vol. 2, no. 1, pp. 18-24, 2012.

Chapter 3: Characterization of a Novel Polypyrrole (PPy) Conductive Polymer Coated Patterned Vertical CNT (pvCNT) Dry ECG Electrode

1. Introduction

Physiological signals, e.g., electrocardiogram (ECG/EKG), electroencephalogram (EEG), electromyogram (EMG), and galvanic skin response (GSR), play a vital role in health monitoring and clinical diagnoses, as well as non-clinical applications, such as neurofeedback and brain–computer interface (BCI) [1–4]. Impedimetric electrodes are required to collect these body signals. Conventional wet electrodes, such as Ag/AgCl electrodes, use a saline- or gel-based electrolyte to decrease the contact impedance and artifacts due to motion and to increase the dielectric constant between the skin surface and the electrode [5]. The gel reduces the resistance between the surface of the metal part of the electrode and the skin below the stratum corneum (SC) layer. These sensors only operate well for a short duration because of gradual degradation of conductivity as the electrode interface impedance deteriorates over time, due to evaporation, leading to a degradation in signal quality [6–12]. Wet or gel electrode applications also require inconvenient skin preparation whereby an expert is typically required to remove dirt, skin debris, and oil from the skin surface. Furthermore, the gel has been observed to be a source of the contact noise [12] and could potentially cause an allergic reaction in the patient. Wet or gel electrodes lead to detrimental reliability over a long period; hence, the current practice is to periodically replace the electrodes, burdening the user and the operator-in-the-loop (e.g., clinician). These technological barriers pose problems for continuous health and wellness monitoring that require neuro-physiological signal monitoring for prolonged periods [5, 13, 14]. Furthermore, the half-cell noise appears at the interface between the gel and the electrode due to diffusion of the gel into the top layer of the skin [12]. The wet and gel Ag/AgCl electrodes are widely used for clinical and research purposes. However, wet electrodes dry within a few hours while gel electrodes only work up to 10 h. Hence, these electrodes are not suitable for long durations and continuous monitoring. These drawbacks have motivated researchers to develop alternatives, such as dry impedimetric electrodes.

Dry electrodes are designed to operate and record biopotential signals without explicit conductive gel and skin preparation and allow for long duration impedimetric sensing without degradation of impedances. However, this method suffers from high interfacing impedances, interfacial potential, contact surface, and noise [6–8]. Planar flexible dry electrodes have been developed for long-term ECG monitoring by depositing gold on polydimethylsiloxane (PDMS) films using plasma treatment [15, 16] or using polypyrrole (PPy) thin film on a copper substrate [17], however these suffer poor skin-contact electrical connectivity. Microneedle dry electrodes fabricated using the process of the microelectromechanical system (MEMS) [18] have recently generated significant interest for use in long-term biopotential signal recording. Silicon microneedle-based dry electrodes for biopotential monitoring are made by etching the wafer and depositing metal in both sides in an array pattern [19]. Flexible microneedle-based electrodes were developed using PDMS with different pins, which pass through hair, but suffer from high contact impedance [16]. Fixable metal-coated polymer bristle-sensors are another promising type of dry electrode that is able to penetrate through a thick layer of hair and has low impedance; however, they are large and uncomfortable for long-term usage [20]. Some dry electrodes that have comfortable interfaces such as conductive sponge [21], ceramic [22], and foam [6] suffer from a high impedance (~10 kΩ) at low frequencies (~100 Hz). Silver ink used in Inkjet-based dry electrodes shows low impedances but the surface connectivity issues remain [23]. Non-contact electrodes are very sensitive to any motion of the electrode with respect to the body as the capacitance dramatically changes by a factor of 10 when the electrode moves 100 μm vertically [24,25]. Textile electrodes were developed by coating cotton woven fabrics with polypyrrole [26] and synthesizing conductive fabrics with graphene cladding [27] which resulted in a good quality ECG signal. There is significant ongoing research looking into developing a high-performance dry electrode [28,29].

Carbon nanotubes (CNTs) are a new technology that has been utilized to develop some biosensors. Multiwall CNTs (MWCNTs) are highly conductive and therefore practically suitable for developing biopotential electrodes [30,31]. Purified CNTs are stable over a long period of time [32]. Some studies have shown that, at low concentration, CNTs have relatively low toxicity [33–35]. CNT-based electrodes display unique properties that provide reliable interfacing to biopotential signals and are desirable due to their ability to penetrate biological membranes [36,38]. Carbon nanotube (CNT)/polydimethylsiloxane (PDMS) or polypyrrole (PPy) composite-based dry ECG electrodes showed long-term wearable monitoring capability and robustness to motion and sweat. However, these electrodes suffered from poor electrical conductivity for the planar top surface, which would not make proper contact with areas of rough skin. Using CNT as an array/forest on the surface of the electrode improved electrical contact by allowing penetration of the outer layers of the skin (stratum corneum). However, they are limited as they cannot form good contacts through skin pores and hairs as CNTs are uniformly grown on the substrate without any gaps [38–40].

We have developed a dry electrode using pvCNT that has lower contact impedance than conventional wet electrodes [41–43]. This electrode is suitable for physiological and neurological signal acquisition with reduced noise. However, in our previously reported development, we noticed that the CNT is weakly attached with mechanically unstable adherence to the stainless steel (SS) substrate of the electrode. Here, we propose a new method to resolve this issue of the pvCNT by applying a conductive polymer, polypyrrole (PPy), to improve mechanical adherence strength while maintaining conductivity. PPy polymer was used in this work for its easy preparation process, environmental safety, and high electrical conductivity.

In this paper, we report a novel dry electrode of Patterned Vertically-aligned Carbon NanoTubes (pvCNT) coated with a conductive polymer (Polypyrrole, PPy) that increases the adherence of CNT pillars to the stainless-steel substrate. The paper demonstrates the improved electrode performance, after coating, with regard to capturing ECG signals in contrast to non-coated and commercial electrodes. The paper also presents a characterization of the coated pvCNT electrode using evaluation metrics such as electrical contact-skin impedance, long-term impedance stability, and ECG signal capture. This paper extends our preliminary findings [43] with detailed characterization and elaboration.

2. pvCNT Electrode Fabrication and Coating

A. pvCNT Fabrication

We have shown in previous work that the prototyped electrodes are developed such that the CNTs are grown in an aligned vertical pattern resulting in a bristle-like structure [41,42]. The pillar heights (~1.5 mm) are sufficient to measure the signal through hairy and rough areas of the skin. For this pvCNT electrode, we have used MWCNTs due to their electrical conductivity and mechanical properties [31]. The pvCNT was fabricated by a commercial CNT fabrication facility (NanoLab, Boston, MA, USA) as follows: Catalytic Chemical Vapor Deposition (C-CVD) technique was used for aligned CNT growth by depositing 10 nm of Al2O3, followed by 1–2 nm of iron using a sputtering process through holes of a mask that was developed and imaged using photoresist to form the patterned array. After stripping the resist, the nanotubes were grown on the patterned substrate using the thermal growth process in several steps: heating, annealing, growth, and cooling down. The catalyst film breaks into islands during the heating and annealing steps, and the diameter and the density of the carbon nanotubes will be defined. The substrate was quickly annealed at 500 °C, cooled down to the growth temperature, and then the substrate was loaded for CNT growth. The average outer diameters of the MWCNT strands were 30 ± 15 nm. The array of pvCNT pillars were grown on a circular stainless-steel substrate with a diameter of 10 mm and thickness of 50 µm. Each pillar had a square base of 100 µm on each side.

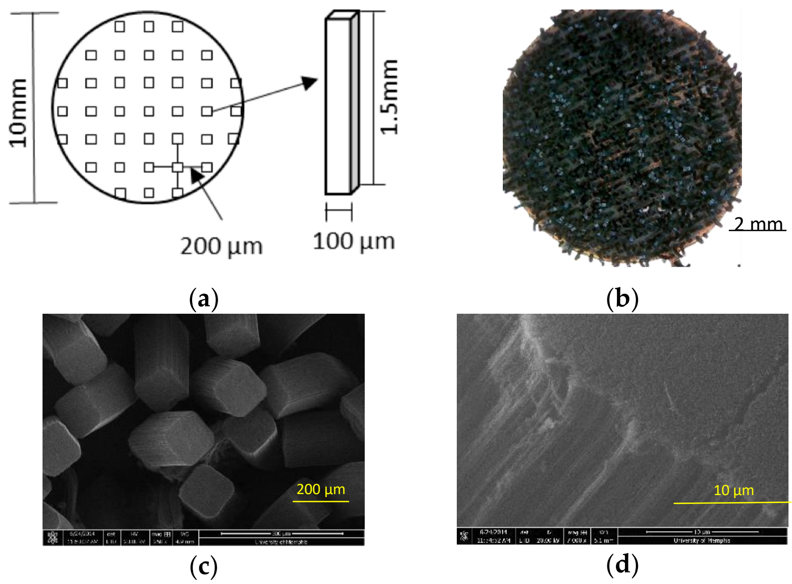

Fig. 3. 1. Schematic design of the pillar and the pattern of patterned vertically-aligned Carbon NanoTubes (pvCNT) growth on stainless steel substrate. (b) Optical microscope image of a pvCNT electrode (200 µm spacing). (c) Scanning electron microscope (SEM) image (top view) of a pvCNT electrode (200 µm spacing) showing the pillars formed with vertically aligned CNT fibers. (d) SEM image of the top corner of a pillar.

The spacing between the pillars was 200 µm in all directions. Other spacings (50 and 100 µm) have been studied and tested in previous work but will not be investigated and tested here as they would expected to perform similarly. The schematic design, photograph and scanning electron microscopy (SEM) images of the pvCNTs, are depicted in Figure 3.1. Note that the top view of the pillars shows that the pillars slightly twist and bend over the height (~1 mm) which is expected for this extreme height of CNT fibers. Figure 3.1d shows the pillar top corner consisting of many CNT strands grouped tightly and vertically. SEM images of the pvCNT electrode were captured at the Integrated Microscopy Center (IMC), The University of Memphis (Memphis, TN, USA).

B. PPy Coating Procedure

Coating is the second step of sensor fabrication, as we proved before, and the strength of adhesiveness of the pvCNT pillars can be improved using a conductive polymer, polypyrrole (PPy). PPy can be changed from an electrical isolator to a good conductor using electrochemical procedures [19]. A liquid PPy from Sigma Aldrich (product number 482552) was used in this experiment. Many researchers have used PPy for coating biosensors [5]. We have used pvCNT electrodes with 200 µm spacing for this study. The pvCNT was prepared by applying 10 µL of 70% ethyl alcohol in order to decrease the surface tension of the CNT. Then, 10 µL of the PPy was added to the electrode and left until the entire substrate was covered. The prepared electrode was then dried using a preheated gun at 300 °C at distance of 10 cm for 30–60 s. Figure 3.2 shows the pvCNT electrode before (left) and after (right) the coating procedure. As evidenced in this figure, the size of the pvCNT pillars shrinks after the coating due to the high surface tension and viscosity of the PPy.

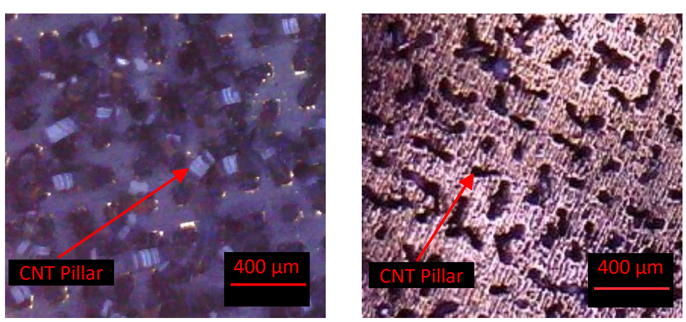

(**a**) (**b**)

Fig. 3. 2. Images of pvCNT electrode without and with polypyrrole (PPy) coating. (a) Prior to PPy coating. (b) After PPy coating.

3. Experimental Method and Setup

A. PPy-coated pvCNT Electrode Conductivity Measurement

The conductivity of the electrode was analyzed by measuring its surface impedance. An Agilent 4294A Precision Impedance analyzer (Agilent Technologies Inc., Santa Clara, CA, USA) was used to analyze the impedance of coated and non-coated pvCNT electrodes using Dielectric Fixture 16451B at room temperature (~23 °C). The measurement data over time was automatically recorded using a Visual Basic script and analyzed using Microsoft Excel (Microsoft Corp, Redmond, WA, USA) and MATLAB (MathWorks, Natick, MA, USA). Measurement of the impedance of the pvCNT electrode was collected using Agilent Fixture 16451B ensuring the two plates were barely in contact with the substrate and the CNTs tips (stopping at a single click of the torque knob).

1) Impedance Measurmnet befor and after Coating

Dielectric Fixture 16451B was attached to the Agilent Impedance Analyzer (IA) and used to measure the impedance of the coated and non-coated pvCNT electrodes. To ensure accurate measurements, the fixture was compensated and calibrated as per the manufacturer's instructions. All measurements were recorded at a frequency range of 40 Hz to 100 kHz.

2) Long-Term Impedance Measurement

In previous work, we showed that the impedance of pvCNT was stable over a long period of time. In this experiment, the coated and non-coated pvCNT impedances were monitored for 24 h. The data was automatically collected and transferred to the PC every hour. Figure 3.3a shows the impedance measurement equipment used.

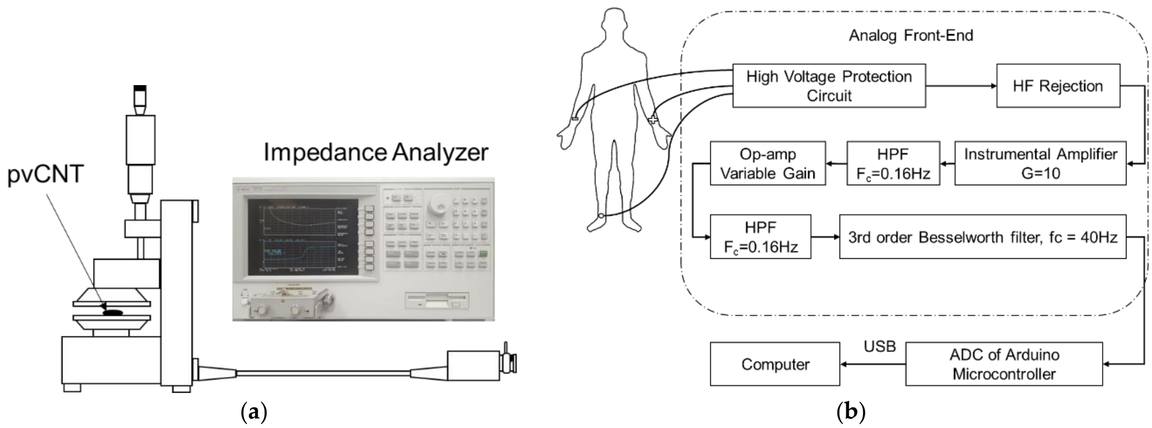

Fig. 3. 3. (a) Impedance measurement setup using Fixture 16451B attached to the Agilent 4294A Impedance Analyzer. (b) The block diagram of the AFE of the OLIMEX shield that are connected to the Arduino board and then to the computer through a USB cable.

B. In Vitro Signal Capture

Half-cell potential is one factor that affects the bio-signal quality as the half-cell potential appears at the interface of the electrode due to gel diffusion and shows up as a direct current (DC) offset. We have shown that the half-cell potential for the pvCNT electrode interfaced with Al foils is very small (~15 mV). Similar experiments were conducted to measure the half-cell potential of the coated pvCNT where a signal from a function generator was applied to the Al foil, captured using the coated pvCNT and then compared to the previous results for non-coated pvCNT and the commercial GS-26.

C. Peel-Off Tests

The peel test was conducted to measure the adhesion and tensile strength of the pvCNT pillar with the substrate. Drafting tape was attached to the top surface of the pvCNT and then peeled off slowly at a ~45° angle while the substrate was held and fixed with double-sided tape. A mini-digital microscope camera (Vividia 2.0MP Handheld USB Digital Microscope, Oasis Scientific Inc., Taylors, SC, USA) was used to inspect the samples before and after each test.

D. In Vivo ECG Signal Capture

The performance of the pvCNT electrode was investigated by recording ECG signals and comparing the quality of the signal measured to signals from traditional wet electrodes Ag/AgCl. An open source commercial hardware EKG/EMG shield (OLIMEX Ltd., Plovdiv, Bulgaria) was used to capture ECG signals. The shield EKG/EMG converts the analog differential signal attached to CH1_IN+/CH1_IN− inputs into a single stream of data as output. The output signal is discretized via dedicated ADC embedded in the MCU onboard attached to the shield. The analog front end of the shield contains multiple stages as follows: a high voltage protection circuit, high frequency and noise rejection, an instrumental amplifier with a gain of 10, a high pass filter with a cutoff frequency of 0.16 Hz, an operational amplifier with variable gain (a gain of 80 was used), another high pass filter at same cutoff frequency, and a third order Besselworth filter with a cutoff frequency at 40 Hz and a gain of 3.56. The total applied gain was around 2848. Figure 3.3b shows the block diagram of the shield. The output signal was attached to the Arduino LEONARDO (Arduino LLC) board and digitized using 10-bit ADC with a sampling rate of 256 Hz then transferred to a computer using micro-USB for further digital processing. A Tektronix oscilloscope was used to monitor and visualize the ECG signal before recording.

The pvCNT electrode was attached to a flexible PCB (flex-PCB) on an exposed Cu pad with a diameter of 10 mm, to provide a low impedance, using double sided z-axis conductive tape (Electrically Conductive Adhesive Transfer Tape 9703, 3M Company, St. Paul, MN, USA). The flex-PCB was designed and prototyped at Cirexx Intl., CA, USA. Three electrodes were placed on the human body at three positions: the left forearm, right forearm, and right leg. All of the measurements of the ECG signals were conducted at room temperature with no skin preparation. The ECG data was collected and recorded using the serial port and analyzed using MATLAB.

Figure 3.4a shows the setup of the pvCNT and the placement of the electrode on the left arm using a rubber band to ensure excellent skin-electrode contact during any body motions. Figure 3.4b shows the OLIMEX EKG/EMG shield attached to Arduino board. This study used the approved Institutional Review Board (IRB) protocol number 4212 (University of Memphis).

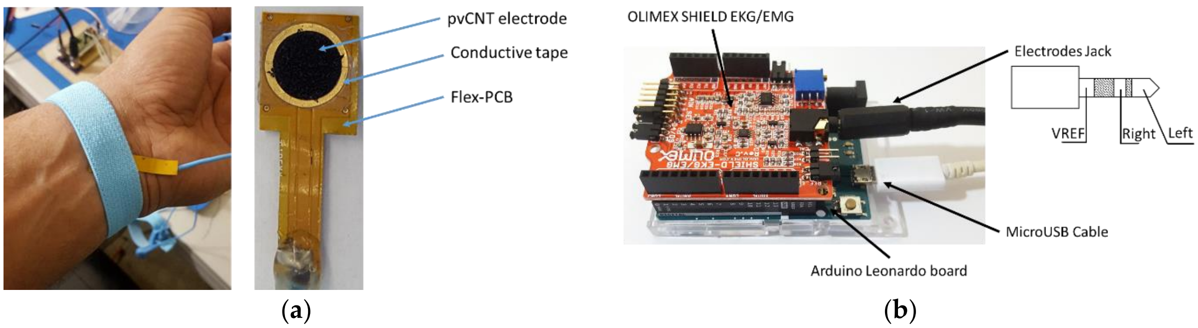

Fig. 3. 4. In vivo electrocardiogram (ECG) signal capture setup. (a) The pvCNT setup attached to the left arm. (b) The SHIELD_EKG_EMG attached with the Arduino Leonardo board.

4. Experimental Results

A. PPy-Coated pvCNT Electrode Conductivity Measurement Results

This section provides a summary of the data captured using the methods described above. All the impedance values in this paper are represented in terms of the amplitude and the phase angle.

1) Impedance Measurmnet Results befor and after Coating

Figure 3.5 shows the short-term impedance where the left shows the magnitude impedance (|Z|) for pvCNT with 200 µm spacing with and without PPy coating, and the right plot shows the phase angle of the impedance for the same electrodes. As expected, the impedance of the PPy-coated pvCNT increased by the impedance of the PPy film. For instance, the impedance of non-coated and PPy-coated pvCNT was 8.15 and 19.4 Ω, respectively, at 40 Hz. However, this higher impedance is well below gel electrode impedance and suitable for low noise impedimetric signal sensing. The phase shift of the coated pvCNT was also increased in the negative direction, possibly due to extra capacitance from to PPy coating.

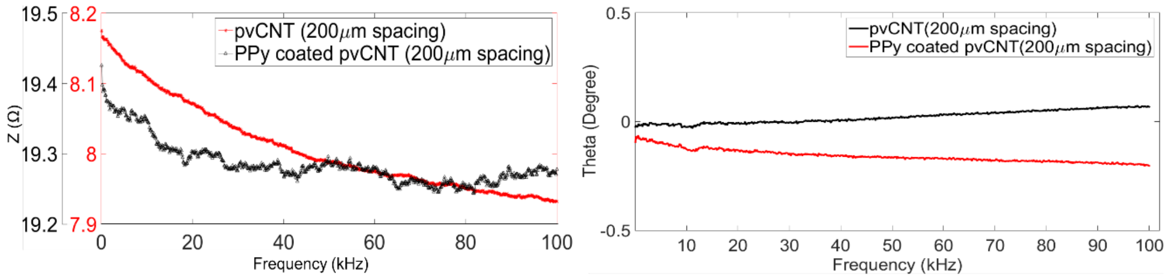

(a) (b)

Fig. 3. 5. The amplitude (a) and phase (b) of the impedance for non-coated and PPy-coated pvCNT electrodes.

The impedance of the coated and non-coated electrodes was observed at different frequencies. Particularly, the variation of the amplitude of the impedance for a non-coated electrode from 40 Hz to 100 kHz was 0.24 Ω, whereas for the coated electrode, the variation was around 0.1 Ω. While the variation of the phase for the non-coated and coated electrodes was less than 0.5°.

2) Long-Term Impedance Measurement Results

The impedance data was captured for frequencies from 40 Hz to 100 kHz. The measurements for the coated pvCNT at two different frequencies (40 Hz and 10 kHz) are shown in Figure 3.6. The results show that the amplitude and phase of the impedance of the coated electrode change very slightly within a range of 5 Ω and 1°, respectively, over 24 h. The amplitude impedance of the coated pvCNT was increased due to the PPy added to the electrode where the average impedance was around 20 Ω.

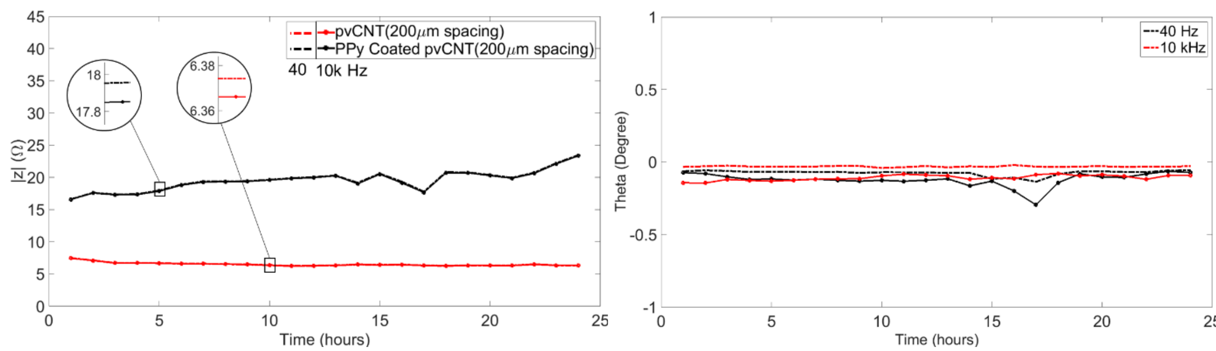

(a) (b)

Fig. 3. 6. The amplitude (a) and phase (b) of the impedance of non-coated pvCNT electrode and PPy-coated pvCNT electrode for a long duration of 24 h.

It is noted that the impedance of PPy-coated pvCNT is higher than the non-coated version for all frequencies and might fluctuate over time. This is due to the extra impedance of the PPy (polymer) that is added to the impedance of the CNT pillars [17]. PPy impedance is also dependent on the environment (humidity, temperature, etc.). The coated electrode resistance is a combination of the resistance of the non-coated electrode and the resistance of PPy layer. Hence, depositing a thin film is important to reduce change of resistance. In our experiments, the typical change in resistance was only 5 Ω.

B. In Vitro Signal Capture Results

Experimental results show that the half-cell potential of the coated pvCNT interfacing with Al foil is 1.3 mV. On the other hand, the potential drops of the pvCNT non-coated and GS-26 electrodes, shown in our previous work [29], were 15 mV and 809.4 mV, respectively.

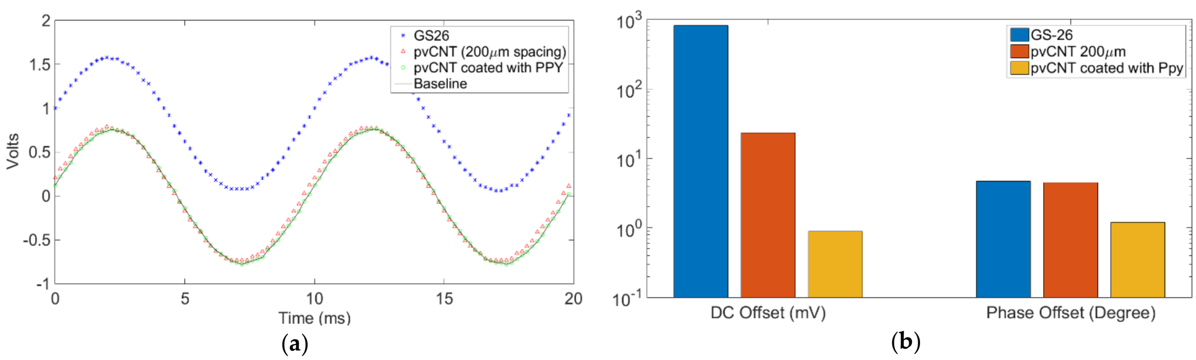

Fig. 3. 7. In vitro test results of the electrodes. (a) Signal capture by coated and non-coated pvCNT dry electrodes compared to the commercial gel GS-26 electrodes interfaced with Al foil. (b) Plots comparing DC offset voltages and phase offsets of these electrodes.

Due to gel diffusion, the potential offset drops on Ag/AgCl were high compared to other electrodes. The applied signal was sinusoidal with a frequency of 100 Hz. Figure 3.7a shows a snapshot of the captured signal and Figure 3.7b shows the different potential drops of each electrode. Due to the polarization that occurred at the interface, a small electric field would rise, shown as a potential offset. Furthermore, the equivalent circuit of the electrode is an RC in parallel, hence, the captured signal will have some phase shift due to the capacitance component.

C. Peel-Off Test Results

Mechanical peel-off tests were performed to check how strongly the CNT pillars were attached to the SS substrate. Figure 3.8 shows the microscopy images of the non-coated and coated pvCNT electrodes prior to and after the peel-off test experiments. As shown in Figure 3.8b, the amount of CNT pillars stuck to the drafting tape was significantly fewer for coated electrodes than for the non-coated electrodes shown in Figure 3.8a. These results show that the CNT pillars of the PPy-coated pvCNT electrodes are attached more strongly than the non-coated electrodes. Drying the PPy after spreading it uniformly through the CNT pillars makes an adhesion layer between the bases of the pillars and the substrate.

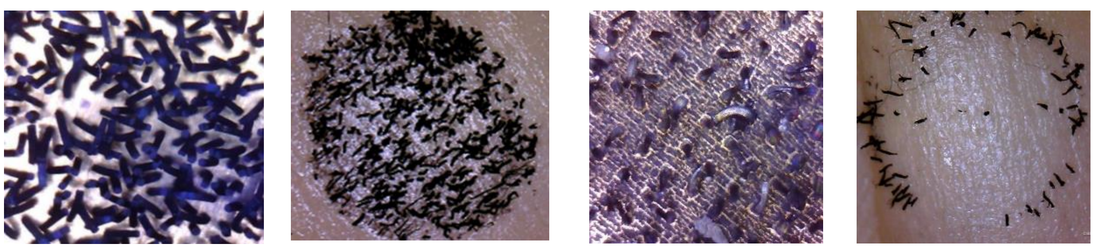

(**a**) Non coated pvCNT (**b**) Coated pvCNT

Fig. 3. 8. Microscopy images of pvCNT prior to and after the peel-off experiments. (a) A non-coated pvCNT electrode prior to the test and the residue left on the tape after the test. (b) PPy-coated pvCNT electrode prior to the test and the residue left on the tape after the test.

D. In Vivo ECG Signal Capture Results

Figure 3.9 shows the ECG signal acquired using the traditional wet electrodes Ag/AgCl (top) and the pvCNT PPy-coated electrode (bottom) described in this work. The pvCNT measurements are very similar to traditional wet electrode measurements. The typical ECG characteristics (QRS-complex, P-wave, and T-wave) were clearly visible as shown in Figure 3.9. The P-wave comes before the QRS-complex which is then followed by the T-wave [1]. The heart rate, in this case, was around 78 beats per minute. Optical images were taken after the experiments to show how many carbon nanotubes had detached and stuck to the skin. Figure 3.10 shows that the PPy-coated pillars are stable and strongly adhered to the stainless-steel substrate.

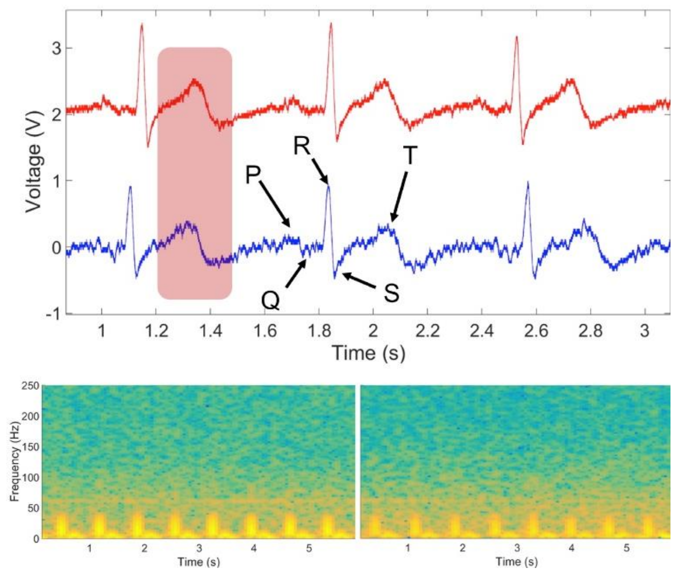

Fig. 3. 9. The ECG signal collected by two electrodes for comparison (Red) Commercial gel electrode, GS-26, and (Blue) PPy coated pvCNT. (Bottom) Time-frequency analysis (Left: GS-26, Right: PPy coated pvCNT) show similar performance and noise characteristics.

Fig. 3. 10. Photographs showing the PPy-coated pvCNT after the ECG signal capture experiments.

5. Discussion

In previous work, we have shown the feasibility of using a novel dry electrode (pvCNT) for physiological and neurological bioelectric or impedimetric signal capturing. The results showed stable and low impedance for short and long periods compared to conventional electrodes. The CNT-based electrodes were fabricated using MWCNT grown in a pillar pattern and vertically aligned on a stainless-steel circular substrate with a diameter of 10 mm. These pillars were weakly attached to the substrate. An electrically conductive polymer polypyrrole (PPy) was used in this study to improve the mechanical stability of the CNT pillars in the pvCNT electrodes. The PPy-coated pvCNTs showed that the impedance of the electrode has increased but the electrodes had a more stable and stronger mechanical adhesion to the SS substrate. In addition, this polymer decreases the toxicity of the CNT making it safer for use on skin. The capability of using the improved pvCNT for monitoring and recording the ECG signals was investigated and the results were compared with commercial gel ECG electrodes (Ag/AgCl). Although the collected ECG signals using pvCNT had more noise (typical for dry ECG electrodes), the typical ECG signal characteristics components, including the P-wave, T-wave, and QRS complex were clearly identifiable and observed.

6. References

[1] Yazicioglu, R.F.; VanHoof, C.; Puers, R. *Bio-Potential Readout Circuits for Portable Acquisition Systems*; Springer: Berlin, Germany, 2008.

[2] Thakor, N.V. Biopotentials and Electrophysiology Measurement. In *The Measurement, Instrumentation and Sensors Handbook*; CRC Press: Boca Raton, FL, USA, 1999.

[3] Martinsen, O.G.; Grimnes, S. *Bioimpedance & Bioelectricity Basics*; Academic Press: Bodmin, UK, 2000.

[4] Plonsey, R.; Barr, R.C. *Bioelectricity: A Quantitative Approach*, 3rd ed.; Springer: New York, NY, USA, 2007.

[5] Patel, S.; Park, H.; Bonato, P.; Chan, L.; Rodgers, M. A review of wearable sensors and systems with application in rehabitation. *J. Neuroeng. Rehabil.* **2012**, *9*, 17.

[6] Lin, C.T.; Liao, L.D.; Liu, Y.H.; Wang, I.J.; Lin, B.S.; Chang, J.Y. Novel dry polymer foam electrodes for long-term EEG measurement. *IEEE Trans. Biomed. Eng.* **2011**, *58*, 1200–1207.

[7] Searle, A.; Kirkup, L. A direct comparison of wet, dry and insulating bioelectric recording electrodes. *Physiol. Meas.* **2000**, *21*, 271–283.

[8] Chi, Y.M.; Jung, T.G; Cauwenberghs, G. Dry-contact and noncontact biopotential electrodes: Methodological review. *IEEE Rev. Biomed. Eng.* **2010**, *3*, 106–119.

[9] Gurger, C.; Krausz, G.; Allison, B.Z.; Edlinger, G. Comparison of dry and gel based electrodes for P300 brain-computer interfaces. *Front. Neurosci.* **2012**, *6*, 1–7.

[10] Huigen, E.; Peper, A.; Grimbergen, C.A. Investigation into the origin of the noise of surface electrodes. *Med. Biol. Eng. Comput.* **2002**, *40*, 332–338.

[11] Webster, J. *Medical Instrumentation: Application and Design*; John Wiley & Sons: Hoboken, NJ, USA, 1998.

[12] Ruffini, G.; Dunne, S.; Farres, E.; Marco-Pallares, J.; Ray, C.; Mendoza, E.; Silva, R.; Grau, C. A dry electrophysiology electrode using CNT arrays. *Sens. Actuators A Phys.* **2006**, *132*, 34–41.
[13] Alemdar, H.; Ersoy, C. Wireless sensor networks for healthcare: A survey. *Comput. Netw.* **2010**, *54*, 2688–2710.
[14] He, B.; Coleman, T.; Genin, G.M.; Hu, X.; Johnson, N.; Liu, T.; Makeig, S.; Sajda, P.; Ye, K. Grand challenges in mapping the human brain: NSF workshop report. *IEEE Trans. Biomed. Eng.* **2013**, *60*, 2983–2992.
[15] Baek, J.; An, J.; Choi, J.; Park, K.; Lee, S. Flexible polymeric dry electrode for long-term monitoring of ECG. *Sens. Actuators A. Phys.* **2008**, *143*, 423–429.
[16] Wang, L.; Liu, J.; Yang, B.; Yang, C. PDMS based low cost flexible dry electrode for long-term EEG measurement. *IEEE Sens. J.* **2012**, *12*, 2898–2904.
[17] Jamadade, S.; Jadhav, S.; Puri, V. Electromagnetic properties of polypyrrole thin film on copper substrate. *Phys. Res.* **2010**, *1*, 205–210.
[18] Chiou, J.C.; Ko, L.W.; Lin, C.T.; Hong, C.T.; Jung, T.P.; Liang, S.F.; Jeng, J.L. Using novel MEMS EEG sensors in detecting drowsiness application. In Proceedings of the Biomedical Circuits and Systems Conference, London, UK, 29 November–1 December 2006; pp. 33–36.
[19] Matthews, R.; Turner, P.J.; McDonald, N.J.; Ermolaev, K.; Mc Manus, T.; Shelby, R.A.; Steindorf, M. Real time workload classification from an ambulatory wireless EEG system using hybrid EEG electrodes. In Proceedings of the 2008 30th Annual International Conference of the IEEE Engineering in Medicine and Biology Society, Vancouver, BC, Canada, 20–25 August 2008; pp. 5871–5875.
[20] Grozea, C.; Voinescu, C.D.; Fazli, S. Bristle-sensors—Low-cost flexible passive dry EEG electrodes for neurofeedback and BCI applications. *J. Neural Eng.* **2011**, *8*, 025008.
[21] Gruetzmann, A.; Hansen, S.; Muller, J. Novel dry electrodes for ECG monitoring. *Physiol. Meas*. **2007**, *28*, 1375–1390.
[22] Gondran, C.; Siebert, E.; Fabry, P.; Novakov, E.; Gumery, P.Y. Non-polarisable dry electrode based on NASICON ceramic. *Med. Biol. Eng. Comput.* **1995**, *33*, 452–457.
[23] Xie, L.; Geng, Y.; Mäntysalo, M.; Xu, L.L; Jonsson, F.; Zheng, L.R. Heterogeneous Integration of Bio-Sensing System-on-Chip and Printed electronics. *IEEE J. Emerg. Sel. Top. Syst.* **2012**, *2*, 672–682.
[24] Kumar, P.S.; Rai, P.; Oh, S.; Kwon, H.; Varadan, V.K. Flexible capacitive electrodes using carbon nanotube and acrylic polymer nanocomposites for healthcare textiles. *Smart Nanosyst. Eng. Med.* **2012**, *2*, 18–24.
[25] Lee, J.M; Pearce, F.; Hibbs, A.D.; Matthews, R.; Morrissette, C. Evaluation of a capacitively-coupled, non-contact (through clothing) electrode or ECG monitoring and life signs detection for the objective force warfighter. In Proceedings of the Combat Casualty Care in Ground Based Tactical Situations: Trauma Technology and Emergency Medical Procedures, DTIC Document, St. Pete Beach, FL, USA, 16–18 August 2004.
[26] Zhou, Y.; Ding, X.; Zhang, J.; Duan, Y.; Hu, J.; Yang, X. Fabrication of conductive fabric as textile electrode for ECG monitoring. *Fibers Polym.* **2014**, *15*, 2260–2264.
[27] Yapici, M.K.; Alkhidir, T.; Samad, Y.A.; Liao, K. Graphene-clad textile electrodes for electrocardiogram monitoring. *Sens. Actuators B Chem.* **2015**, *221*, 1469–1474.

[28] Sullivan, T.J.; Deiss, S.R.; Cauwenberghs, G.; Jung, T. A low-noise, low-power EEG acquisition node for scalable brain-machine interfaces. *SPIE Bioeng. Bioinspir. Syst. III* **2007**, *6592*, 659203.

[29] Ha, S.; Kim, C.; Chi, Y.M.; Akinin, A.; Maier, C.; Ueno, A.; Cauwenberghs, G. Integrated circuits and electrode interfaces for noninvasive physiological monitoring. *IEEE Trans. Biomed. Eng*. **2014**, *61*, 1522–1537.

[30] Zhang, Y.; Bai, Y.; Yan, B. Functionalized carbon nanotubes for potential medicinal applications. *Drug Discov. Today* **2010**, *15*, 428–435.

[31] White, C.T.; Todorov, T.N. Carbon nanotubes as long ballistic conductors. *Nature* **1998**, *393*, 240–243.

[32] Tran, T.Q.; Headrick, R.J.; Bengio, E.A.; Myo Myint, S.; Khoshnevis, H.; Jamil, V.; Duong, H.M.; Pasquali, M. Purification and Dissolution of Carbon Nanotube Fibers Spun from the Floating Catalyst Method. *ACS Appl. Mater. Interfaces* **2017**, *9*, 37112–37119.

[33] Bareket-Keren, L.; Hanein, Y. Carbon nanotube-based multi electrode arrays for neuronal interfacing: Progress and prospects. *Front. Neural Circuits* **2013**, *6*, 1–60.

[34] Smart, S.K.; Cassady, A.I.; Lu, G.Q.; Martin, D.J. The biocompatibility of carbon nanotubes. *Carbon* **2006**, *44*, 1034–1047.

[35] Chlopek, J.; Czajkowska, B.; Szaraniec, B.; Frackowiak, E.; Szostak, K.; Beduin, F. In vitro studies of carbon nanotubes biocompatibility. *Carbon* **2006**, *44*, 1106–1111.

[36] Ruffini, G.; Dunne, S.; Farres, E.; Watts, P.C.P.; Mendoza, E.; Silva, S.R.P.; Grau, C.; Marcho-Pallares, J.; Fuentemilla, L.; Vandecasteele, B. ENOBIO—First tests of a dry electrophysiology electrode using carbon nanotubes. In Proceedings of the 2006 International Conference of the IEEE Engineering in Medicine and Biology Society, New York, NY, USA, 30 August–3 September 2006; pp. 1826–1829.

[37] Ruffini, G.; Dunne, S.; Fuentemilla, L.; Grau, C.; Farres, E.; Marco-Pallares, J.; Watts, P.C.P.; Silva, S.R.P. First human trials of a dry electrophysiology sensor using a carbon nanotube array interface. *Sens. Actuators A. Phys.* **2008**, *144*, 275–279.

[38] Radhakrishana, J.K.; Bhusan, H.; Pandian, P.S.; Rao, K.U.B.; Padaki, V.C.; Aatre, K.; Xie, J.; Abraham, J.K.; Varadan, V.K. Growth of CNT array, for physiological monitoring applications. *Proc. SPIE* **2008**, *6931*, 69310.

[39] Baskey, H.B. Development of carbon nanotube based sensor for wireless monitoring of electroencephalogram. *DRDO Sci. Spectr.* **2009**, *59*, 161–163.

[40] Jung, H.; Moon, J.; Baek, D.; Lee, J.; Choi, Y.; Hong, J.; Lee, S. CNT/PDMS composite flexible dry electrodes for long-term ECG monitoring. *IEEE Trans. Biomed. Eng.* **2012**, *59*, 1472–1479.

[41] Abu-Saude, M.; Consul-Pacareu, S.; Morshed, B.I. Feasibility of Patterned Vertical CNT for Dry Electrode Sensing of Physiological Parameters. In Proceedings of the 2015 IEEE Topical Conference on Biomedical Wireless Technologies, Networks, and Sensing Systems (BioWireleSS), San Diego, CA, USA, 25–28 January 2015; pp. 1–4.

[42] Abu-Saude, M.; Morshed, B.I. Patterned Vertical Carbon Nanotube (pvCNT) Dry Electrodes for Impedimetric Sensing and Stimulation. *IEEE Sens. J*. **2015**, *15*, 5851–5858.

[43] Abu-Saude, M.; Morshed, B.I. Polypyrrole (PPy) Conductive Polymer Coating of Dry Patterned Vertical CNT (pvCNT) Electrode to Improve Mechanical Stability. In Proceedings of the IEEE Topical Conf. Biomedical Wireless Technologies, Networks, and Sensing Systems (BioWireleSS), Austin, TX, USA, 24–27 January 2016; pp. 84–87.

Chapter 4: Accessing Differential Measures with a Conjugate Coil-pair for Wireless Resistive Analog Passive (WRAP) ECG Sensors with PPy Coated pvCNT

1. Introduction

Biopotential signals such as electrocardiogram (ECG/EKG), electroencephalogram (EEG), electromyogram (EMG), and galvanic skin response (GSR) require impedimetric interfacing with skin. Theses neurophysiological signals play a vital role for disease diagnosing, health monitoring, and non-clinical applications [1]. The demand of using an alternative method for continuous and user friendly monitoring has increased specially in situations when physical wires connections are unsuitable such as implantable, body-worn, and remote sensors [2]. Furthermore, the conventional gel/wet electrodes operate well for short-term as the conductivity decreases overt time due to the evaporation when exposed to the environment [3].

Dry electrode is an alternative method for traditional wet electrodes and has the capability of ease-of-use and long duration measurement without degradation of impedance. We have reported a novel dry interfacing electrode using patterned vertically aligned CNTs (pvCNT) coated with conductive polymer (PPy) that mechanically stable and has very stable and low impedance [4]. MWCNTs are used due to its electrical conductivity [5]. pvCNT enable a good contact over the rough and hairy skin surfaces.

Traditional biopotential measuring requires complex electronics, power source, and wires and that will increase the cost and the size of the device. This can be a challenge in a situation where the wired connections are impractical such as wearable or implantable applications [2]. Passive wireless sensing is an alternative method to measure bioelectric signals where the device is highly simplified, battery-less (zero power), and no physical connection, therefore, continuous patient monitoring would be more practical and can be used in body-worn sensors to collect physiological signals unobtrusively [6-8]. The first passive wireless transensor was developed for measuring the intraocular pressure in 1967 by implanting a pair of spiral coils inside the eye [9]. Also, a similar type of resonator was used to measure intra-cardiac blood pressure [10,11] using a capacitive pressure sensor. ECG signal was measured using a wireless radio system based on variable capacitive diodes (varactors) as the frequency shifting component in the resonance circuit [12] but the system requires a battery to power up. A variable capacitance diode (varactor) was used as a capacitive component with passive LC resonator for measuring ECG where biopotential electrodes were connected over the varactor ends [13]. The change in the varactor capacitance induced by the biopotential signal can be measured over an inductive link as modified reflected impedance. We have previously developed a Wireless Resistive Analog Passive (WRAP) sensors [14,15] that can transmit analog signals without using additional digital chips for harvesting the power which is required in the in wireless digital passive sensors. The novel WRAP sensor is based on an LC resonance that is inductively coupled between two printed spiral coils (PSCs). Various physiological signals have been captured such as respiration rate, heart rate, and core body temperature [14-17]. The differential input of two ECG electrodes is required for ECG signal measurements. The differential amplifiers reject most of the common mode noise and amplify differences between two signals such as 3-Lead ECG measurements. In this work, we have designed a novel WRAP sensor for measuring differential biopotential signals using two conjugate spiral coils as secondary (sensor side) and one primary coil (readout). Two depletion mode N-channel dual gate MOSFETs were used to connect the differential inputs that change the loading of the two secondary coils according to the biopotential signals. As a result, only the differential biopotential signals are transmitted over the conductive link by modulating the carrier signal at the primary while the common signals of both sensor coils are canceled out. The system is integrated with dry electrodes PPy coated pvCNT that is connected to the human body. The primary and secondary coil designs have been optimized and improved by our research group previously [16].

2. Hardware Description

A. pvCNT Electrode

The pvCNT electrodes are developed where MWCNTs are grown in a patterned vertically aligned to the stainless steel substrate (Ø = 10 mm, 2 mils thick) forming a bristle-like structure [18, 19]. The pillars were grown on 100µm-squared base with heights between 1 to 1.5 mm and the distance between each pillar is 200µm in an array formation. This structure provides the capability of measuring the signal through hairy and rough areas of the skin. The pvCNTs were fabricated using Chemical Vapor Deposition system (CVD). Figure 4.1 shows the optical images of pvCNT electrode.

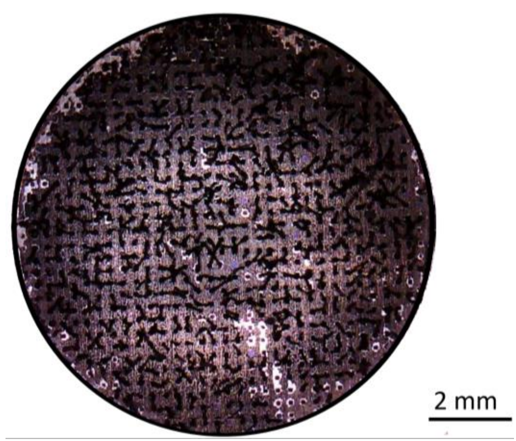

Fig. 4. 1. Optical image of a PPy coated pvCNT electrode.

B. Coil Design

The most essential parameter of measurement system design is the quality and the strength of the link (i.e. the inductive coupling) between the primary and the secondary boards. The dimension of the antennas depends on the operating frequency. In this work we have used 8.27 MHz, thus the size of the antennas would not be extremely small but still feasible for the first prototype. The planar design was chosen so that the construction of the prototype would be easy, small in size, and relatively accurate. All the loop antennas are designed on printed circuit boards (PCBs) as a planar spiral coils (PSC) which can be modeled as inductors.

One of the advantages of using spiral coil cross-section is that the skin effect occurring in conductors with AC current is a volumetric effect thus higher surface area on conductor is better at high frequency than great volume [20]. The coupling coefficient between spiral antennas would be the best when both are placed and aligned coaxially. Furthermore, spiral antennas are more tolerant to misalignment [21]. Coupling coefficient k is a convenient way to specify the coupling efficiency between inductors with arbitrary inductance and is defined by:

$$k = \frac{M}{\sqrt{L_1 L_2}} \qquad (1)$$

Where M is the mutual inductance and L_1 and L_2 are the self-inductances of the coils. When mutual inductance increases the coupling coefficient also increases. The mutual inductance becomes greater as the diameter of the coils increases. However, the self-inductance of the coils increases, the mutual inductance dominates in this case so that increasing the diameter of the coils has a positive effect on the coupling coefficient. The relationship between the size of the coils and the distance between those coils presented in Eq. (2) [22]. Where d_p and d_s are the diameters of the primary and secondary coils and d represent the coaxial distance.

$$d = \frac{1}{2}\sqrt{d_p - d_s} \qquad (2)$$

The optimal coupling can be achieved by making the diameter of the primary coil greater than the diameter of the sensor coil. Our research group previously has developed an iterative method to find the optimal coil pair [16] however; the procedure is left undiscussed in this paper. Figure 4.2. Shows the selected design as it has the highest efficiency among other three designs.

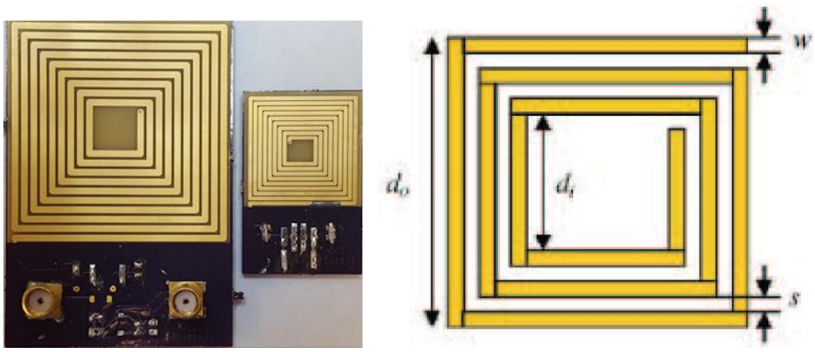

	L (μH)	R_S (Ω)	C_P (pF)	d_O (mm)	d_i (mm)	w (mil)	s (mil)	n	Q	η	C (pF)
P	2.0	0.76	0.65	40	7.1	50	20	9	228	0.85	68.2
S	1	0.65	1	20	3.5	31	6	9	133		133

Fig. 4. 2. The selected coils design and its specification. L, R_s, and C_p are the equivalent electrical components of the coil. n, Q, η, and C are the number of turns, quality factor, power transfer efficiency, and tuning capacitor, respectively.

Cadence Allegro (Cadence Design Systems Inc., San Jose, CA, USA) was used to design the Printed Circuit Boards (PCBs). The outer diameter of the primary and the secondary coils were 40 and 20 mm, respectively.

C. Measurement system

A schematic figure of a simplified WRAP sensor for biopotential signals access is shown in Figure 4.3 (a). The equivalent circuit for the WRAP sensor is a parallel combination of RLC as depicted in Figure 4.3 (b). The measurement device consists of three spiral coils. Two identical coils (L2 and L3) are used on the sensor side and one coil (L1) is used as a scanner device Figure 4.3 (c). The primary coil is coupled to the sensor coils through an inductive link functioning as antennas and can be reduced to single circuit elements with impedances of Xsen1 and Xsen2 as shown in Figure 4.3 (d). Biopotential signals are captured using an N-channel dual gate MOSFET (depletion mode) due to its high sensitivity for small input voltages (Vin). These MOSFETs have a thin layer of silicon N-type placed below the gate, which makes it normally-ON. Furthermore, the input resistance of the depletion-mode transistor is high due to its construction; hence, the depletion mode MOSFET is suitable to use as a voltage control resistance for biopotential measurements. The input voltage is converted to a correlated resistive variation of source-drain resistance of the MOSFET (RSD). Two SMA connectors were used on the scanner board, one for the carrier input that oscillates at an RF carrier wave (8.37 MHz used in this work), and the other one is across the coil L1, that carries the modulated signal to another other PCB with electronic circuits for detecting, filtering, and amplification. The capacitors C1 and C2 are used to match the 50Ω antenna and adjust the resonance frequency with L1 respectively.

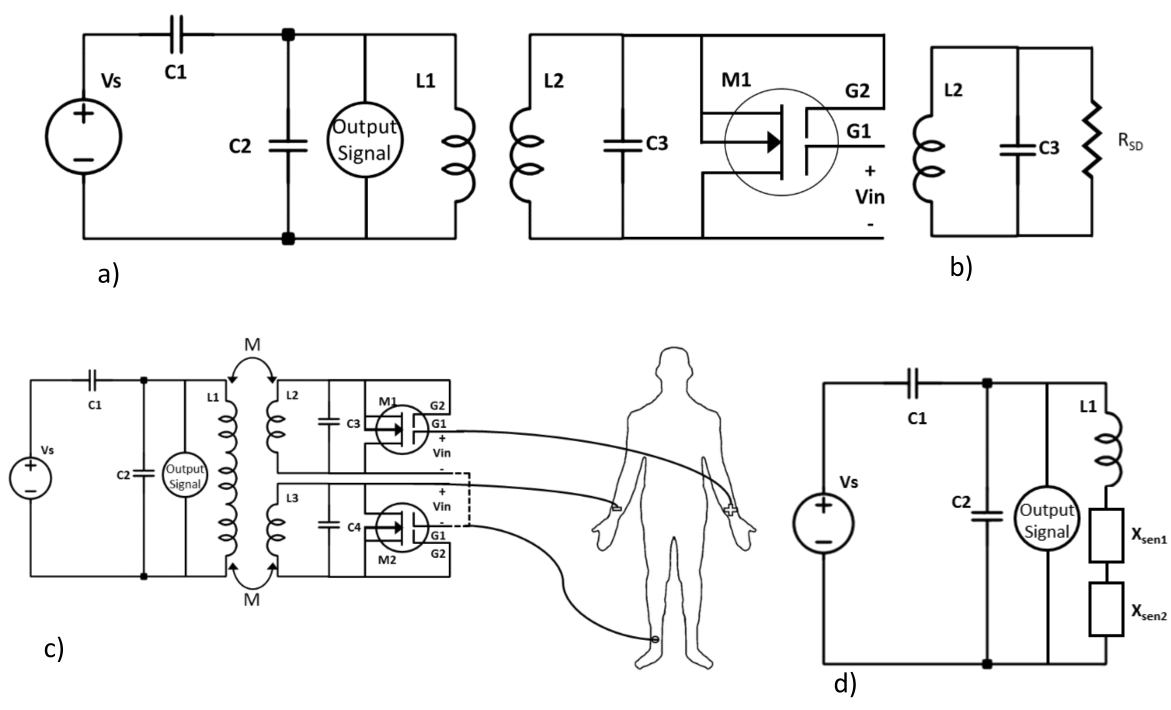

Fig. 4. 3: a) Schematic of the primary and the secondary coils for biopotential sensing. b) The equivalent circuit of secondary. c) Two WRAP sensors are used for sensing of the differential input voltages to access ECG signals from a human body. d) The sensors are reduced to impedances Xsen1 and Xsen2.

The sensor boards are identical and they have similar circuit component values (C3 and C4) that are used to tune the antennas at the resonance frequency. Gate-2 of the MOSFETs M1 and M2 were connected to the coupled signal to increase the sensitivity to a µV range of Vin connected at Gate1. Three electrodes were connected to the human body (e.g. two channels to capture an ECG signal).

The planar coils of the sensor boards were placed to face each other and Kapton tape was used as an isolation material as shown in Figure 4.4 (a). A fixture was designed to keep the boards in parallel at a co-axial position Figure 4.4 (b).

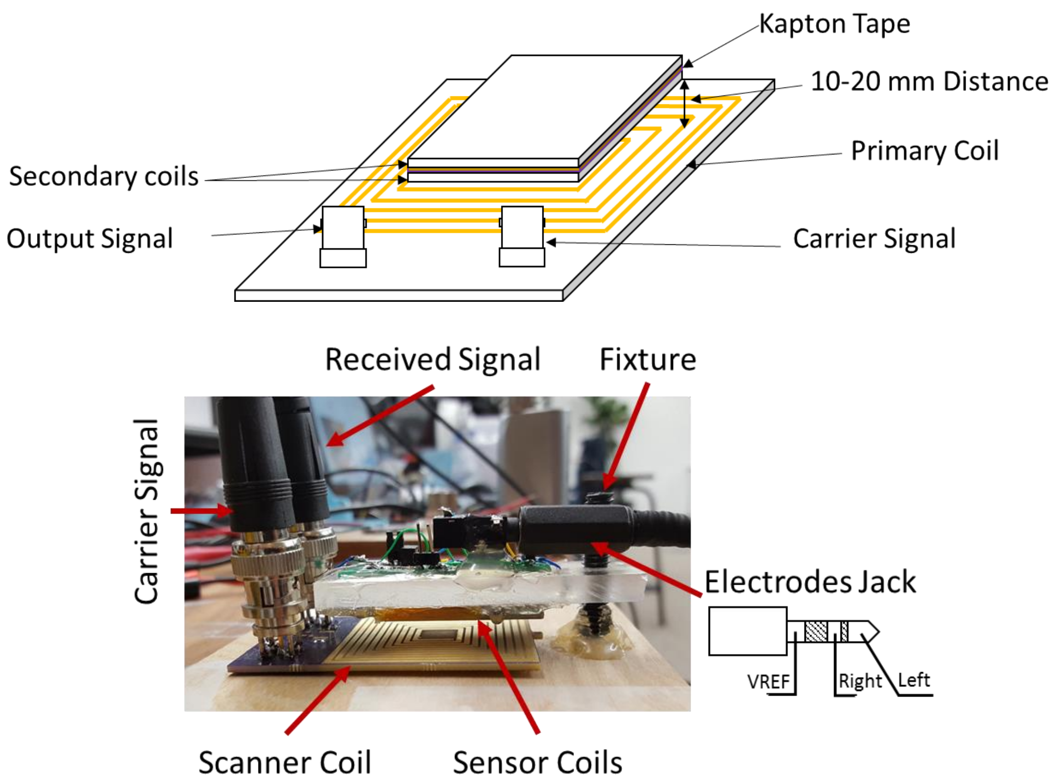

Fig. 4. 4: (Top) Diagram depicting the conjugate coil paper (separated by Kapton tape), and the scanner coil positioned at the co-axial position. (Bottom) A photograph of the setup used for the scanner and the sensors to capture signals in differential mode.

3. Theory of Operation

Each resonance sensor connected to the reader over a conductive link has impedances, Z2 and Z3, as given in Equation 3 and 4 [23].

$$Z_2 = \left(jwL_2 \mid\mid \left(\frac{1}{jwC_3}\right) \mid\mid R_{SD1}\right) \quad (3)$$
$$Z_3 = \left(jwL_3 \mid\mid \left(\frac{1}{jwC_4}\right) \mid\mid R_{SD2}\right) \quad (4)$$

Where RSD1 and RSD2 are the corresponding source-drain resistive variation of MOSFET 1 (M1) and MOSFET 2 (M2), respectively, of the two conjugate sensors.

The current through these sensors, I2 and I3, is proportional to the input voltages (Vin) of these two MOSFETs, say V2 and V3. Mathematically,

$$V_2 \alpha\ I_2 \quad (5)$$

$$V_3 \alpha\ I_3 \quad (6)$$

These sensor currents, in addition to primary current, I1, dictates the voltage, V1, across the primary coil. To solve the effect of the two coils, we can use superposition theorem. Only considering a change of V2 as ΔV2, and determining the corresponding change in V1:

$$V_{1(2)} = j\omega L_1 I_1 - j\omega M I_2 \quad (7)$$

Where ω is the angular frequency of the induced magnetic field of the primary and M represents the mutual inductance between the primary and secondary coils. Primary current can also be represented as:

$$I_1 = \frac{Z_2}{j\omega M} I_2 \quad (8)$$

Where M is the mutual inductance of the two coils. Substituting I1 from (8) to (7), we find:

$$V_{1(2)} = \left(\frac{Z_2 L_1}{M} - j\omega M\right) I_2 \quad (9)$$

Similarly, we can find the change of V1 for a change of V3 using superposition theorem:

$$V_{1(3)} = \left(\frac{Z_3 L_1}{M} - j\omega M\right) I_3 \quad (10)$$

As the coils L2 and L3 are arranged in conjugate orientation, the total effective change of V1 for a change of both V2 and V3 will be:

$$\Delta V_1 = V_{1(2)} - V_{1(3)} = \left(\frac{Z_2 L_1}{M} - j\omega M\right) I_2 - \left(\frac{Z_3 L_1}{M} - j\omega M\right) I_3 \qquad (11)$$

As the two sensor circuits are identical, the impedances Z2 is the same as Z3. Thus, (11) can be reduced to:

$$\Delta V_1 = \left(\frac{Z_2 L_1}{M} - j\omega M\right)(I_2 - I_3) \qquad (12)$$

Utilizing (5) and (6), we can write:

$$\Delta V_1 = K(V_2 - V_3) \qquad (13)$$

Where K is the proportionality constant determined by the inductance of the primary coil, the mutual inductance, and the impedance of the sensor coils. Equation (13) represents a differential amplifier expression where the primary voltage is dependent on the difference between the two input voltages.

In our setup, we placed the two spiral coils in each sensor in opposite direction forming a conjugate coil pair. Therefore, if V_2 and V_3 are identical, the effect on V_1 are canceled out leading to a common mode rejection. This unique technology allows the device to capture only the differential signals and cancel out the common mode voltages.

4. Method for Data Collection

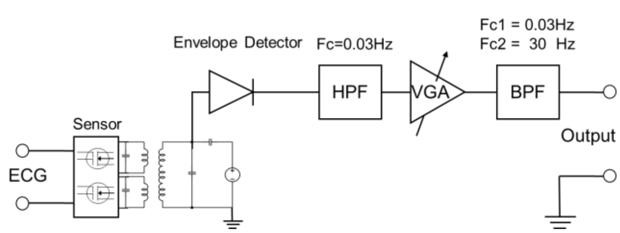

Fig. 4. 5: Block diagram of ECG signal capture process and analysis flowchart where HPF is high pass filter, VGA is variable gain amplifier, and BPF is band pass filter.

The biosignal will modulate the impedance of the resonance circuit, which in turn modulates the carrier signal. By demodulating this signal with an envelope detector, the variations of the ECG in the sensing unit can be detected. The received signal was detected using an envelope detector followed by a unity gain voltage follower with a high pass filter, a variable gain amplifier, and a bandpass filter with $fc1 = 0.03$ Hz and $fc2 = 30$ Hz as shown in Figure 4.5. The output is connected to an oscilloscope (Model: MDO3024, Tektronix, Inc., Santa Clara, CA, USA) and the captured data from the oscilloscope is saved in .csv file format. A signal generator (Model: DG4162, Rigol Technologies Inc., Beijing, China) was used to generate carrier signal to interrogate the passive sensors. This data is later compiled, analyzed, and plotted in Matlab (Mathworks Inc., Natick, MA).

A. Bench Test Experiment Setup

Two test bench experiments have been done to test the sensitivity of the depletion mode MOSFET and the functionality (i.e. differential mode) of the sensor. In the first experiment, only one sensor board was used as shown in Figure 4.1 (a). The voltage was applied through BNC attenuator to achieve microvolt range. In the other experiment, two sensor boards were setup as conjugate coil-pair and two input voltages Vin1 and Vin2 were applied at the input. Three function generators (Model: DG4162, Rigol Technologies Inc., Beijing, China) were used in this setup, one for the carrier frequency and the other one for the input voltages. All ground terminals of the secondary boards were common and different than the ground of the primary coil.

B. ECG Measurement Setup

In the first ECG measurement, the performance of the passive sensor was further investigated by recording ECG signals and compared to the quality of ECG signal measured using an open source commercial hardware EKG/EMG shield (OLIMEX Ltd, Bulgaria) as shown in Figure 4.4 (right). *In vivo*, ECG data was captured using commercial gel ECG electrodes Ag/AgCl (GS-26) for the passive sensor while dry electrodes for the EKG/EMG shield as shown in Figure 4.4 (left). The left arm was connected to the Vin1, right arm to Vin2, and right leg to the reference point as shown in Figure 4.1 (c). The shield EKG/EMG converts the analog differential signal attached to CH1_IN+/CH1_IN- inputs into a single stream of data as output. The output signal was connected directly to the oscilloscope. All the ECG measurements were taken at the same time from both sensors.

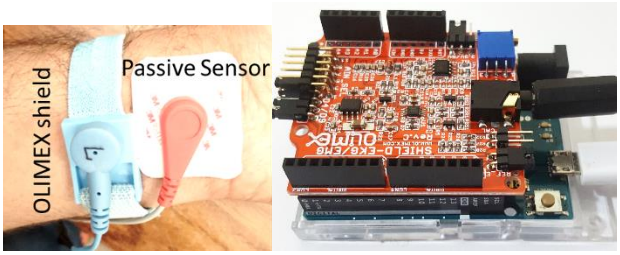

Fig. 4. 6: ECG electrode setup for signal capture (left) and EKG/EMG shield from OLIMEX connected on an Arduino Uno board (right).

C. ECG with pvCNT Measurement Setup

Another set of ECG measurements were done using pvCNT. The pvCNT electrode was attached to a flexible PCB (flex-PCB) on an exposed Cu pad with a diameter of 10 mm, to provide a low impedance, using double-sided z-axis conductive tape (Electrically Conductive Adhesive Transfer Tape 9703, 3M Company, St. Paul, MN, USA). The flex-PCB was designed and prototyped at Cirexx Intl., CA, USA. Three electrodes were placed on the human body at three positions: the left forearm, right forearm, and right leg. All of the measurements of the ECG signals were conducted at room temperature with no skin preparation.

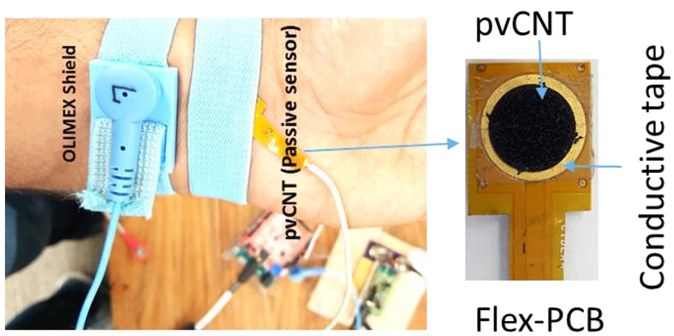

Fig. 4. 7: The pvCNT setup attached to the left arm.

5. Results

A. Bench Test Results

In the first experiment, a micro range voltage using BNC attenuator of 40 dB was applied at low frequencies to meet the requirement of measuring biopotential signals. The device was able to transfer signal of 40µV. Figure 4.5 shows the received signal of 100 µV at a frequency of 100 Hz (top) is before and (bottom) after filtering the signal. The signal was captured and processed using Matlab.

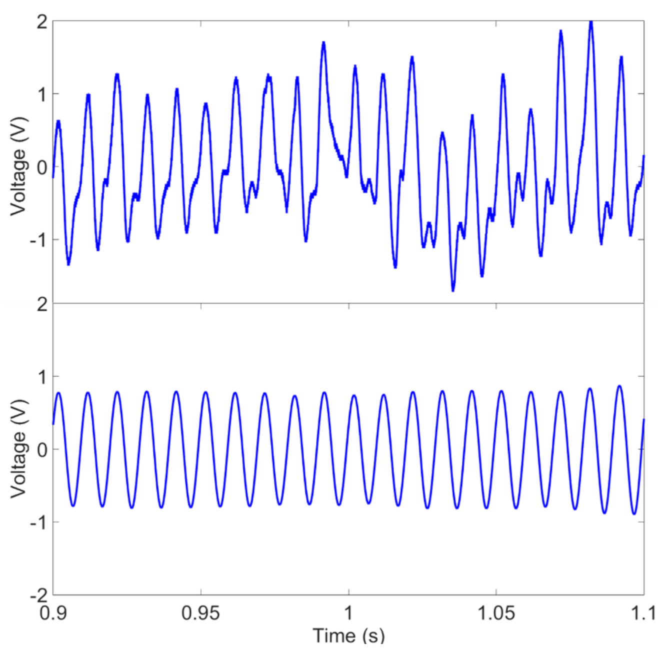

Fig. 4. 8: The output signal of applying 100 µV. Raw (Top) and filtered data (Bottom).

The first experiment of the differential mode setup was conducted to measure the CMRR for the differential sensor. For this experiment, the received signal was connected directly only to a unity gain low pass filter to remove the carrier signal. The average common (ACM) and differential (ADM) mode gains are 0.1703 and 1.24 respectively; therefore, the CMRR is 17.24 dB. Figure 6 shows a linear response of the sensor when one input is fixed and the other input is linearly changed.

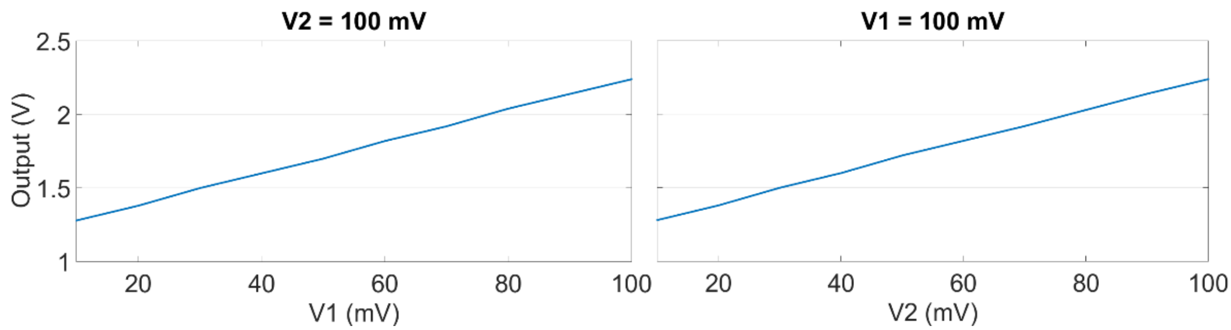

Fig. 4. 9: The response of the differential sensor when one input fixed and the other one changes.

Figure 7 shows the received signal (Blue) as the phase between Vin1 (Green) and Vin2 (Red) is equal to 0, 90, and 180 degrees, respectively. Both Vin1 and Vin2 are sinusoidal signals with a peak-to-peak voltage of 100 mV and frequency of 100 Hz. The results show that the output signal is significantly attenuated when both input signals are identical, while the output signal is amplified when they have a maximum difference.

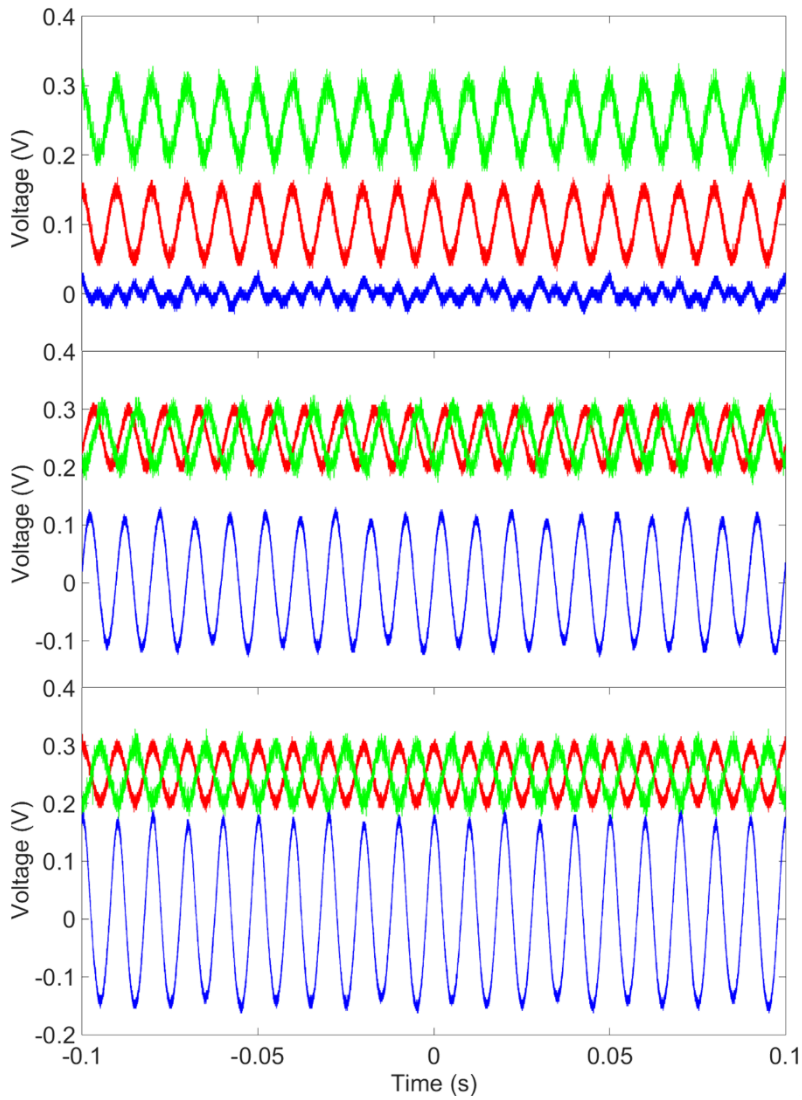

Fig. 4. 10: The output mode of the differential mode setup. The phase difference between Vin1 and Vin2 (Top) 0 (Middle) 90 degree and (Bottom) 180 degree.

B. ECG Measurement Results

The setup in Figure 1(c) was used for ECG signal measurement, where the reference of input voltages was connected together and then connected to the right leg. The setup in Figure 1(c) was used for ECG signal measurement, where the drain of MOSFET 1 and Gate 1 of MOSFET 2 were connected together and then connected to the right leg. Figure 8 shows the raw data of the ECG signal recorded using EKG/EMG shield (Red) and the passive sensor (Blue) for 10 seconds (100k points at sampling frequency 10k sample per second). Some noise can be seen in the unfiltered signal using time-frequency analysis of ECG EKG/EMG shield (Left) and the passive sensor (Right). The ECG signals recorded using the passive sensor had more components of the utility line 60Hz noise and its harmonics. All the ECG components (R-peaks, QRS-complexes, T-waves, and P-waves) are easily recognizable from the raw data without any downstream processing as shown in Figure 9 (Top). A low pass filter was applied to the signal using Matlab for both signals and the results are depicted in Figure 9 (Bottom).

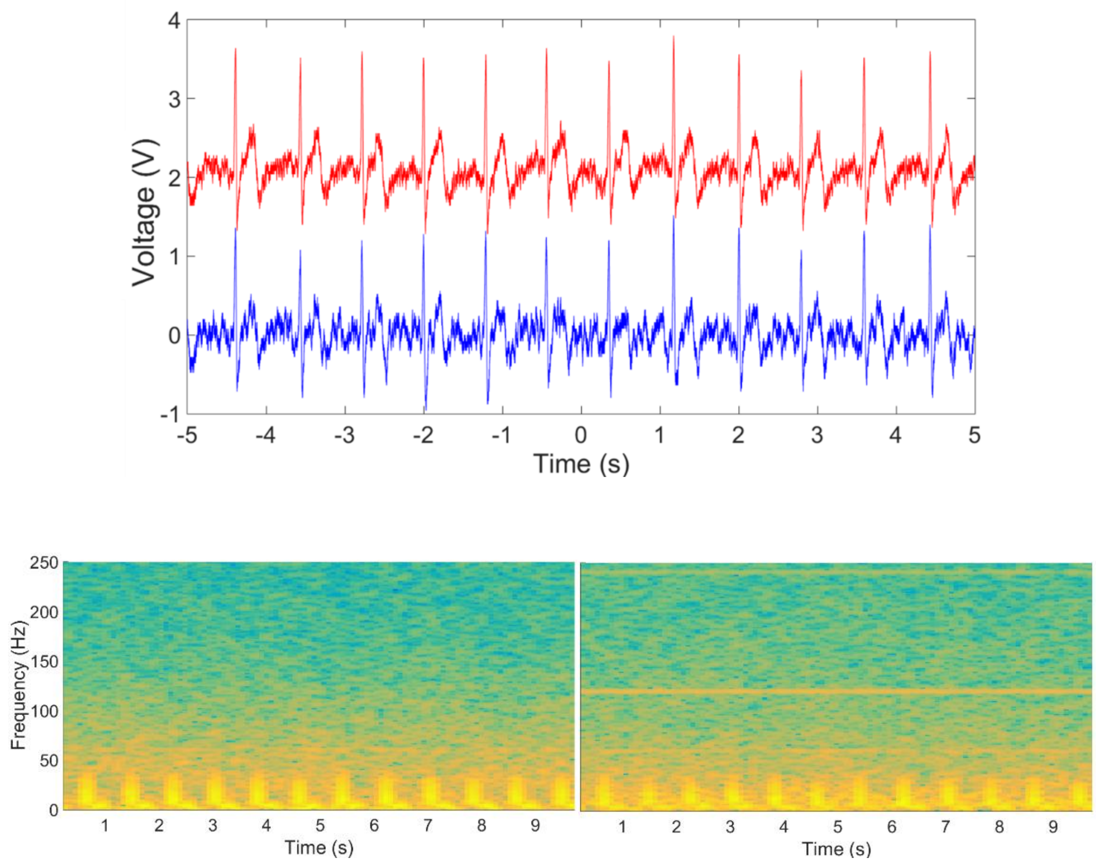

Fig. 4. 11: (Top) The raw data of the recorded ECG signals using EKG/EMG shield (Red) and the passive sensor (Blue) for 10 seconds. (Bottom) the time-frequency analysis of ECG using EKG/EMG shield (Left) and the passive sensor (Right)

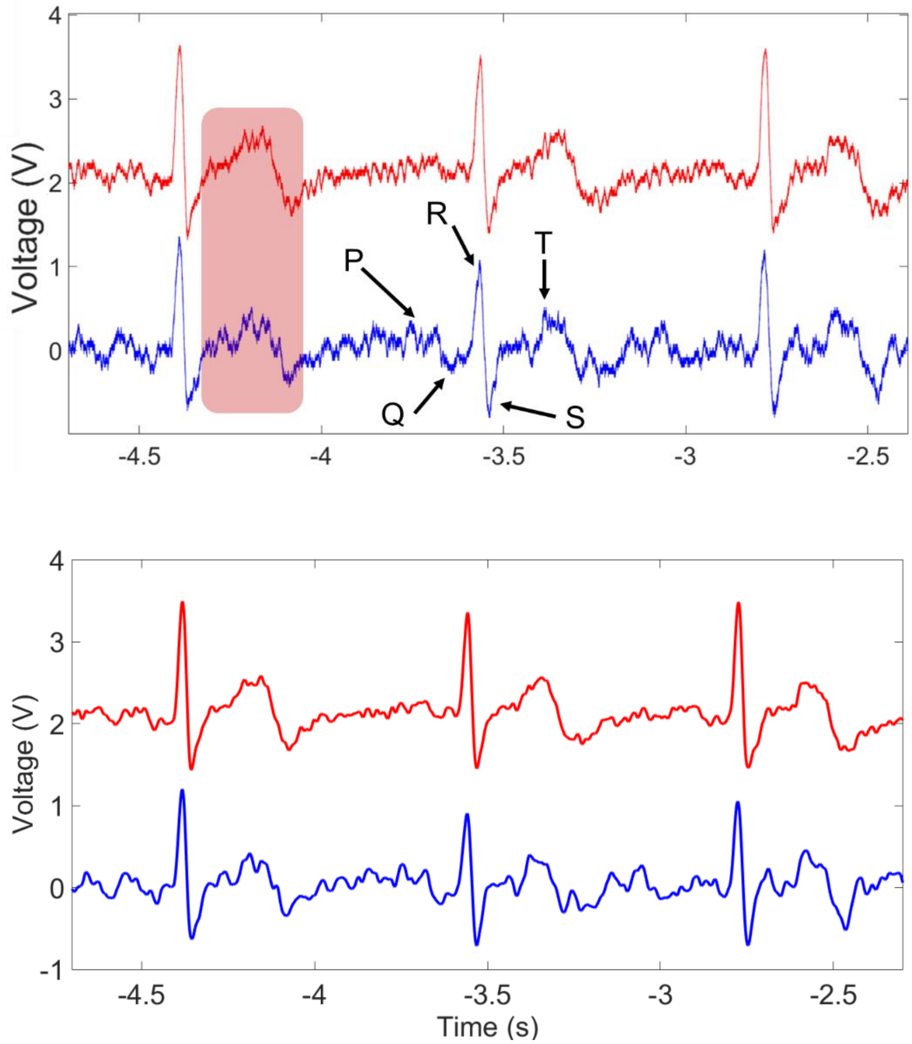

Fig. 4. 12: (Top) The ECG components (R-peaks, QRS-complexes, T-waves, and P-waves). (Bottom) and the filtered ECG signal.

C. ECG with pvCNT Measurement Results

Figure 13. Shows the ECG signal acquired using the pvCNT PPy coated electrode. Although the collected ECG signals using pvCNT has more noise, the typical ECG signal characteristics components, including the P-wave, T-wave, and QRS complex were clearly identifiable and observed as P-wave comes before QRS-complex and T-wave comes after. The heart rate in this case was around 77.8 beats per minute.

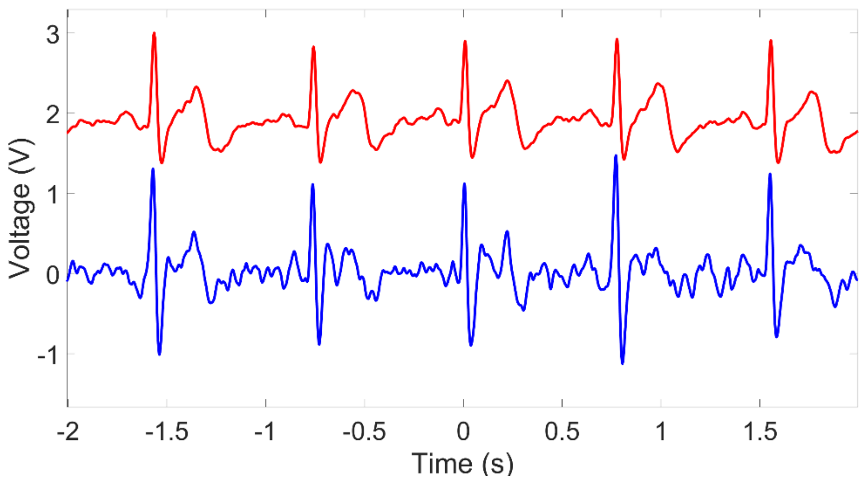

Fig. 4. 13: The ECG components (R-peaks, QRS-complexes, T-waves, and P-waves). (Bottom) and the filtered ECG signal.

Figure 14. Shows the raw and filtered ECG signal acquired using the pvCNT PPy coated electrode after bypassing the envelope detector.

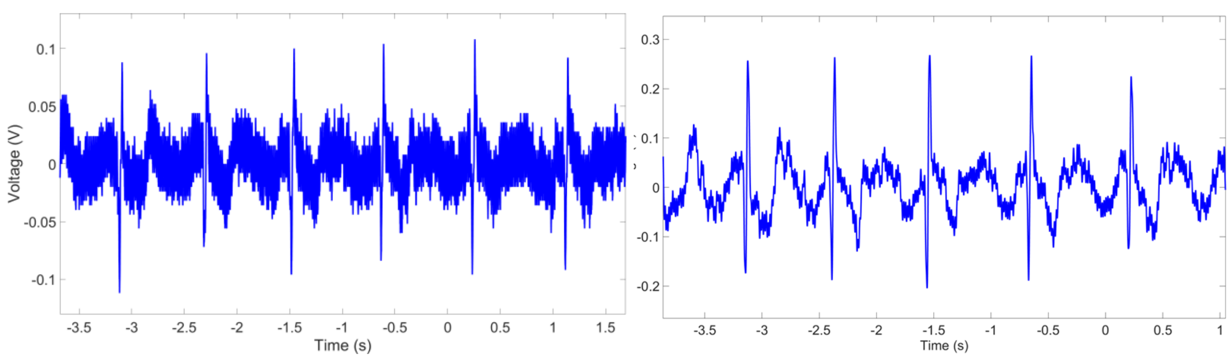

Fig. 4. 14: (left) is the raw data of the recorded ECG signals using pvCNT with the passive sensor and (right) is the filtered signal.

6. Conclusions

A novel, wireless resonance device to measure biopotentials has been presented and shown to be able to measure biopotentials. The novel setup (conjugate coil-pair) of WRAP sensors uses two WRAP sensors utilizing depletion mode MOSFETs for measuring ECG signal from limb lead configuration. The system successfully was able to capture biopotentials as low as 40 µV, in addition to the ECG signal in vivo. Also in previous work, we have shown a feasibility of using a novel PPy coated dry electrode (pvCNT) for physiological and neurological bioelectric or impedimetric signal capturing. In this work, we integrated both, the passive wireless device with PPy coated pvCNT, for measuring ECG signals. The results demonstrate the promise of developing a battery-less WRAP ECG sensor integrated with dry CNT based electrode (pvCNT) that can be worn on the body or even possibly be implanted inside the human body and would be a suitable for continuous ECG recording.

7. References

[1] Thakor, N.V. Biopotentials and Electrophysiology Measurement. In The Measurement, Instrumentation and Sensors Handbook; CRC Press: Boca Raton, FL, USA, 1999.

[2] J. Coosemans, M. Catrysse, and R. Puers, “A readout circuit for an intra-ocular pressure sensor,” Sens. Actuators A, Phys., vol. 110,nos. 1–3, pp. 432–438, 2004.

[3] Searle, A.; Kirkup, L. A direct comparison of wet, dry and insulating bioelectric recording electrodes. Physiol. Meas. 2000, 21, 271–283.

[4] Abu-Saude, M., Morshed, B.I. Characterization of a Novel Polypyrrole (PPy) Conductive Polymer Coated Patterned Vertical CNT (pvCNT) Dry ECG Electrode. Chemosensors 2018, 6, 27.

[5] C. T. White , T. N. Todorov, “Carbon nanotubes as long ballistic conductors”, Nature, vol. 393, pp. 240-243, 1998.

[6] Y. M. Chi, T. Jung, and G. Cauwenberghs, Dry-contact and noncontact biopotential electrodes: methodological review, IEEE Reviews in Biomedical Engineering, vol. 3, pp. 106-119, 2010.

[7] A. Sabban, Comprehensive study of printed antennas on human body for medical applications, Intl. J. Advance in Medical Sci., vol. 1, no. 1, pp. 1-10, 2013.

[8] A. Dementyev, and J. R. Smith, A wearable UHF RFID-based EEG system, IEEE Intl. Conf. RFID, pp. 1-7, 2013.

[9] C. C. Collins, “Miniature passive pressure transensor for implanting in the eye,” IEEE Trans. Biomed. Eng., vol. BME-14, no. 2, pp. 74–83, Apr. 1967.

[10] K. Takahata, A. DeHennis, K.D. Wise, Y.B. Gianchandani, Stentenna: a micromachined antenna stent for wireless monitoring of implantable microsensors, in: IEEE Engineering in Medicine and Biology 25th Annual Conference, 2003.

[11] N. Najafi, A. Ludomirsky, Initial animal studies of a wirelss, batteryless, mems implant for cardiovascular applications, Biomedical Microdevices 6 (1) (2004) 61–65.

[12] J.H. Filshie, I.J.H. Duncan, J.S.B. Clark, Radiotelemetry of avian electrocardiogram, Journal of Medical and Biological Engineering and Computing 18 (1980) 633–637.

[13] J. Riistama, E. Aittokallio, J. Verho, J. Lekkala.Totally passive wireless biopotential measurement sensor by utilizing inductively coupled resonance circuits, Sensors and Actuators A: Physical, Volume 157, Issue 2, 2010, Pages 313-321.

[14] S. Consul-Pacareu, D. Arellano, and B. I. Morshed, "Body-worn fullypassive wireless analog sensors for physiological signal capture through load modulation using resistive transducers," in Proc. IEEE Healthcare Innov. Conf. (HIC), Oct. 2014, pp. 67–70.

[15] S. Consul-Pacareu, D. Arellano, and B. I. Morshed, "Body-worn fullypassive wireless analog sensors for biopotential measurement through load modulation," in Proc. IEEE Biowireless Conf., San Diego, CA, USA, Jan. 2015, pp. 1–3.

[16] B. Noroozi, and B.I. Morshed, "Formal Method for PSC Design Optimization of 13.56 MHz Resistive Wireless Analog Passive Sensors (rWAPS)," presented at the IEEE Radio and Wireless Week Conf., Austin TX, Jan. 24-27, 2016.

[17] B. I. Morshed, B. Harmon, M. S. Zaman, M. J. Rahman, S. Afroz, and M. Rahman, "Inkjet Printed Fully-passive Body-worn Wireless Sensors for Smart and Connected Community (SCC)", J. Low Power Electron. Appl., vol. 7, no. 4, article 26, pp. 1-21, 2017.

[18] M. Abu-Saude, S. Consul-Pacareu, and B. I. Morshed, "Feasibility of Patterned Vertical CNT for Dry Electrode Sensing of Physiological Parameters", IEEE Radio Wireless Conference (BioWireleSS), pp. 1-4, Jan. 2015.

[19] M. J. Abu-Saude and B. I. Morshed, "Patterned Vertical Carbon Nanotube (pvCNT) Dry Electrodes for Impedimetric Sensing and Stimulation", IEEE Sensors J., vol. 15, no. 10, pp. 5851-5858, 2015.

[20] C. Fernndez, O. Garca, R. Prieto, S. Cobos, J. Gabriels, G. Van Der Borght, Design issues of a core-less transformer for a contact-less application, in: Applied Power Electronics Conference and Exposition, 2002.

[21] N. Donaldson, T. Perkins, Analysis of resonant coupled coils in the design of radio frequency transcutaneous links, Journal of Medical and Biological Engineering and Computing 21 (1983) 612–627.

[22] Erc/rec 70–03 - erc recommendation 70–03 relating to the use of short range devices (srd), October 2007.

[23] K. Finkenzeller, The RFID Handbook, John Wiley and Sons, 2003.

Chapter 5: Conclusions and Future Directions

1. Key Results

The key findings of this work can be summarized as follows:

1. **PvCNT dry electrodes:** We were able to design a CNT based electrode for dry impedimetric sensing. The pvCNT is an ensemble of an array of MWCNT that forms pillars vertical to the circular stainless steel substrate (Ø = 10 mm) with four different spacing between the pillars (50, 100, 200, and 500 µm) and heights of the pillars were between 1 to 1.5 mm. A comparative test with commercial ECG electrodes shows that pvCNT has lower electrical impedance, stable impedance over very long time, and comparable signal capture in vitro. Long duration study shows minimal degradation of impedance over 7 days period. The results demonstrate the feasibility of using pvCNT dry electrodes for physiological parameter sensing.
2. **PPy coating of pvCNT electrodes:** We were able to strengthen the mechanical stability of the electrode using a coating mechanism of pvCNT with a thin layer of conductive polymer, Polypyrrole (PPy). The coating procedure involved applying 10 µL of PPy after preparing the pvCNT with 70% ethyl alcohol solution and flash drying at 300°C. A comparative test with commercial ECG electrodes and non-coated version show that coated pvCNT has lower electrical impedance compared to commercial electrode whereas higher impedance compared to non-coated version. The signal capture was comparable for all electrodes in vitro. The peel test reveals much stronger mechanical adhesion of the pvCNT with the SS substrate when coated with PPy. The results demonstrate the feasibility of coating pvCNT dry electrodes with PPy for robustness.

3. **Novel WRAP ECG sensor with integrated pvCNT electrodes:** We presented a novel approach for monitoring body signals with a zero power (battery-less), fully passive electronic patch sensors that can be attached to the body. The system uses conjugate coil pair technique that able to sense differential signals such as electrocardiogram (ECG) using N-channel dual-gate MOSFET (depletion mode) to convert the biopotential signal to the correlated drain-source resistance. The results show that connecting a pair of sensors in this way could allow accurate measurement of a differential biopotential. This work demonstrates voltage sensitivity down to 40 µV towards realizing a battery-less, body-worn WRAP ECG sensor for monitoring ECG signals.

2. Future Research Directions

1. Our preliminary studies on CNT-based electrode show that pvCNT dry electrode shows the potential of pvCNT as a dry electrode for physiological monitoring of patient-centric healthcare for use beyond clinical settings. In addition, the PPy coating provides the pvCNT electrode with higher mechanical strength. One future direction can be to study pillar structure shape and geometry (such as hive structure, cylindrical etc.) to increase the mechanical strength of the pillar with higher breathability, and use different type of substrate and transfer technique to improve the adhesion between the pillar and the substrate as well as integrating the pvCNT electrodes with flexible body worn electronic circuits.
2. The conjugate coil-pair of the WRAP sensors was successfully able to capture biopotential as low as 40 µV and ECG signal in vivo. However, the sensor can be improved further, and the SNR can be increased by designing a single board with the conjugate coil, rather than using the two boards where the two coils are in the top and the bottom of the board. Moreover, the distance between the primary and the secondary coils could be increased by using different

sizes of the coils. Furthermore implementing the circuit using flexible electronics can improve usability and user experience for long duration wearable ECG sensors.

APPENDIX

I. Simulation

LTSpice was used for simulation to check the sensitivity of the MOSFET.

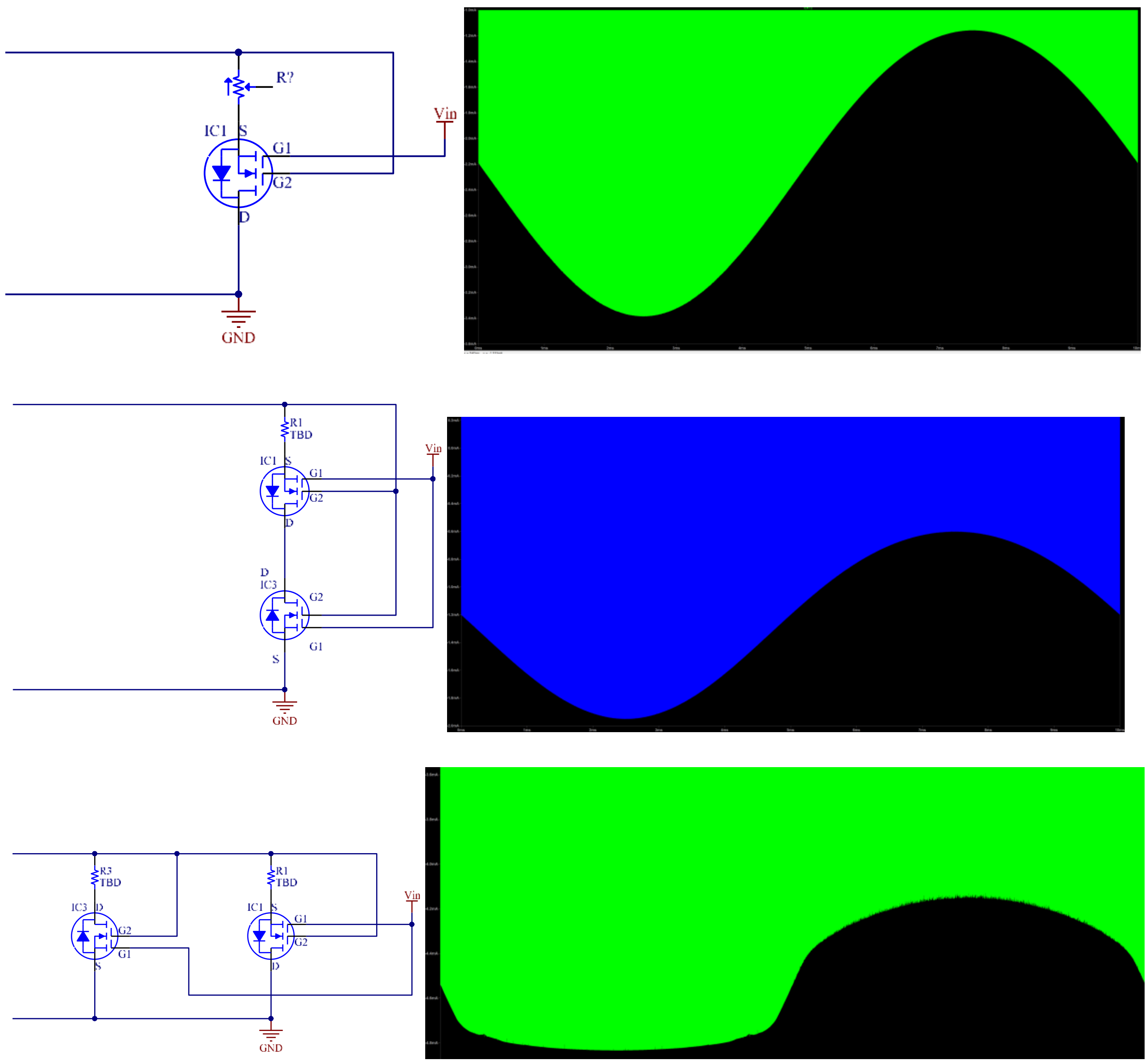

Fig. A. 1 LTSpice simulation to check the sensitivity of the dual-gate MOSFET (Depletion-mode) using different combination.

II. Wireless passive sensor experiments

Finding the resonance frequency:

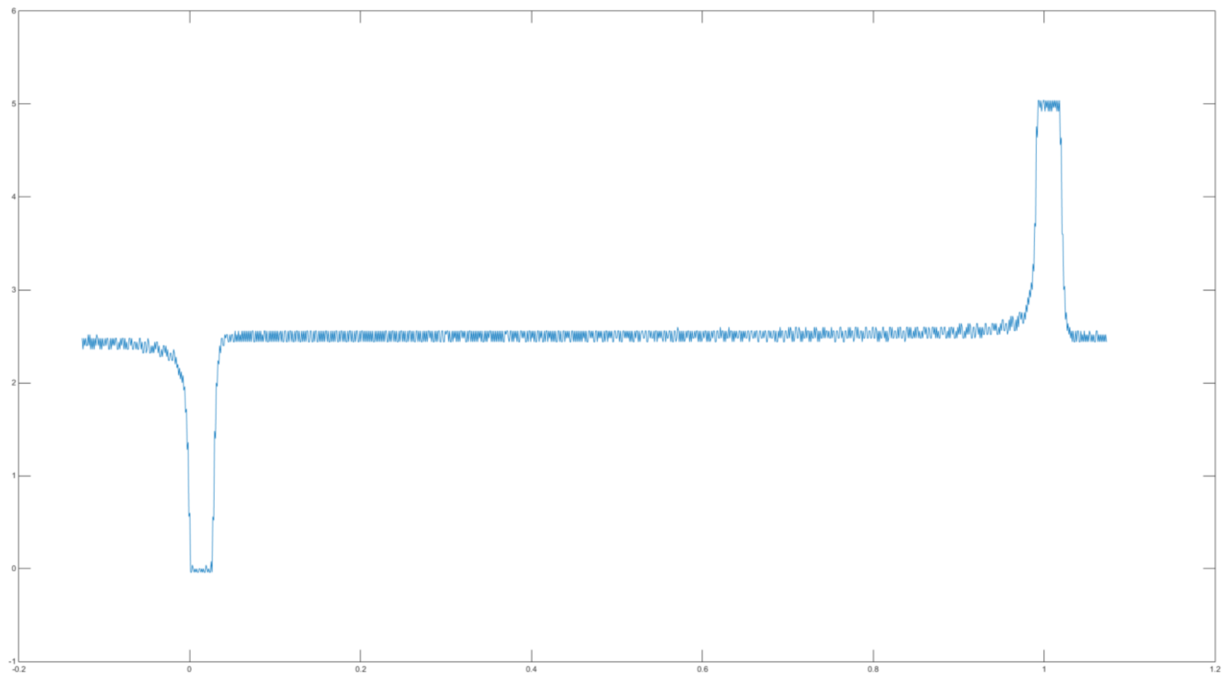

Fig. A. 2 Sweep (8 MHz - 8.5 MHz)

Applying 40uV, 100Hz input voltage:

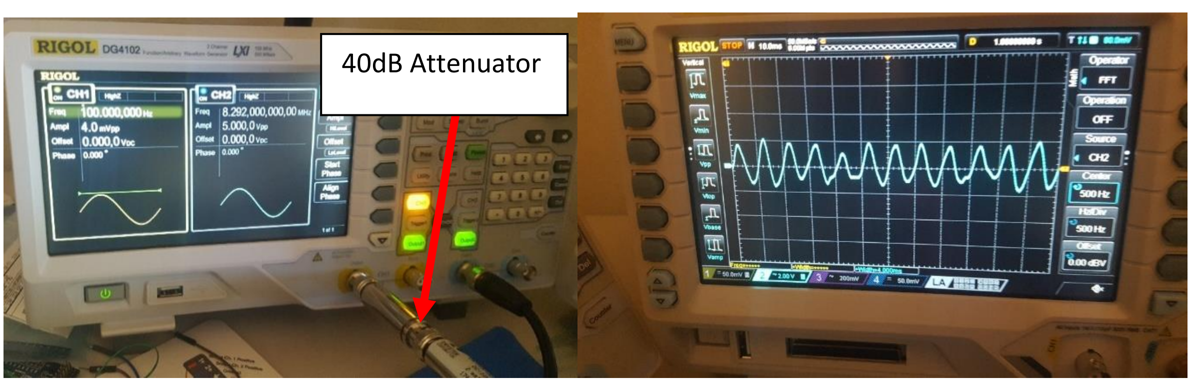

Fig. A. 3 Applying 40μV with 40db attenuator and its result on the left

III. Matlab

```
%%Reading and processing ECG signal:
%%
clear all
close all

fontSize=30;
linewidth=3;
filename='tek0007ALL.csv';
Fs=1/csvread(filename,8,1, [8 1 8 1]);
M = csvread(filename,21,0);
%M = M(:,1)*(-1)
%t=0:1/Fs:length(M)/Fs-1/Fs
figure()
hold on
plot(M(:,1),M(:,2)+0.6, 'r')
hold on
plot(M(:,1),M(:,3), 'b')
xlabel('Time (s)','fontSize',fontSize,'FontName','Arial');
ylabel('Voltage (V)','fontSize',fontSize,'FontName','Arial');
%title('CNT Impedance','fontSize',fontSize,'FontName','Arial');
%axis([0.038 102 0 350]);
set(gca,'fontsize',26)

t=M(:,1)';
data=M(:,3)';
data_ref=M(:,2)';
figure()
plot(data,'b','LineWidth',linewidth)
xlabel('Time (s)','fontSize',fontSize,'FontName','Arial');
ylabel('Voltage (V)','fontSize',fontSize,'FontName','Arial');
%title('CNT Impedance','fontSize',fontSize,'FontName','Arial');
%axis([0.038 102 0 350]);
set(gca,'fontsize',fontSize)

[pxx, fx] = pwelch(data,[],[],[],Fs);
plot(fx,pxx);

% data=downsample(data,40)
% t = downsample(t,40)
% Fs=250
%%
%de-trend
plot(t, data,'r');
data = detrend(data);
hold on
plot(t, data, 'b');
%%
N = length(data_ref);
dft = fft(data_ref);
dft = dft(1:N/2+1);
psd = (1/(Fs*N)) * abs(dft).^2;
psd(2:end-1) = 2*psd(2:end-1);
freq = 0:Fs:N:Fs/2;
```

```
plot(freq,10*log10(psd))
grid on
title('Periodogram Using FFT')
xlabel('Frequency (Hz)')
ylabel('Power/Frequency (dB/Hz)')

periodogram(data,rectwin(length(data)),length(data),Fs)
%%
%time-Frequency analysis
spectrogram(data_ref,[],[],[],Fs,'yaxis')

segmentLength = round(numel(data)/4.5); % Equivalent to setting segmentLength
= [] in the next line
spectrogram(data,round(segmentLength/5),round(80/100*segmentLength/5),[],Fs,'
yaxis')
ylim([0 250])
set(gca,'fontsize',fontSize)
figure,
segmentLength = round(numel(data_ref)/4.5); % Equivalent to setting
segmentLength = [] in the next line
spectrogram(data_ref,round(segmentLength/5),round(80/100*segmentLength/5),[],
Fs,'yaxis')
ylim([0 250])
set(gca,'fontsize',fontSize)
spectrogram(data,round(segmentLength/5), ...
    round(80/100*segmentLength/5),[],Fs,'yaxis')
ylim([0 500])
spectrogram(data,round(segmentLength/5),round(80/100*segmentLength/5),[],Fs,'
yaxis','MinThreshold',-70)
%%
dataWind=data.*hamming(length(t),'periodic')';
plot(t,data,'b')
hold on
plot(t,dataWind,'r')

%%
%%
bsFilter = designfilt('bandstopiir','FilterOrder',2, ...
               'HalfPowerFrequency1',59,'HalfPowerFrequency2',61, ...
               'DesignMethod','butter','SampleRate',Fs);
data_no_60=filter(bsFilter,dataWind);

figure();
plot(data_no_60)
xlabel('Time (s)')
ylabel('Voltage (V)')
[pxx, fx] = pwelch(data_no_60,[],[],[],Fs);
plot(fx,pxx);

%%
Order  = 7;  % Order
Fc =75;  % Cutoff Frequency

% Construct an FDESIGN object and call its BUTTER method.
h  = fdesign.lowpass('N,Fp,Ap', Order, Fc,1, Fs);
```

```
LPF = design(h, 'cheby1');
dataFiltered=filter(LPF,data_no_60);

plot(t,dataFiltered,'b');

%[pxx, fx] = pwelch(dataFiltered,[],[],[],Fs/10);
%plot(fx,pxx);

%% BPF
Fc1 = 8.5;   % First Cutoff Frequency
Fc2 = 9;  % Second Cutoff Frequency
N   = 4;  % Order

% Construct an FDESIGN object and call its BUTTER method.
h  = fdesign.bandpass('N,F3dB1,F3dB2', N, Fc1, Fc2, Fs);
BPF = design(h, 'butter');
BPFiltered=filter(LPF,data);
plot(t,BPFiltered,'b');
[pxx, fx] = pwelch(BPFiltered,[],[],[],Fs);
plot(fx,pxx);
%%
%moving
MovOrder=floor(length(data)/500);
a = 1;
b = ones(1, MovOrder)/MovOrder;

dataFilteredMoving = filter(b,a,dataFiltered);
figure()
plot(t,dataFiltered,'r');
hold on
plot(t,dataFilteredMoving,'b','LineWidth',linewidth)
xlabel('Time (s)','fontSize',fontSize,'FontName','Arial');
ylabel('Voltage (mV)','fontSize',fontSize,'FontName','Arial');
%title('CNT Impedance','fontSize',fontSize,'FontName','Arial');
%axis([-1 1 -1 1]);
set(gca,'fontsize',fontSize)

%%
bsFilter = designfilt('bandstopiir','FilterOrder',2, ...
               'HalfPowerFrequency1',8,'HalfPowerFrequency2',9, ...
               'DesignMethod','butter','SampleRate',Fs);
data_cus=filter(bsFilter,dataFiltered);

figure();
plot(data_cus)
xlabel('Time (s)')
ylabel('Voltage (V)')
[pxx, fx] = pwelch(data_cus,[],[],[],Fs);
plot(fx,pxx);

%%
smoothECG = smoothdata(data);
plot(smoothECG,'b');
hold on
plot(data,'r')
```

```
%%

lpFilt = designfilt('lowpassiir', 'PassbandFrequency', 3, ...
        'StopbandFrequency', 270, 'PassbandRipple', 1, 'StopbandAttenuation',
...
        50, 'SampleRate', Fs);
fvtool(lpFilt)
data_filt=filter(lpFilt,data);
plot(t, data_filt ,'b','LineWidth',linewidth)
data_filt=filter(lpFilt,data_ref);
hold on
plot(t, data_filt + 0.4 ,'r','LineWidth',linewidth)
%axis([-4.7 -2.3 -1 4]);
xlabel('Time (s)','fontSize',fontSize,'FontName','Arial');
ylabel('Voltage (V)','fontSize',fontSize,'FontName','Arial');
set(gca,'fontsize',fontSize)
```

CNT project

% Long-Term Analysis (CNT)

```
clear all
close all
clc
fileName='10Glycol90PPY.xls';
sheet=3;
xlRange='B11:G811';
[status,sheets] = xlsfinfo(fileName);
numOfSheets = numel(sheets);
fontSize=30;
linewidth=3;

colors=['r';'b';'g';'k';'m'];
cnt='200\mum'; % this value will appear in labels and titles
electrodes={'200' ,'100','GS26','End'}
%% Reading data - Start from sheet 3
selectelectrode=3; % 1 for 200 ,2 for 100, and 3 for GS26
index1=find(strcmp(sheets,electrodes(1,selectelectrode)))+1
index2=find(strcmp(sheets,electrodes(1,selectelectrode+1)))-1
clearvars data;
i=0;
for sheet=3:numOfSheets
 i=i+1;
 data(:,:,i)=xlsread(fileName,sheet,xlRange);
end

%% validate data to remove the error
j=1
for j=1:size(dataZ,3)

dif=diff(dataZ(:,2,j));
dif_theta=diff(dataTheta(:,2,j));
%plot(dif)
[m i_max]=max(abs(dif));
[m_theta i_max_theta]=max(abs(dif_theta))
```

```
mx=dif(i_max)
mx_theta=dif_theta(i_max_theta)
if (i_max>=400)
  dataZ(i_max+1:801,2,j)=dataZ(i_max+1:801,2,j)-mx;
else
    dataZ(1:i_max,2,j)=dataZ(1:i_max,2,j)+mx;
end
if (i_max_theta>=400)
  dataTheta(i_max_theta+1:801,2,j)=dataTheta(i_max_theta+1:801,2,j)-mx_theta;
else
    dataTheta(1:i_max_theta,2,j)=dataTheta(1:i_max_theta,2,j)+mx_theta;
end
end

hour=6;
plot(dataZ(:,1,hour),dataZ(:,2,hour))
plot(dataTheta(:,1,hour),dataTheta(:,2,hour))

%% 3D plot
c=1;
for i=1:numOfSheets-2
 plot3(ones(1,801)+i-1,dataZ(:,1,i),dataZ(:,2,i),colors(c,:))
 hold on
 c=c+1;
 if c>5
     c=1;
 end
end
%%
dataZ2=squeeze(dataZ(:,2,:));
dataZ2=dataZ2';
%dataZ2=flipud(dataZ2);
mesh(dataZ(:,1,1),(1:size(dataZ2,1)),dataZ2,'LineWidth',linewidth);

ylabel('Time (Hours)','fontSize',24,'FontName','Arial');
xlabel('Frequency (Hz)','fontSize',24,'FontName','Arial');
zlabel('|z| (\Omega)','fontSize',24,'FontName','Arial');
title(['CNT Impedance ',cnt,' ',strcat(num2str(numOfSheets-2),'
hours')],'fontSize',24,'FontName','Arial');
set(gca,'fontsize',24)
set(gca,'Ydir','reverse')
%axis([0 100e3 0 size(dataZ2,1) 0 6]);
%% subplot
for k=1:9
    subplot(3,3,k);
    c=1;
for i=5*k-4:5*k
plot(dataZ(:,1,i),dataZ(:,2,i),colors(c,:))
legend('1','2','3','4','5')
xlabel('Frequency (Hz)');
ylabel('|z| (\Omega)');
title([strcat(num2str(5*k-4),' Hours'),' to ' ,strcat(num2str(k*5),' Hours')]
);
%legend(sheets(5*k-4+2),sheets(5*k-4+3),sheets(5*k-4+4),sheets(5*k-
4+5),sheets(5*k-4+6))
hold on
```

```
c=c+1;
end

end
%% Plot the data for diff freq
start=113;
finish = 138;
figure(3);
index=find(dataZ(:,1,1)>49950 & dataZ(:,1,1)<50050);
x=dataZ(1,2,start:finish) ;% for 40 hz
x=reshape(x,1,size(x,3));

plot(x,'k-.x','LineWidth',linewidth);

hold on;

x=dataZ(9,2,start:finish) ;% for 950 1100 hz
x=reshape(x,1,size(x,3));

plot(x,'r-.o','LineWidth',linewidth);

x=dataZ(80,2,start:finish) ;% for 950 1100 hz
x=reshape(x,1,size(x,3));

plot(x,'g-.s','LineWidth',linewidth);

x=dataZ(401,2,start:finish); % for 950 1100 hz
x=reshape(x,1,size(x,3));

plot(x,'m-.^','LineWidth',linewidth);

x=dataZ(801,2,start:finish); % for 950 1100 hz
x=reshape(x,1,size(x,3));

plot(x,'b-..','LineWidth',linewidth);

h=legend('40 Hz', '1kHz', '10kHz', '50kHz','100kHz');
set(h,'FontSize',30,'FontName','Arial');
xlabel('Time (hours)','fontSize',30,'FontName','Arial');
ylabel('|z| (\Omega)','fontSize',30,'FontName','Arial');
%title(['CNT Impedance ',cnt],'fontSize',30,'FontName','Arial');
axis([0 25 0 50]);
set(gca,'fontsize',fontSize)
%% Plot the data for diff freq
figure(4);
index=find(dataTheta(:,1,1)>49950 & dataTheta(:,1,1)<50050);
x=dataTheta(1,2,start:finish) ;% for 40 hz
x=reshape(x,1,size(x,3));

plot(x,'k-.x','LineWidth',linewidth);
hold on;

x=dataTheta(9,2,start:finish) ;% for 950 1100 hz
x=reshape(x,1,size(x,3));

plot(x,'r-.o','LineWidth',linewidth);
```

```
x=dataTheta(80,2,start:finish) ;% for 950 1100 hz
x=reshape(x,1,size(x,3));

plot(x,'g-.s','LineWidth',linewidth);

x=dataTheta(401,2,start:finish); % for 950 1100 hz
x=reshape(x,1,size(x,3));

plot(x,'m-.^','LineWidth',linewidth);

x=dataTheta(801,2,start:finish); % for 950 1100 hz
x=reshape(x,1,size(x,3));

plot(x,'b-..','LineWidth',linewidth);

h=legend('40 Hz', '1kHz', '10kHz', '50kHz','100kHz');
set(h,'FontSize',30,'FontName','Arial');
xlabel('Time (hours)','fontSize',30,'FontName','Arial');
ylabel('Theta (Degree)','fontSize',30,'FontName','Arial');
%title(['CNT Impedance ',cnt],'fontSize',30,'FontName','Arial');
axis([0 25 -15 1]);
set(gca,'fontsize',fontSize)
%%
% Short
chosenHour=116;
figure (4);
 plot(dataZ(:,1,1)/1000,dataZ(:,2,chosenHour),'m','LineWidth',linewidth)

%h=legend('pvCNT(One Pillar)',4);
%set(h,'FontSize',fontSize,'FontName','Arial');
xlabel('Frequency (kHz)','fontSize',fontSize,'FontName','Arial');
ylabel('|z| (\Omega)','fontSize',fontSize,'FontName','Arial');
%title('CNT Impedance','fontSize',fontSize,'FontName','Arial');
set(gca,'fontsize',fontSize)
hold on
%axis([0 100 17 17.5]);

% plot |Z|
figure (5);
plot(dataTheta(:,1,1)/1000,dataTheta(:,2,chosenHour),'m','LineWidth',linewidt
h)

xlabel('Frequency (kHz)','fontSize',fontSize,'FontName','Arial');
ylabel('Theta (Degree)','fontSize',fontSize,'FontName','Arial');
%title('CNT Impedance','fontSize',fontSize,'FontName','Arial');

set(gca,'fontsize',fontSize)
hold on
%axis([0 100 -1 0]);

%% Plot the Amplitud for diff 40 and 10k freq
start=113;
finish = 136;
figure(3);
index=find(dataZ(:,1,1)>49950 & dataZ(:,1,1)<50050);
```

```
x=dataZ(1,2,start:finish) ;% for 40 hz
x=reshape(x,1,size(x,3));
x200=dataZ200(1,2,1:24)
x200=reshape(x200,1,size(x200,3));

plot(x,'k-.','LineWidth',linewidth);
hold on;
plot(x200,'r-.','LineWidth',linewidth);


x=dataZ(80,2,start:finish) ;
x=reshape(x,1,size(x,3));
x200=dataZ200(80,2,1:24)
x200=reshape(x200,1,size(x200,3));
plot(x,'k-s','LineWidth',linewidth);
plot(x200,'r-s','LineWidth',linewidth);

%h=legend('40 Hz', '10kHz');
h=legend('pvCNT(200\mum spacing)', 'PPy Coated pvCNT(200\mum spacing)');
set(h,'FontSize',fontSize,'FontName','Arial');
xlabel('Time (hours)','fontSize',fontSize,'FontName','Arial');
ylabel('|z| (\Omega)','fontSize',fontSize,'FontName','Arial');
%title(['CNT Impedance ',cnt],'fontSize',30,'FontName','Arial');
axis([0 25 0 45]);
set(gca,'fontsize',fontSize)

%% Plot the Theta for diff 40 and 10k freq
figure(4);
index=find(dataTheta(:,1,1)>49950 & dataTheta(:,1,1)<50050);
x=dataTheta(1,2,start:finish) ;% for 40 hz
x=reshape(x,1,size(x,3));

x200=dataTheta200(1,2,1:24) ;% for 40 hz
x200=reshape(x200,1,size(x200,3));

plot(x,'k-.','LineWidth',linewidth);
hold on;
plot(x200,'r-.','LineWidth',linewidth);


x=dataTheta(80,2,start:finish) ;% for 950 1100 hz
x=reshape(x,1,size(x,3));

x200=dataTheta200(80,2,1:24) ;% for 40 hz
x200=reshape(x200,1,size(x200,3));

plot(x,'k-s','LineWidth',linewidth);
plot(x200,'r-s','LineWidth',linewidth);

h=legend('40 Hz',  '10 kHz');
set(h,'FontSize',30,'FontName','Arial');
xlabel('Time (hours)','fontSize',30,'FontName','Arial');
ylabel('Theta (Degree)','fontSize',30,'FontName','Arial');
%title(['CNT Impedance ',cnt],'fontSize',30,'FontName','Arial');
axis([0 25 -1 1]);
set(gca,'fontsize',fontSize)
```

```
%% Short-Term Analysis (CNT)
clear all
close all
fileName='50100200.xlsx';
sheet=3;
xlRange='B11:G811';
i=0;
[status,sheets] = xlsfinfo(fileName);
numOfSheets = numel(sheets);
for sheet=1:numOfSheets-1
 i=i+1;
 data(:,:,i)=xlsread(fileName,sheet,xlRange);
end

dataZ=[data(:,2,:) data(:,3,:)]

fontSize=30;
linewidth=3;
%% plot
figure (1);
 plot(dataZ(:,1,1)/1000,dataZ(:,2,1),'r','LineWidth',linewidth)
 hold on
 plot(dataZ(:,1,2)/1000,dataZ(:,2,2), 'b','LineWidth',linewidth)
 hold on
 plot(dataZ(:,1,3)/1000,dataZ(:,2,3), 'k','LineWidth',linewidth)

h=legend('pvCNT(50\mum spacing)', 'pvCNT(100\mum spacing)', 'pvCNT(200\mum
spacing)',4);
set(h,'FontSize',fontSize,'FontName','Arial');
xlabel('Frequency (kHz)','fontSize',fontSize,'FontName','Arial');
ylabel('|z| (\Omega)','fontSize',fontSize,'FontName','Arial');
%title('CNT Impedance','fontSize',fontSize,'FontName','Arial');
axis([0 100 0 10]);
set(gca,'fontsize',fontSize)



figure (2);

semilogx(dataZ(:,1,1),dataZ(:,2,1),'r')
 hold on
 semilogx(dataZ(:,1,2),dataZ(:,2,2), 'b')
 hold on
 semilogx(dataZ(:,1,3),dataZ(:,2,3), 'k')
h=legend('50\mum', '100\mum', '200\mum',4);
set(h,'FontSize',20,'FontName','Arial');
xlabel('Frequency (Hz)','fontSize',fontSize,'FontName','Arial');
ylabel('|z| (\Omega)','fontSize',fontSize,'FontName','Arial');
%title('CNT Impedance','fontSize',fontSize,'FontName','Arial');
axis([0 100000 3 10]);
set(gca,'fontsize',fontSize)


[ax,hlines]=plotyn(dataZ(:,1,1)/1000,dataZ(:,2,1),dataZ(:,1,1)/1000,dataZ(:,2
,2),dataZ(:,1,3)/1000,dataZ(:,2,3))
 leghandle = legend(hlines, '50\mum', '100\mum', '200\mum');
```

```
set(leghandle,'FontSize',fontSize,'FontName','Arial');
```

IV. COMSOL Simulation

COMSOL simulations for three base structures (Square, circle, and hexagon)

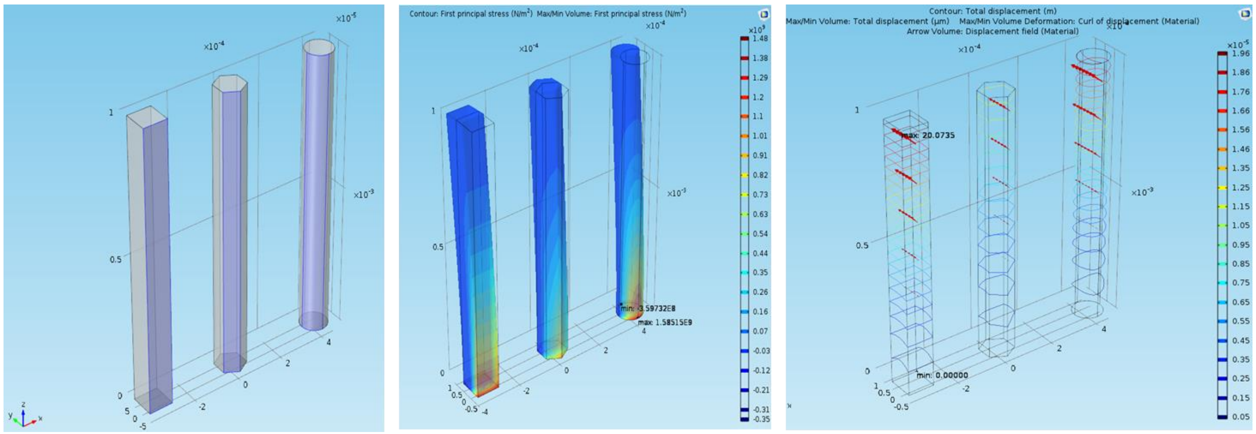

Fig. A. 4 The force was applied to the top surface of the pillar horizontally.

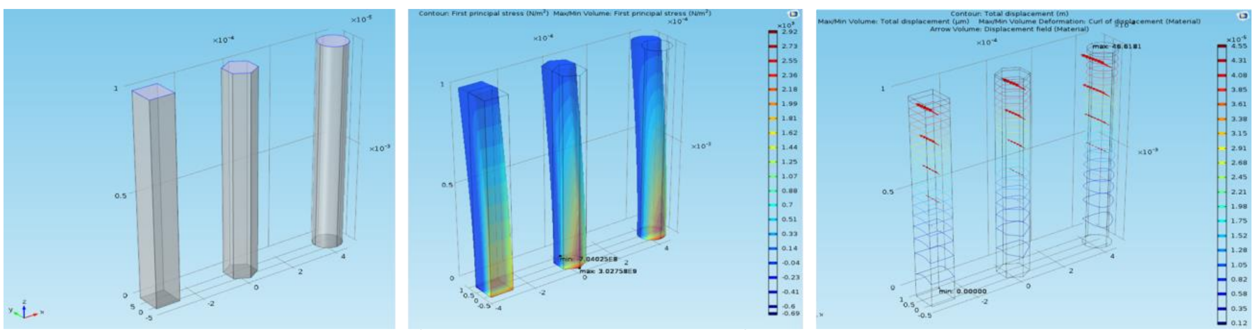

Fig. A. 5 The force was applied to the side of the pillar horizontally.

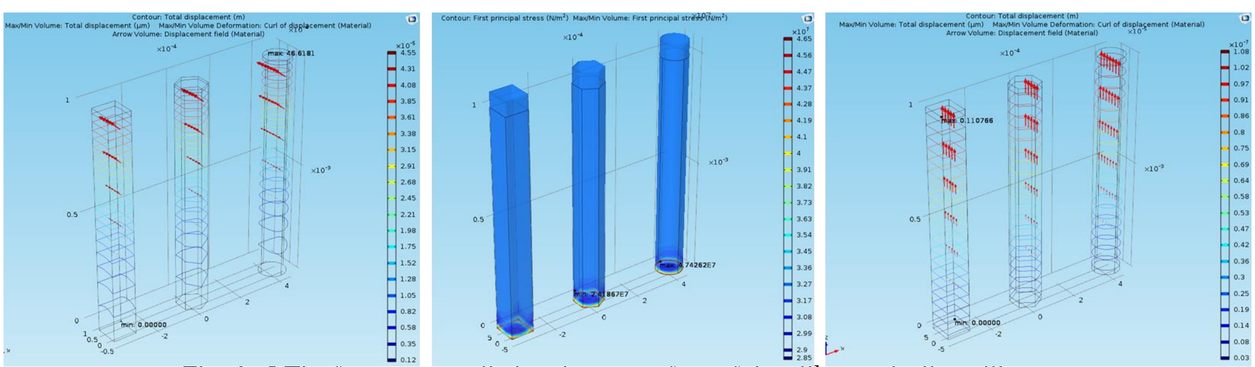

Fig. A. 6 The force was applied to the top surface of the pillar vertically pulling up.